Lecture Notes

Generation of ultraintense Laserpulses

Prof. Dr. Stefan Karsch

LMU München
Fakultät für Physik, Lehrstuhl Krausz
Am Coulombwall 1
85748 Garching

Wintersemster 2013

Contents

1 Description of Laser Light

1.1 Spectro-temporal description

1.1.1 Main parameters of laser electric field:

T_0	period duration
$\lambda_0 = c \cdot T_0$	wavelength
$\omega_0 = \dfrac{2\pi}{T_0}$	(angular-) frequency
$k_0 = \dfrac{2\pi}{\lambda_0}$	wave number
$\sqrt{2}\Delta\tau$	pulse duration (FWHM)
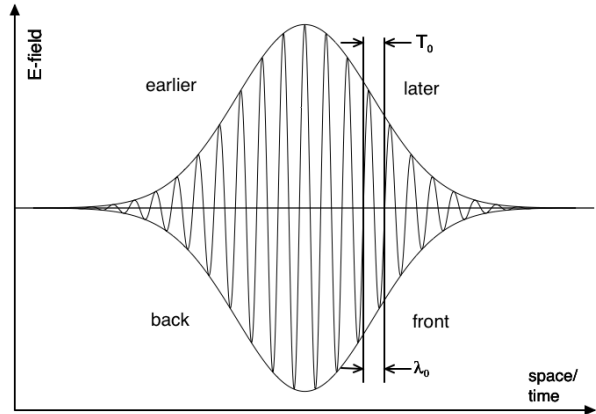
Figure 1: Electric field of light pulse.

1.1.2 Temporal description using real Functions:

Electric field:

lin. polarization:

$$\vec{E}(x,t) = \vec{E}_A(x,t) \cdot \cos\left(\omega_0 \cdot t - \vec{k} \cdot \vec{x} + \Phi(x,t)\right)$$

$E_A(x,t)$: envelope function
$\Phi(x,t)$: phase
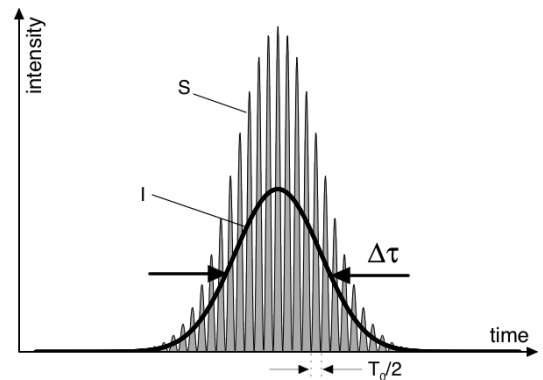
Figure 2: Intensity and Poynting-vector.

Magnetic Field:

For a full electrodynamic description of the light field, the magnetic field component has to be specified as well. For light propagating in vacuum, its value at any time can be inferred from the electric field by considering the potential equations for the electromagnetic fields, which are a direct consequence of Maxwell's equations. Using this approach, E and B can be expressed in terms of a scalar potential Φ and a vector

potential $\vec{A}$.

$$\left. \begin{array}{ll} E & = -\frac{\partial}{\partial t}\vec{A} - \vec{\nabla}\Phi \\ B & = \vec{\nabla} \times \vec{A} \end{array} \right\} \frac{\vec{A}(\vec{x}, t) = \vec{A}_0 \cdot \cos(\omega t - \vec{k}\vec{x} + \varphi)}{\Phi = 0 (\text{in absence of free charge})}$$

Inserting the Ansatz for $\vec{A}$ into the first equation, we get:

$$\left. \begin{array}{ll} \vec{E}(\vec{x}, t) & = \omega \vec{A}_0 \sin(\omega t - \vec{k}\vec{x} + \varphi) \\ \vec{B}(\vec{x}, t) & = \vec{k}\vec{A}_0 \sin(\omega t - \vec{k}\vec{x} + \varphi) \end{array} \right\} |\vec{E}| = \omega|\vec{A}_0| = \frac{\omega}{|\vec{k}|}|\vec{B}_0| = c|\vec{B}_0|$$

This simple consideration yields:
$|\vec{B}| = \frac{|\vec{E}|}{c}$, B is in phase with E, but perpendicular to it.
In vacuum, the Poynting vector S denotes the instantaneous energy flux density:

$$\vec{S} = \epsilon_0 c^2 (\vec{E} \times \vec{B})$$

Since $\vec{E}$ and $\vec{B}$ are in phase, $\vec{S}$ rapidly oscillates between 0 and $\epsilon_0 c E_0^2$, and is best viewed as the instantaneous light pressure (pressure = energy density!). Because of this oscillatory behaviour, $\vec{S}$ is very hard to measure directly and with an absolute value.
The temporal average of $\vec{S}$ is called light intensity, $\vec{I} = \langle \vec{S}(t) \rangle$, and is the commonly accessible quantity in an experiment. The intensity can thus be given in terms of $\vec{E}$ or $\vec{B}$.

$$|\vec{I}| = \langle \vec{S}(t) \rangle = \epsilon_0 c^2 \langle \vec{E}(t) \times \vec{B}(t) \rangle = \epsilon_0 c \langle \vec{E}(t)^2 \rangle = \epsilon_0 c^3 \langle \vec{B}(t)^2 \rangle$$

Executing the temporal average, we find:

$$|\vec{I}| = \frac{\epsilon_0 c}{2}(E_0(t))^2 = \frac{\epsilon_0 c^3}{2}(B_0(t))^2$$

Thus, $\vec{E}$ and $\vec{B}$ can be calculated in terms of $|\vec{I}|$.

1.2 Description in frequency space

An arbitrary light wave in frequency space can be written as:

$$E(\omega) = E_A(\omega) \cdot \cos(\omega t + \varphi(\omega)) \qquad \text{real description}$$

$$E(\omega) = \frac{1}{2}\{\tilde{E}(\omega) \cdot e^{i\omega t} + \tilde{E}^*(\omega) \cdot e^{-i\omega t}\} \quad \text{complex description}$$

where $\quad \tilde{E}(\omega) = E_A(\omega) \cdot e^{i\varphi(\omega)} \qquad\qquad$ complex amplitude (incl. spectrum and phase)
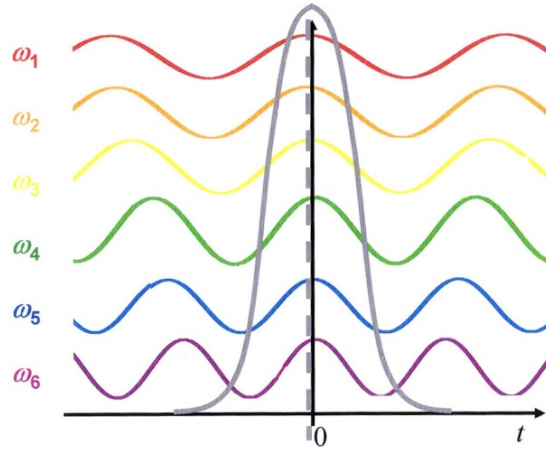
Figure 3: Addition of monochromatic waves yields a short pulse.

As evident from figure 3, a short pulse or pulse train can be understood as the phase-coherent sum of many discrete monochromatic waves with one local maximum of each wave coinciding at a given time (i.e. $t = 0$). .

While a pulse train can be constructed from a finite sum of discrete waves (modes), a single pulse requires an infinite number of modes, which can only be expressed by an integral:

$$\tilde{E}(t) = \frac{1}{\sqrt{2\pi}} \int_{-\infty}^{\infty} \tilde{E}(\omega) \cdot e^{i\omega t} d\omega = \mathcal{FT}\left(\tilde{E}(\omega)\right)$$

This fact can be understood by noting that in order to ensure that there is no periodicity, there can be no least common multiple of the set of wavelengths. This requires the set to be infinite.

The real component of the temporal field can be obtained by adding the above expression and its complex conjugate:

$$E(t) = \frac{1}{2}\{\tilde{E}(t) \cdot e^{i\omega t} + \tilde{E}(t) \cdot e^{-i\omega t}\}$$

On the other hand, the spectral composition of a known pulse (i.e. envelope and phase) in time is:

$$\tilde{E}(\omega) = \frac{1}{\sqrt{2\pi}} \int_{-\infty}^{\infty} \tilde{E}(t) \cdot e^{-i\omega t} dt = \mathcal{IFT}\left(\tilde{E}(t)\right) \text{ (corresponds to inverse Fourier transform)}$$

> $\tilde{E}(t)$ and $\tilde{E}(\omega)$ are equivalent, complete descriptions of the laser pulse.
> They can be mutually converted into each other by complex Fourier transforms.

Side consideration: FOURIER TRANSFORMS

Transformation rules		Calculation rules	
$f(x) \begin{array}{c} \to FT \to \\ \leftarrow IFT \leftarrow \end{array} F(s)$		$g(x) \to G(s)$	
		$f(x) \to F(s)$	
$A = \text{const}$	$\delta(s - 1/A)$	$f^*(x)$	$F^*(-s^*)$
$r(x) \begin{cases} r(x) = 1, \ |x| < 1 \\ r(x) = 0.5, \ |x| = 1 \\ r(x) = 0, \ |x| > 1 \end{cases}$	$2 \cdot \frac{\sin s}{s}$	$f(-x)$	$F(-s)$
		$f(a \cdot x)$	$\frac{1}{|a|} \cdot F\left(\frac{s}{a}\right)$
		$f(x - a)$	$e^{-ias} \cdot F(s)$
$\frac{1}{2}e^{-|x|}$	$2 \cdot \frac{1}{1+s^2}$	$f^{(k)}(x)$	$(is)^k \cdot F(s)$
e^{-Ax^2}	$\frac{1}{\sqrt{2A}} \cdot e^{-\frac{s^2}{4A}}$	$[A \cdot f(x) + B \cdot g(x)]$	$[A \cdot F(s) + B \cdot G(s)]$
		$f(x) \cdot g(x)$	$(F * G)(s)$
$\frac{1}{\sqrt{2B}} \cdot e^{-\frac{x^2}{4B}}$	e^{-Bs^2}	$|f(x)^2|$	$(F * F)(s)$

Side consideration: Gaussian function

Formulas :

$$A = A_0 \cdot e^{-\frac{(x-x_0)^2}{\xi^2}}$$
$$= A_0 \cdot e^{-\frac{(x-x_0)^2}{2\sigma^2}}$$
$$= A_0 \cdot e^{-\frac{4\ln(2)(x-x_0)^2}{\Delta x^2}}$$

x_0 peak location, mean value

ξ gaussian width, $\frac{1}{e}$ width, $\frac{1}{e^2}$ intensity

Δx FWHM width

σ standard deviation
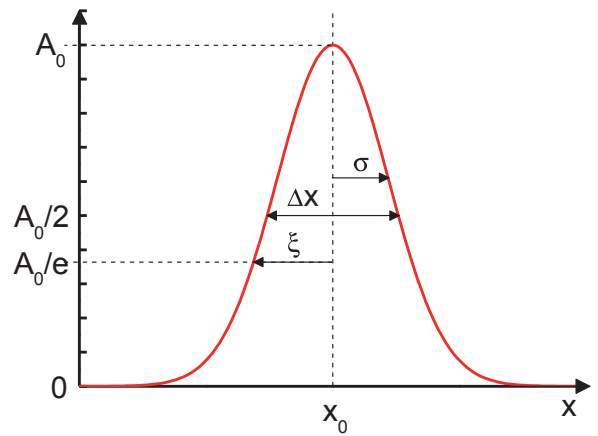
Figure 4: Gaussian function.

Hint: Calculations usually work with the electric field of the laser, which we cannot directly measure, in contrast to the intensity. In order not to become confused, it is therefore important to memorize that before comparing measured data to theory the translation of intensity into field has to be made.

Assume now that $x_0 = 0$, $A_0 = 1$:

$$\frac{1}{e} = e^{-\frac{x^2}{\xi^2}} \Rightarrow x^2 = \xi^2 \Rightarrow x_{\frac{1}{e}} = \xi$$

$$\text{HWHM:} \quad \frac{1}{2} = e^{-\frac{\Delta x^2_{HWHM}}{\xi^2}} \Rightarrow \ln\left(\frac{1}{2}\right) = -\left(\frac{\Delta x_{HWHM}}{\xi}\right)^2$$

$$\Rightarrow \Delta x_{HWHM} = \xi\sqrt{\ln(2)} = \xi \cdot 0.8326$$

$$\text{FWHM:} \quad \Rightarrow \Delta x_{FWHM} = \xi \cdot 2\sqrt{\ln(2)} = \xi \cdot 1.6651$$

Substitute ξ with $\sqrt{2}\sigma : \sigma = \frac{\xi}{\sqrt{2}}$.

	Widths			Heights
	$\Delta x\cdot$	$\xi\cdot$	$\sigma\cdot$	$\frac{1}{2} = 0.5$
$\Delta x =$	1	$2\sqrt{\ln 2} = 1.665$	$2\sqrt{2\ln 2} = 2.355$	$\frac{1}{e} = 0.368$
$\xi =$	$\frac{1}{2\sqrt{\ln 2}} = 0.6$	1	$\sqrt{2} = 1.414$	$\frac{1}{\sqrt{e}} = 0.607$
$\sigma =$	$\frac{1}{2\sqrt{2\ln 2}} = 0.425$	$\frac{1}{\sqrt{2}} = 0.707$	1	

Normalization:

$$A = \frac{A_0}{\sigma\sqrt{2\pi}}e^{-\frac{(x-x_0)}{2\sigma^2}} = \frac{A_0}{\xi\sqrt{\pi}}e^{-\frac{(x-x_0)}{\xi^2}}$$

Examples for frequency/temporal description:

- light pulse with gaussian temporal dependence:
  $E_A(t) = E_0 \cdot e^{-(t/\xi_t)^2}$ with constant phase $\varphi(t) = const.$

$$\rightarrow \text{IFT} \Rightarrow E(t) \propto e^{-At^2} \quad \text{with} \quad A = \frac{1}{\xi_t^2}$$

$$\Rightarrow E(\omega) \propto e^{-\frac{\omega^2}{4A}} = e^{-\frac{\omega^2\xi_t^2}{4}} = e^{-\left(\frac{\omega\xi_t}{2}\right)^2}$$

$$\Rightarrow \xi_\omega = \frac{2}{\xi_t}$$

$E_A(\omega) \propto e^{-(\omega\cdot\xi_t/2)^2}$ $\Rightarrow$ gaussian spectrum $\xi_\omega = 2/\xi_t$

$\Delta\tau_I = \sqrt{2\cdot\ln 2} \cdot \xi_t, \Delta\omega_I = \sqrt{2\cdot\ln 2} \cdot \xi_\omega$ $\Rightarrow \Delta\tau_I \cdot \Delta\nu_I = \frac{4\cdot\ln 2}{2\pi} = 0.441$

Note that $\Delta\tau_I = \Delta\tau_E/\sqrt{2}, \Delta\omega_I = \Delta\omega_E/\sqrt{2}$!

The time-bandwidth product is calculated using the temporal and spectral FWHM widths in intensity!

Usually, a spectrum measurement yields λ, not ν:

$$\Delta\tau \cdot \Delta\lambda \geq \frac{2 \cdot \ln 2}{\pi} \cdot \frac{\lambda^2}{c} \quad \Rightarrow \Delta\tau[\text{fs}] \cdot \Delta\lambda[\text{nm}] \approx 1.47 \cdot 10^{-3} \cdot (\lambda[\text{nm}])^2$$

- Pulse with sech(t)-dependence:

$$E_A(t) = E_0 \cdot \text{sech}(t/\tau_s) = \frac{2}{e^{t/\tau_s} + e^{-t/\tau_s}}$$

$$\Delta\tau_I \cdot \Delta\nu_I = 0.315$$

These are lower limits for the time-bandwidth product $\Delta\tau \cdot \Delta\nu$, that can only be achieved of the phase is constant or a linear function in t. Such pulses are called "bandwidth limited" or "transform limited".

In the presence of nonlinear temporal phase contributions, $\Delta\tau \cdot \Delta\nu$ increases, leading to "chirped pulses" (the instantaneous frequency changes in time).

1.3 Spatial pulse description: "Gaussian optics":

A gaussian transverse beam profile is a self-consistent analytical solution of the diffraction integrals, and can be considered a good approximation for certain laser types. These are mostly low- power systems, since Gaussian beams are not very efficient in using the available surface area of optical components.

Gaussian profile (in E-field and Intensity):

$$E = E_0 \cdot e^{-(r/w)^2}$$
$$I = I_0 \cdot e^{-2(r/w)^2}$$

Normalized energy content within radius r:

$$W(r) = \frac{2}{\pi w^2} \cdot \int_0^r 2\pi r \cdot e^{-2\left(\frac{r}{w}\right)^2} \mathrm{d}r$$
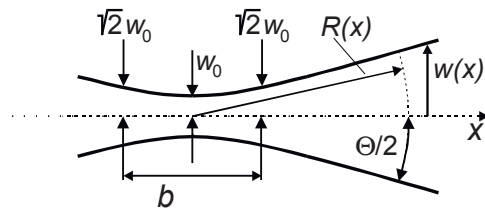
Figure 5: Gaussian optics: beam waist and diffraction.

For

$$r = w \qquad\qquad 86.5\%$$
$$r = 1.5w \qquad\qquad 98.9\%$$
$$r = 2w \qquad\qquad 99.9\%$$
$$r = 3w \qquad\qquad > 1 - 10^{-6}$$

Propagation:

If a Gaussian beam has a waist ($w = w_0$), defined by a locally flat wavefront, diffraction increases its diameter upon further propagation according to:

$$w(x) = w_0 \cdot \left[1 + \left(\frac{\lambda_0 x}{\pi w_0^2} \right)^2 \right]^{1/2}$$

The distance during which the beam area $w(x)^2$ is smaller than twice the waist area w_0^2 is called the confocal parameter b: ($b = 2x$ *Rayleigh-length*).

$$b = \frac{2\pi w_0^2}{\lambda} = 2 \cdot L_r$$

This is an important parameter considering the interaction of laser light, since within b the intensity can be kept above half the maximum intensity. For smaller w_0 the distance over which a high intensity can be maintained drops quadratically. If a long interaction is desired, w_0 has to be kept large enough. The total power to reach a certain intensity grows linearly with the interaction length. The total power is given by the integral over the intensity distribution of the beam:

$$P = \int_0^\infty I_0 \cdot e^{-2(r/w)^2} 2\pi r \cdot \mathrm{d}r = \pi \cdot I_0 \cdot \frac{w^2}{2}$$
$$\Rightarrow \text{on-axis peak intensity } I_0 :$$
$$I_0 = \frac{2}{\pi} \cdot \frac{P}{w_0^2}$$
$$\Rightarrow \text{mean intensity within } r = w :$$
$$I = \frac{2 \cdot (1 - e^{-2})}{\pi} \cdot \frac{P}{w^2}$$

From now on, the treatment is done for the electric field, not the intensity!

The radius of the wave fronts equals x for large x, but approaches infinity (i.e. a flat wavefront) for $x \to 0$:

$$R(x) = x \cdot \left[1 + \left(\frac{\pi w_0^2}{\lambda_0 x} \right)^2 \right]$$

The sign change of the wavefront curvature when going from $x = -\infty$ to $x = \infty$ corresponds to an additional phase term, the so-called *Guoy* phase $\zeta(x)$.

$$\zeta(x) = \arctan\left(\frac{x}{L_r}\right)$$

This additional phase term can be understood when considering the average longitudinal phase advance of a focused bundle. Since a focused beam consists of a superposition of plane waves with different angles, the average longitudinal phase advance of the whole bundle has to be less than for an axis-parallel plane wave. However, the axis-parallel part of the bundle has the same phase as said plane wave, and hence has to be faster than the average bundle. This corresponds exactly to the change in wavefront curvature at focus.

An even more naive interpretation is the fact that after focus the beam is inverted, i.e. the sign of the electric field has changed, corresponding to a phase shift by π.

The asymptotic beam *divergence* angle θ is found by dividing $w(x)$ by x for large x:

$$\tan\left(\frac{\theta}{2}\right) = \lim_{x \to \infty}\left(\frac{w(x)}{x}\right) = \frac{1}{\pi} \cdot \frac{\lambda}{w_0} \approx 0.318 \cdot \frac{\lambda}{w_0}$$

Alternatively, if a beam is focused with an asymptotic *converging* angle θ, the waist size can be determined from θ and λ using the above equation. This is done under the assumption that the focusing optics does not significantly clip the Gaussian beam:

Beam diameter $A = 4w$ (99.9% of the beam energy is transmitted through the focusing optics).

$$\Rightarrow \text{waist size} \quad w_0 = \frac{1}{\pi} \cdot \frac{\lambda}{\tan(\theta/2)} \quad 1/e \ \text{ radius of waist}$$

$$\text{or} \quad \Delta d_0 = \frac{4\ln 2}{\pi} \cdot \lambda \cdot \frac{f}{\Delta d} \quad \text{(FWHM of waist, for FWHM } \Delta d \text{ at focussing optics)}$$

Remember, we're still dealing with the electric field...

1.4 Top-hat beam profile:

In high intensity lasers, the beam profile often follows a super-gaussian (higher-order Gaussian) or top-hat distribution. This is done in order to illuminate the available optics with homogeneous fluence profile, hence minimizing damage caused by intensity peaks in the beam.

For simplicity, the top-hat profile is considered here. For a flat input wavefront, the

spatial intensity distribution in focus (far-field) is the Fourier transform of the intensity profile on the last focusing optics (near field)[1]. First, consider a 1-dimensional situation (far-field diffraction off a slit, width D (in units of λ)). The aperture function is a rectangle:

$$rect\left(\frac{x}{D}\right) = \left\{ \begin{array}{ll} 1 & |x| <= D/2 \\ 0 & \text{otherwise} \end{array} \right.$$

Then the intensity distribution in the far field is given by the sinc²-function:

$$I(\theta) = E^2(\theta) = \left(FT\left(rect\left(\frac{x}{D}\right)\right)(\theta)\right)^2 = \left(\frac{1}{\sqrt{2\pi}}D \cdot sinc\left(\frac{\theta D}{2}\right)\right)^2 = \frac{1}{2\pi}D^2\left(\frac{\sin\left(\frac{\theta D}{2}\right)}{\left(\frac{\theta D}{2}\right)}\right)^2$$

Here, θ is the angle of observation.

a) sinc and sinc²-function (diffraction off a slit)
b) $J_1(x)/x$ and $(J_1(x)/x)^2$ (diffraction off a hole)
c) Airy-distribution
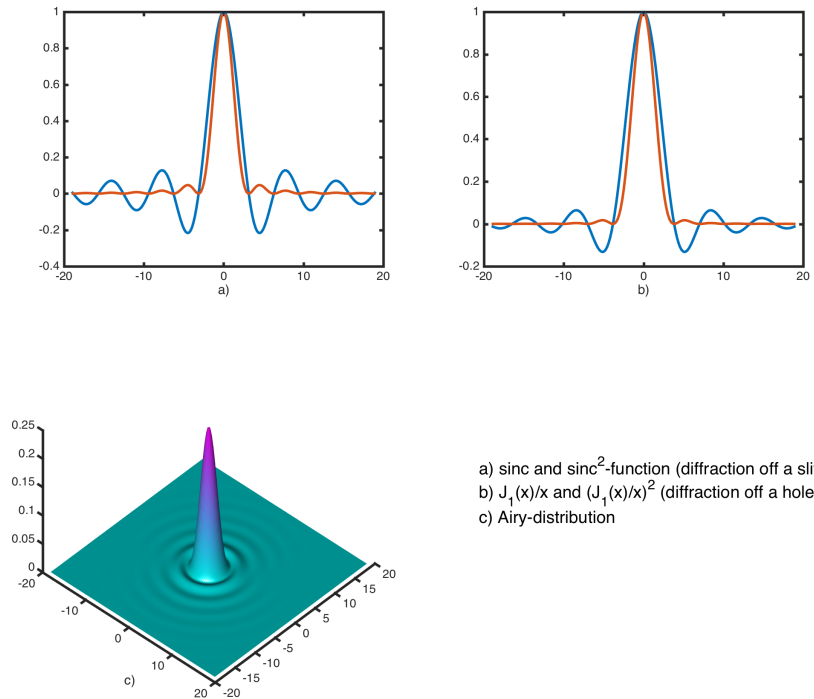
Figure 6: The Airy pattern on the interval $kD/2\sin(\theta) = [-10, 10]$, and the encircled power within the radius $kD/2\sin(\theta)$.

---

[1]Keep in mind that this refers to the field, not the intensity distribution. The correct calculation goes as follows: 1) Measure the near-field intensity (and possibly the phase). 2) take square root to get the field (which for a top-hat is a top-hat). 3) perform FT on the field. 4) Take square of FT'd field to get intensity in far-field.

For a 2-D round aperture, the intensity is given by (analogous to 1D-case):

$$I(\theta) = I_0 \left(\frac{2 J_1 \left(k \frac{D}{2} \sin(\theta) \right)}{k \frac{D}{2} \sin(\theta)} \right)^2 = I_0 \left(\frac{2 J_1(x)}{x} \right)^2, \quad x = k \frac{D}{2} \sin(\theta)$$

Here J_1 is the Bessel function of the first kind of order one and $k = 2\pi/\lambda$ is the wavenumber, and θ the angle of observation. The first zero crossing of the Bessel function $J_1(x)$
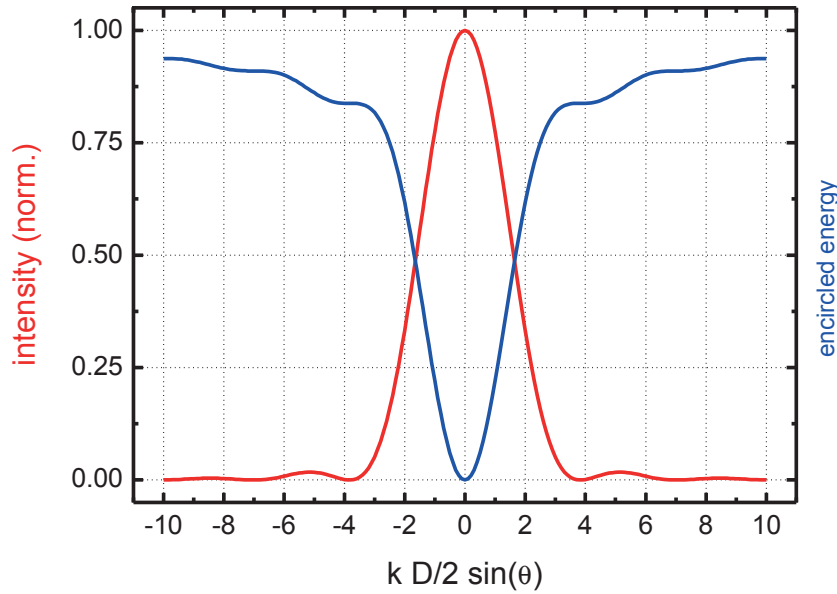
Figure 7: The Airy pattern on the interval $kD/2 \sin(\theta) = [-10, 10]$, and the encircled power within the radius $kD/2 \sin(\theta)$.

at $x = 3.8317$ marks the size of the first dark ring in the diffraction pattern and hence the size of the Airy disk. Hence, $kD/2 \sin(\theta) = 3.8317$ or

$$\sin(\theta) = \frac{3.83}{k \frac{D}{2}} = \frac{3.83\lambda}{2\pi \frac{D}{2}} = 1.22 \frac{\lambda}{D}$$

This condition is the well-known Rayleigh criterion for the resolution of optical instruments. This angle leads to a radius of the first dark ring

$$r_1 = f \cdot \sin(\theta) = 1.22 \cdot f \frac{\lambda}{D} = 1.22\lambda F$$

with the distance f to the observation point (or focal length of the optic) and the F-number $F = f/D$.

The FWHM size of the Airy disk can be computed by requiring

$$I(x) = 0.5 = \left(\frac{2J_1(x)}{x}\right)^2$$

which occurs at $\quad J_1(x) = \frac{x}{2\sqrt{2}}, \quad$ hence $\quad x = 1.6163$ and

$$D_{FWHM} = \frac{2 \cdot 1.6163}{\pi} \cdot f\frac{\lambda}{D} \approx 1.03\lambda F$$

Integration of the expression for $I(\theta)$ with respect to θ gives the total energy within a circle of given size in the diffraction plane:

$$E(\theta) = E_0 \cdot (1 - J_0^2(x) - J_1^2(x))$$
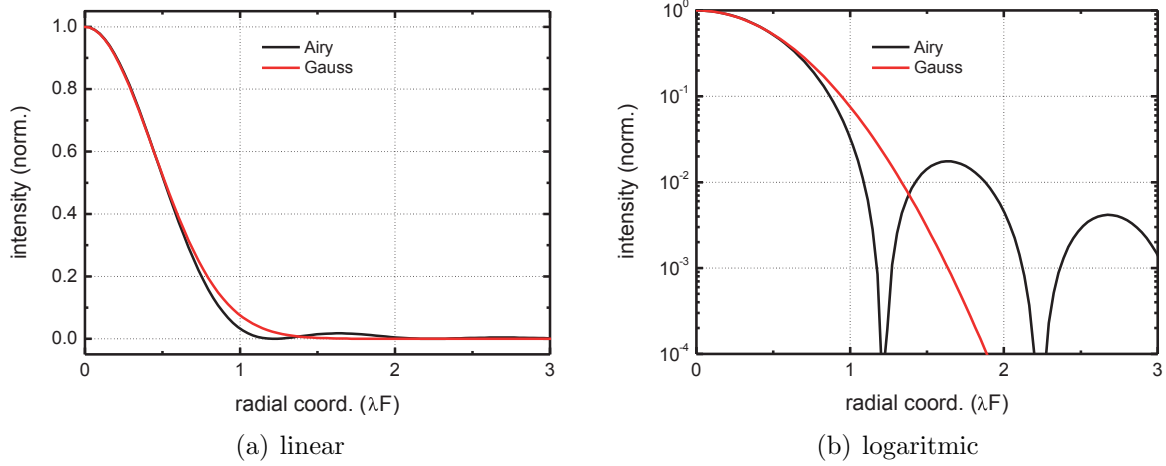
Figure 8: Comparison of Airy pattern and Gauss distribution of the same integral volume on a linear (left) and logarithmic (right) scale.

The amount of total energy within the first, second and third dark ring are 83.8%, 91.0% and 93.8%, respectively.

Focal intensities:

$\Rightarrow$ on-axis peak intensity I_0 : $I_0 = \dfrac{\pi \cdot P}{\lambda^2 \cdot F^2}$

$\Rightarrow$ mean intensity within $1/e^2$ diameter: $I_{av} = I_0 \cdot 0.394$

It is sometimes desirable to fit a gaussian distribution to an Airy-type pattern in order to facilitate the calculation of important beam properties. Requiring that the Gaussian profile has the same integral as the Airy pattern leads to (see Fig.8):

$$I(x) = I_0 \cdot e^{-\frac{2x^2}{w^2}}, \quad \text{with } w = 0.44\lambda F$$

1.5 Phase effects

Up to now, the envelope function of a light pulse and its evolution in space has been described in some detail. In contrast, we will now focus on mainly temporal (but also spatial) effects cased by changes to the phase of a light pulse. These can have dramatic effects for the pulse envelope, as will be illustrated in the following examples.

1.5.1 Nonlinear propagation / self phase modulation

Consider an intense laser pulse propagating in a transparent medium. In strong fields, the polarization response of the medium becomes nonlinear when the elongation of the electron cloud in an atom cannot be described as harmonic anymore. In such cases, the refractive index (approximated here as equal for all wavelengths) can be expressed as a series expansion in I:

$$n = n_0 + \Delta n(I) = n_0 + n_2 \cdot I + \ldots$$

Example: *Ti:Sapphire, $\lambda = 800 nm$*

$$n_0 = 1.76$$
$$n_2 \approx 3 \cdot 10^{-20} \mathrm{m}^2/\mathrm{W}$$

Note that in normally dispersive media $n_2 > 0$, such that an increase in intensity always leads to a higher refractive index, and consequently to a <u>lower</u> group velocity.

<div align="center"><u>High intensity slows down light!</u></div>

The electric field can be written as a fourier transform of the complex spectrum with an intensity-dependent phase:

$$\tilde{E}(x,t) = \int_{-\infty}^{\infty} E_0(\Delta\omega) \cdot e^{-i(\omega t - kx)} \mathrm{d}(\Delta\omega) = \int_{-\infty}^{\infty} E_0(\Delta\omega) \cdot e^{-i\omega\left(t - \frac{x}{c}(n_0 + \Delta n(I))\right)} \mathrm{d}(\Delta\omega)$$

This indicates that a local intensity-dependent phase shift has an influence on the temporal (and spatial) properties of the beam.

An important practical parameter is he so-called B-integral, which counts the accumulated phase shift due to nonlinear effects after propagation in units of $2\pi/\lambda$:

$$B = \frac{2\pi}{\lambda_0} \cdot \int \frac{\Delta n(I)}{n_0} \mathrm{d}l <= 1$$

As long as B is smaller than unity during its propagation through the laser (i.e. the accumulated phase shift $< \lambda$), the effects do not become too excessive to be handled.

(a) Spatial effect: self-focussing (SF)

In a laser pulse with gaussian transverse profile, the nonlinear phase follows a radial profile according to:

$$\Delta\varphi(r) = -x \cdot \frac{\omega}{c} \cdot n_2 \cdot I(r) \quad \text{with} \quad I(r) = I_0 \cdot e^{-2\left(\frac{r}{w}\right)^2}$$

This leads to a phase retardation in areas of high intensities, and hence to an inward curvature of the wavefront. After propagation, the beam self-focuses as shown in figure 9. The local retardation of the wavefronts caused by $\Delta\varphi(r)$ leads to a shift in space:
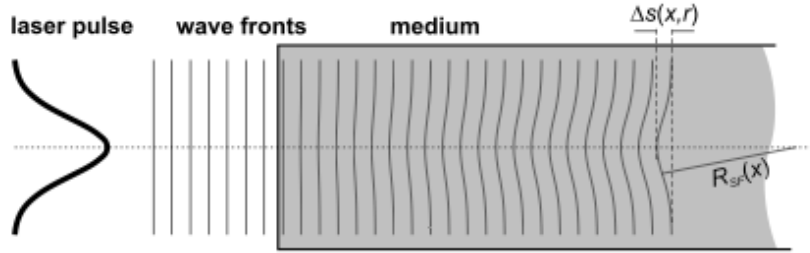
Figure 9: Self-focusing in a nonlinear medium.

$$\Delta s(x, r) = (x(I(r)) - x_0) = (\nu(I(r)) - \nu_0) \cdot t$$
$$= \left(\frac{c}{n(I(r))} - \frac{c}{n_0}\right) \cdot t = \frac{ct}{n(I(r))}\left(1 - \frac{n(I(r))}{n_0}\right)$$
$$= -\underbrace{\frac{ct}{n(I(r))}}_{x}\left(\frac{n_2}{n_0} \cdot I(r)\right) = -x \cdot \frac{n_2 I_0}{n_0} \cdot e^{-2\left(\frac{r}{w}\right)^2} \underbrace{\approx}_{e^{-x}=1-x^2+\dots} -x \cdot \frac{n_2 I_0}{n_0} \cdot \left(1 - 2\frac{r^2}{w^2}\right)$$

Double radial differentiation yields the radius of the wavefront in the center of the beam:

$$R_{SF}(x) \approx \frac{n_0}{n_2} \cdot \frac{w^2}{4x \cdot I_0} = O\left(\frac{1}{x}\right)$$

This obvious focusing effect is counteracted by diffraction. In order to find the threshold where self-focusing overcomes diffraction, it is necessary to recall the radius of a wavefront due to diffraction:

$$R(x) = x \cdot \left[1 + \left(\frac{\pi w_0^2 n_0}{\lambda_0 x}\right)^2\right]$$

which can be approximated for small x:

$$R_D(x) \approx x \cdot \left(\frac{\pi w_0^2}{\frac{\lambda_0}{n_0} x}\right)^2 = \frac{\pi^2 w_0^4 n_0^2}{\lambda_0^2 \cdot x} = O\left(\frac{1}{x}\right)$$

Catastrophic self-focusing occurs for $R_{SF} \leq R_D$:

$$\frac{n_0}{4 \cdot n_2 I_0} \leq \frac{\pi^2 \cdot w_0^2 \cdot n_0^2}{\lambda^2}$$

and consequently for a powers greater than:

$$P \approx \frac{w_0^2 \cdot \pi \cdot I_0}{2} > P_\sigma = \frac{\alpha \cdot \lambda^2}{8\pi \cdot n_0 \cdot n_2} \quad (\alpha \approx 2 \text{ :empirical factor})$$

(b) Spectro-temporal effect: self-phase modulation (SPM)

With a gaussian temporal profile of the laser pulse, the nonlinear phase contribution varies in time analogous to the previous case:

$$\Delta\varphi(t) = x \cdot \frac{\omega}{c} \cdot n_2 \cdot I(t) \quad \text{with} \quad I(t) = I_0 \cdot e^{-2\left(\frac{t}{\xi_t}\right)^2}$$

and the total instantaneous phase is given by:

$$\Phi(t) = \omega_0 t - \frac{2\pi}{\lambda_0} n(I) x$$

Consequently, the instantaneous frequency reads:

$$\omega(t) = \frac{\mathrm{d}\Phi(t)}{\mathrm{d}t} = \omega_0 - \frac{2\pi x}{\lambda_0}\frac{\mathrm{d}n(I)}{\mathrm{d}t} = \omega_0 + \frac{8\pi x n_2 I_0}{\lambda_0 \xi_t^2} \cdot t \cdot e^{-2\left(\frac{t}{\xi_t}\right)^2} \equiv \omega_0 + \alpha \cdot t \cdot e^{-2\left(\frac{t}{\xi_t}\right)^2}$$

The resulting pulse after a propagation distance x exhibits a temporally varying instantaneous frequency that increases nearly linearly with t in around the peak of the pulse. The nonlinear phase change thus creates new frequencies. Since the linear chirp region around the pulse center contains the largest fraction of the pulse energy, it can be efficiently compressed into a shorter pulse than before (albeit with temporal wings originating from the region of negative chirp at the foot of the pulse). Note that the pulse envelope is not affected by SPM directly, but is subsequently distorted via dispersion effects.
  In a simple picture, the pulse maximum propagates slower than the foot of the pulse. This "stretches" the leading and "squeezes" the trailing edge of the pulse.

Effects:

- different phase velocities within the pulse

- generation of new frequencies ($n_2 > 0$): leading edge "red", trailing edge "blue"

- Change of spectral envelope $\tilde{E}(\omega)$
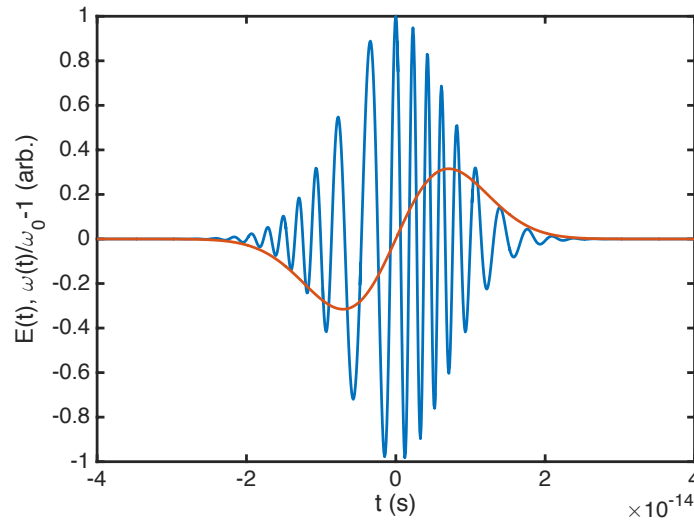
Figure 10: Self-phase modulation: different local intensities lead to a instantaneous phase shift and consequently to a time-varying instantaneous frequency. In effect, new frequencies are generated.

- After dispersion: Change of temporal envelope $\tilde{E}(t)$

Since phase advance is best described in frequency space (via $n(\omega)$) and intensity changes in time, self-phase modulation is usually modeled numerically by alternately switching between these two descriptions. This is the basis for the "Fourier split-step method", which works as follows:

- evaluate the intensity-dependent phase $\Delta\varphi(I(t))$ after propagating Δx

- IFT to spectrum and spectral phase

- propagate from $\Delta x/2$ to $3\Delta x/2$ and accumulate frequency-dependent phase $\Delta\varphi(\omega)$

- FT back to temporal pulse

- Compute $\Delta\varphi(I(t))$ between Δx and $2\Delta x \ldots$
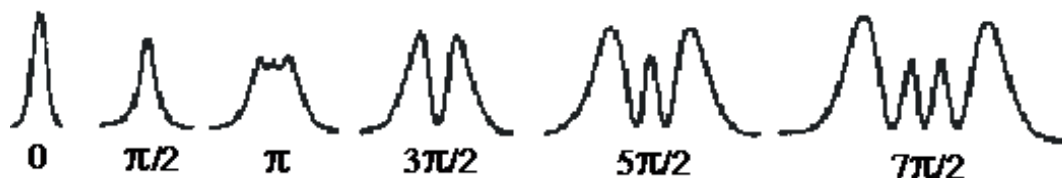
Figure 11: Change of frequency spectrum by self-phase modulation.

1.6 CPA-principle

<u>Gain in a laser chain:</u> pulse energy and -power increase upon propagation.

- non-linear refractive index ($\Delta n = n_2 \cdot I$) grows:
  self phase modulation, self focussing, damage.

<u>Measures:</u>

(a) increase beam size (reduces intensity)

(b) increase pulse duration (reduces peak power)

<u>CPA-principle:</u> (**C**hirped **P**ulse **A**mplification):

(a) before the amplification: lengthen pulse in time (by factor 10^3–10^5) by introducing positive dispersion.

(b) after amplification: compress pulses back to original duration by introducing the opposite (i.e. negative) dispersion in a fully reflective or large beam diameter setup.

2 Dispersion

2.1 Propagation of pulses, dispersion effects

Consider the electric field of a laser pulse:

$$\tilde{E}(x,t) = \int_{-\infty}^{\infty} E_A(\omega) \cdot e^{-i(\omega t - \varphi(\omega))} \mathrm{d}\omega \quad \text{with} \quad \varphi(x,\omega) = k(\omega) \cdot x = \frac{x}{c} \cdot \omega \cdot n(\omega)$$

This corresponds to a relative change in the absolute phase for different frequencies. After propagation, the different colors in the pulse have travelled different optical paths, according to the respective refractive index $n(\omega)$.

$\varphi(\omega)$ can be written as a Taylor expansion:

$$\varphi(\omega) = \sum_{m=0}^{\infty} \frac{(\omega - \omega_0)^m}{m!} \cdot \left(\frac{\partial^m}{\partial \omega^m} \varphi(\omega) \right)_{\omega = \omega_0} = \sum_{m=0}^{\infty} \frac{(\omega - \omega_0)^m}{m!} \cdot D_m$$

The D_m are called dispersion coefficients and are found by evaluating the mth-derivative of $\varphi(\omega)$ with respect to ω (not λ, which is a common mistake!) at ω_0:

$$D_m = \left(\frac{\partial^m}{\partial \omega^m} \varphi(\omega) \right)_{\omega = \omega_0} \overset{\varphi = k \cdot x}{=} x \cdot \left(\frac{\partial^m k}{\partial \omega^m} \right)_{\omega = \omega_0} \overset{k \cdot c = \omega \cdot n}{=} \frac{x}{c} \cdot \left(\frac{\partial^m (\omega \cdot n(\omega))}{\partial \omega^m} \right)_{\omega = \omega_0}$$

- pulse propagation with a linear spectral phase (all Taylor coefficients with $m > 1$ are 0): Shift in time vs. propagation describes the group velocity:

$$\tilde{E}(x,t) = \int_{-\infty}^{\infty} E_A(\omega) \cdot e^{i((\omega_0 + \Delta\omega) \cdot t - (\varphi(\omega_0) + D_1 \Delta\omega))} \mathrm{d}\omega$$

$$= e^{i(\omega_0 t + \phi(\omega_0))} \int_{-\infty}^{\infty} E_A(\omega) e^{i(\Delta\omega(t - D_1))} \mathrm{d}\omega$$

$$= e^{i\omega_0(t - x/v_p)} \cdot E_A(t - x/v_g)$$

with $v_p = \omega_0 / k(\omega_0)$ velocity of wavefronts (phase velocity)

$$v_g = \frac{x}{D_1} = \frac{\mathrm{d}\omega}{\mathrm{d}k} \text{ velocity of pulse (group velocity)}$$

- pulse propagation with a quadratic spectral phase (all Taylor coefficients with $m > 2$ are 0): Pulse broadening during propagation.

  Assumptions:

  1. Start with transform-limited Gaussian pulse ($\varphi(\omega) \equiv 0, \equiv$ linear) of the following form

$$\tilde{E}(t) = E_0 \cdot e^{-(t/(\sqrt{2} \cdot \xi_I))^2} \cdot e^{i(\omega_0 t - \varphi(t))} \qquad \Delta\tau = 2 \cdot \sqrt{\ln 2} \cdot \xi_I$$

2. introduce linear *chirp*: 2nd derivative of spectral phase

$$\varphi(\omega) = D_0 + \frac{(\Delta\omega)^2}{2} \cdot D_2$$

$\Rightarrow$ pulse shape: $\tilde{E}(t, D_2) = E_1(t, D_2) \cdot e^{i(\omega_0 t - \varphi(t, D_2))}$ with t: local time (from IFT-FT)

amplitude: $E_1(t, D_2) = \frac{E_0 \cdot \xi_I}{\sqrt[4]{\xi_I{}^4 + D_2{}^2}} \cdot e^{-\left((t \cdot \xi_I)/\sqrt{2 \cdot \left(\xi_I{}^4 + D_2{}^2\right)}\right)^2}$

phase: $\varphi(t, D_2) = -\frac{D_2}{2 \cdot \left(\xi_I{}^4 + D_2{}^2\right)} \cdot t^2 + \frac{1}{2} \cdot \arctan\left(\frac{D_2}{\xi_I{}^2}\right)$

frequency: $\omega(t) = \frac{\partial(\omega_0 t - \varphi)}{\partial t} = \omega_0 + \frac{D_2}{\left(\xi_I{}^4 + D_2{}^2\right)} \cdot t$ (linear *chirp*)

Higher order dispersion effects

Description via "dispersion components" D_m (Taylor expansion of the spectral phase):

$$D_m = \left(\frac{\partial^m\left(\phi(\omega)\right)}{\partial\omega^m}\right)_{\omega=\omega_0} \overset{\phi=k\cdot x}{=} x \cdot \left(\frac{\partial^m k}{\partial\omega^m}\right)_{\omega=\omega_0} \overset{k \cdot c = \omega \cdot n}{=} \frac{x}{c} \cdot \left(\frac{\partial^m\left(\omega \cdot n(\omega)\right)}{\partial\omega^m}\right)_{\omega=\omega_0}$$

- D_0 describes <u>phase</u> propagation

$$D_0 = \frac{x}{c} \cdot \omega_0 \cdot n_0 = 2\pi \cdot \frac{x}{(\lambda_{0,vak}/n_0)}$$ (phase in units of $2\pi/\lambda$)

- D_1 describes <u>pulse</u> propagation (group delay, GD)

$$D_1 = \frac{x}{c} \cdot \frac{\partial(\omega \cdot n)}{\partial\omega} = x \cdot \frac{\partial k}{\partial\omega} = \frac{x}{v_g} = t_g$$

- D_2 describes pulse broadening (group delay dispersion, GDD)

$$D_2 = \frac{x}{c} \cdot \frac{\partial^2(\omega \cdot n)}{\partial\omega^2} = x \cdot k''$$

for Gaussian pulses: $\Delta\tau(x) = \Delta\tau(0) \cdot \sqrt{1 + \left(4 \cdot \ln 2 \cdot \frac{D_2}{(\Delta\tau(0))^2}\right)^2}$

For $D_2 \gg \Delta\tau(0)^2$, D_2 effects increase quadratically with decreasing $\Delta\tau(0)$
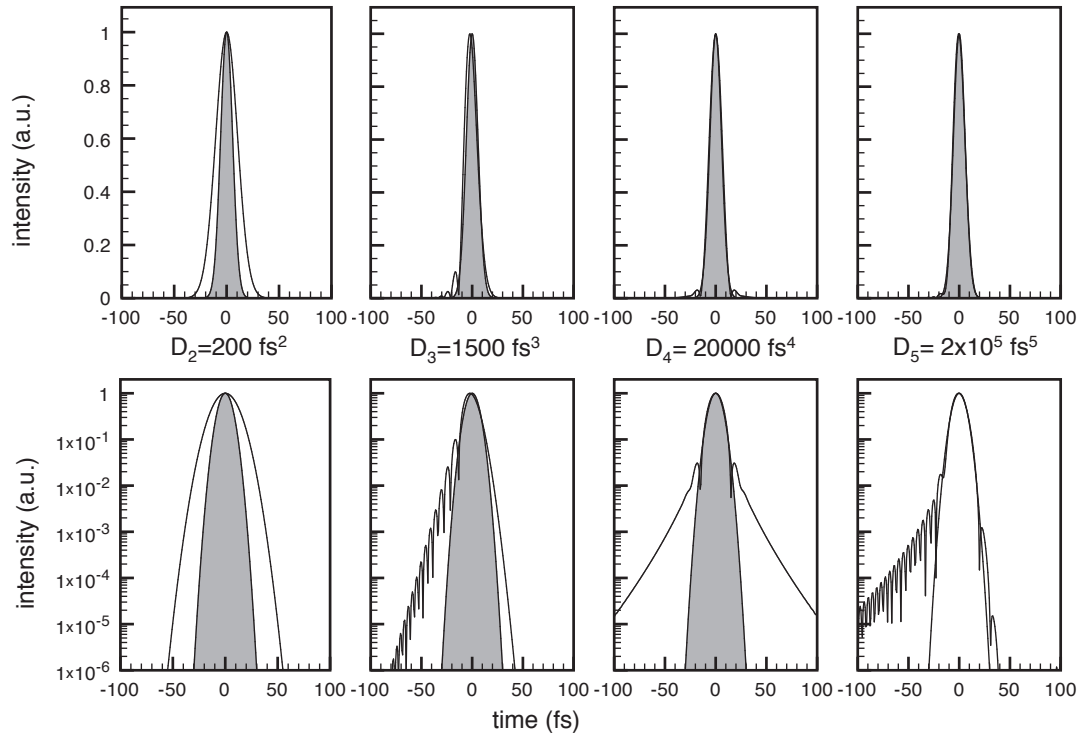
Figure 12: Influence of each dispersion coeffient on the pulse shape, in linear and logarithmic scales (top and bottom, respectively). Original pulse: Gaussian, $\Delta\tau = 13$ fs, $\Delta\lambda = 75$ nm

- D_3 third order dispersion (TOD)

- $D_{4...}$ higher order dispersion (FOD, ...)

- ...   + higher orders

Convention D_n is usually given in units of $(\text{fs})^n$, i.e. D_1 in fs, D_2 in fs^2 etc., although the calculation yields $(\text{seconds})^n$. Therefore, D_1 has to be multiplied by 10^{-15}, D_2 by 10^{-30}, etc.

Sign conventions: Positive (or normal) dispersion $\rightarrow$ *carrier frequency increases with time:* longer wavelengths (red part) travel faster than shorter ones (blue part)$\rightarrow$ positive GDD. Reflects normal material dispersion: Red wavelengths see lower refractive index than blue ones.

Negative (or anomalous) dispersion $\rightarrow$ *carrier frequency decreases with time:* longer wavelengths (red part) travel slower than shorter ones (blue part) $\rightarrow$ negative GDD.

Main sources of dispersion:

- **Bulk Material:** wavelength dependent refractive index

- **Chirped mirrors:** multilayer dielectric structure with wavelength-selective reflectivity a different depths (i.e. optical path lengths)

- **Prism pair:** cumulative effect of the angular dispersion as well as the material dispersion

- **Diffraction grating pair:** angular dispersion

- **Grism:** combination of grating and prism

2.2 Material dispersion

The change of refractive index with wavelength in an optical material leads to a different phase velocity of the individual frequency components on a short laser pulse. This difference in propagation speed leads to a frequency-dependent total phase for these components, and hence to a non-constant spectral phase of the pulse. Material dispersion is the most common cause for changes in the spectral phase of a laser pulse after propagation, and has to be understood and controlled if a short laser pulse has to be delivered to a target by an optical system.

Almost all common optical materials:

- exhibit normal dispersion (i.e. $\lambda_1 > \lambda_2$: $n(\lambda_1) < n(\lambda_2)$)

- create positive chirp (i.e. $D_2 > 0$).

Material dispersion is present in all transmissive (including air!) laser components and has to be compensated. However, it can also be used to introduce a desired amount of dispersion.

Abnormal dispersion occurs only close to a resonance in the dielectric function (absorption line). A good approximation of material dispersion for most common materials can be given by expressing the material's refractive index with the "Sellmeier formula". In its most common form, it yields a good approximation by fitting three resonance lines λ_i and amplitude factors A_i to the measured refractive index curve in a certain wavelength range.

$$\text{Sellmeier formula: } n(\lambda) = \sqrt{1 + \sum_{i=1}^{3} \frac{A_i \cdot \lambda^2}{\lambda^2 - \lambda_i^2}} \ \ (\lambda \text{ in units of } \mu\text{m})$$

(Data for A_i and λ_I, or alternative Sellmeier formulas and their coefficients can be found for a wide range of materials e.g. in www.refractiveindex.info or on manufacturer's websites)

Mat.	A_1	A_2	A_3	$\lambda_1^2[\mu m^2]$	$\lambda_2^2[\mu m^2]$	$\lambda_3^2[\mu m^2]$
Sapphire	1.02380	1.05826	5.28079	0.00377588	0.0122544	321.3616
BK7	1.039612	0.2317923	1.0104694	0.006000699	0.020017914	103.560653
Silica	0.6961663	0.4079426	0.8974794	0.004679148	0.013512063	97.9340025
SF14	1.6918254	0.2859199	1.12595145	0.013315154	0.061264744	118.405242

These Sellmeier coefficients can be used to calculate the dispersion coefficients in a consistent fashion: Definition: $\eta(\omega) = \omega \cdot n(\omega) = \sqrt{\omega^2 + \omega^2 \cdot \sum_{i=1}^{3} A_i \cdot \frac{\omega_i{}^2}{\omega_i{}^2 - \omega^2}}$ $\Rightarrow$

$D_m = \frac{x}{c} \cdot \left(\frac{\partial^m \eta}{\partial \omega^m} \right)_{\omega = \omega_0}$ nth differentiation with respect to ω yields the D$_n$ $\Rightarrow$

$$\eta' = \frac{d}{d\omega}(\omega \cdot n) = n + \omega n'$$

$$\eta'' = \frac{d^2}{d\omega^2}(\omega \cdot n) = \frac{d}{d\omega}(n + \omega n') = n' + n' + \omega n'' = 2n' + \omega n''$$

$$\eta''' = \frac{d^3}{d\omega^3}(\omega \cdot n) = \frac{d}{d\omega}(2n' + \omega n'') = 2n'' + n'' + \omega n''' = 3n'' + \omega n'''$$

$$\eta'''' = \frac{d^4}{d\omega^4}(\omega \cdot n) = \frac{d}{d\omega}(3n'' + \omega n''') = 3n''' + n''' + \omega n'''' = 4n''' + \omega n''''$$

with the following derivatives of n:

$$n' = \frac{\omega}{n} \sum_{i=1}^{3} \frac{A_i \omega_i^2}{(\omega_i^2 - \omega^2)^2}$$

$$n'' = \frac{n'}{\omega} - \frac{n'^2}{n} + \frac{4\omega^2}{n} \sum_{i=1}^{3} \frac{A_i \omega_i^2}{(\omega_i^2 - \omega^2)^3}$$

$$n''' = \frac{3n'^3}{n^2} + \frac{3}{\omega}\left(n'' - \frac{n'}{\omega}\right) - 12\frac{\omega n'^2}{n} \sum_{i=1}^{3} \frac{1}{\omega_i^2 - \omega^2} + 24\omega^2 n' \sum_{i=1}^{3} \frac{1}{(\omega_i^2 - \omega^2)^2}$$

$$n'''' = -15\frac{n'^4}{n^3} + 72\frac{n'^3\omega}{n^2} \sum_{i=1}^{3} \frac{1}{\omega_i^2 - \omega^2} + 18\frac{n'^3}{n^2\omega} - 144\frac{\omega^2 n'^2}{n} \sum_{i=1}^{3} \frac{1}{(\omega_i^2 - \omega^2)^2} -$$

$$- 72\frac{n'^2}{n} \sum_{i=1}^{3} \frac{1}{\omega_i^2 - \omega^2} + \frac{3}{\omega^2}\left(n'' - \frac{n'}{\omega}\right) + 192\omega^3 n' \sum_{i=1}^{3} \frac{1}{(\omega_i^2 - \omega^2)^3} + 144\omega n' \sum_{i=1}^{3} \frac{1}{(\omega_i^2 - \omega^2)^2}$$

Note that a discrete list of refractive indices created from the above Sellmeier formula is not continuously differentiable beyond differentiation order $n = 2$, hence large errors for higher order derivatives occur if repeated straightforward numerical differentiation is applied. The above analytical expressions yield correct values up to D_4. Alternative numerical approach: Fit n^{th} order polynomial ($n > m_{max}$), and perform polynomial differentiation (i.e. Matlab).

Mat.	n_0	D_0	$D_1[fs]$	$D_2[fs^2]$	$D_3[fs^3]$	$D_4[fs^4]$
Saphire	1.76019	138245	59387	581	421	$-$ 156
BK7	1.51078	118656	50924	447	321	$-$ 106
Silica	1.45332	114143	48939	363	275	$-$ 114
SF14	1.74294	136890	59558	1785	1147	$+$ 358

Table 1: Dispersion coefficients for some optical materials. At $\lambda_0 = 800$nm central wavelength and $x = 1$cm (optical path length).

After having established the fact that all optical materials (including air!) cause a positive chirp and hence temporal elongation of the laser pulse, it becomes clear that the art of compensating that effect by introducing negative chirp ($D_2 < 0$) in a clever arrangement of optics is a central part of high-intensity laser design. In fact, the sum of all $D_{n,i}$ from all materials and optics in the laser chain has to be zero for $n > 1$.

2.3 Chirped Mirrors

Gradual change in the optical thickness of different coating layers results in changing the Bragg wavelength within the multilayer structure. $\rightarrow$ Different wavelengths penetrate to a different depth.

Features:

- both positive or negative dispersion

- higher order dispersion control

- ultrabroadband spectral range $\rightarrow$ more than one octave

- ideal for few cycle pulse generation

- free from SPM

- high reflectivity $> 99\%$
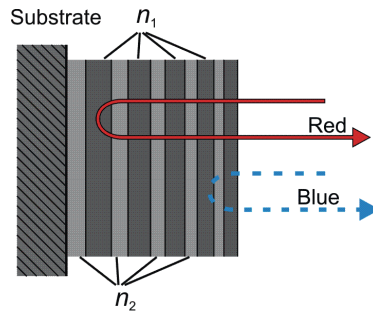
Figure 13: Chirped mirror providing negative dispersion
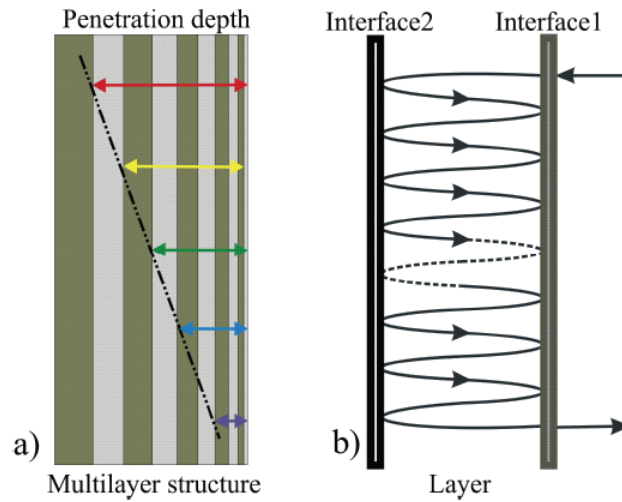
Figure 14: Delay generation mechanisms in chirped mirrors

- *limited dispersion,* absolute value depends on the spectral bandwidth: typical design for ~ 1 octave at $\lambda_0 = 800$nm provides $|D_2| \sim 50\text{fs}^2$

Additional to the penetration depth for different colors, resonators for a given wavelength range can be introduced at certain depths to selectively trap and delay that range, further increasing the overall dispersion (14)

Such a mirror design is presented in 15:
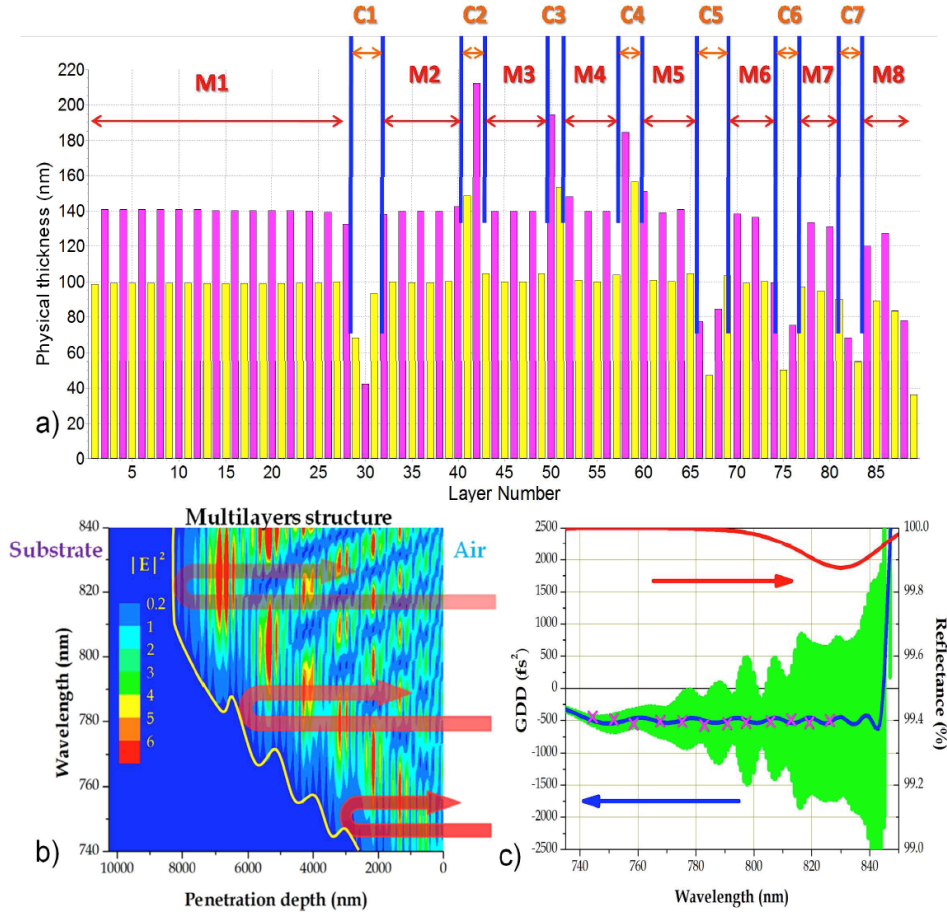
Figure 15: Structure and characteristics of our multilayer HDM.

(a) Physical thicknesses of the alternate layers of tantalum pentoxide (Ta_2O_5) and silicon dioxide (SiO_2) are shown with yellow and pink columns, respectively. Individual layer thicknesses range between 35 nm and 210 nm and the total physical thickness of the structure is approximately 10 μm. The structure can be represented as a combination of eight mirrors (M1-M8) and seven resonant cavities (C1-C7) resulting in GDD originating from the penetration and resonance effects, respectively. In general the cavities C1-C7 consist of several layers of different materials.

(b) The distribution of the modulus-square of the electric field ($|E|^2$) displaying the penetration in the HDM structure shown in panel (a). The storage effect of the cavities manifests itself in localized enhancements of the trapped fields. The yellow line plots the GD variation introduced by the penetration effect only.

(c) Calculated reflectance (red) and GDD (blue) curve of the HDM for the designed angle of incidence of 10°. Measured GDD with white light interferometer (magenta crosses). The green area represents the probable range of GDD values.

(Image taken from: V. Pervak et al., Optics Express 17, 19204 (2009))

2.4 GVD caused by angular dispersion

As a preparation for various types of angularly dispersing setups (prism / grating / grism compressor / stretcher), we will derive the effects of angular dispersion on the GVD of a light pulse. We assume an optical element introducing angular dispersion at A. Here, β is the angle between a ray of frequency ω and a ray at the reference frequency ω_0.
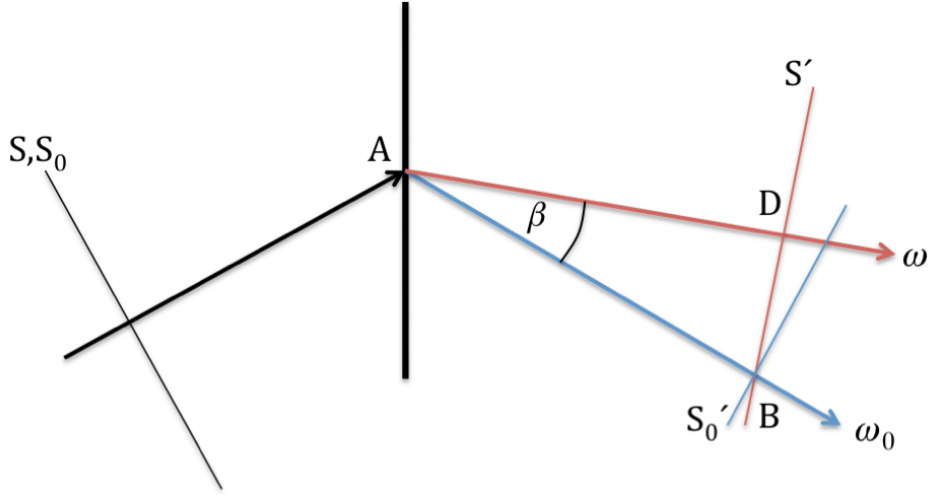
Figure 16: Here S, S_0 and S',S_0' represent the wave fronts of two rays corresponding to the center frequency ω_0 (blue line) and an arbitrary frequency ω (red line), respectively.

The phase delay in any linear optical element is given by

$$\varphi(\omega) = \frac{\omega}{c}P(\omega); \text{ where } P(\omega) = \overline{AD} \text{ "frequency dependent optical path"}$$

In the above setup,

$$\overline{AD} = P\left(\omega\right) = \overline{AB} \cdot \ \cos\left(\beta\right) = P\left(\omega_0\right) \cdot \ \cos\left(\beta\right) = x \ \cos\left(\beta\right)$$

which yields an angular phase advance of:

$$\varphi_{ang.}(\omega) = \frac{\omega}{c}x \cdot \cos(\beta(\omega))$$

The D_i are then given as the i-th derivative of $\varphi_{ang.}(\omega)$ with respect to ω, e.g.:

$$D_{2ang.} = \left.\frac{\partial^2}{\partial\omega^2}\varphi_{ang.}(\omega)\right|_{\omega_0} = \frac{1}{c}\left.\left(2 \cdot \frac{d}{d\omega}P(\omega) + \omega\frac{d^2}{d\omega^2}P(\omega)\right)\right|_{\omega_0}$$

$$= \left.-\frac{x}{c}\left\{\sin\beta\left[\frac{2d\beta}{d\omega} + \omega\frac{d^2\beta}{d\omega^2}\right] + \omega \ \cos\beta\left(\frac{d\beta}{d\omega}\right)^2\right\}\right|_{\omega_0}$$

Similarly,

$$
\begin{aligned}
D_{3ang.} &= \left.\frac{\partial^3 \varphi_{ang.}(\omega)}{\partial \omega^3}\right|_{\omega_0} = \left.\frac{1}{c}\left(3\frac{d^2}{d\omega^2}P(\omega) + \omega\frac{d^3}{d\omega^3}P(\omega)\right)\right|_{\omega_0} \\
&= \left.-\frac{x}{c}\left\{\cos\beta\cdot\left[3\left(\frac{d\beta}{d\omega}\right)^2 + 3\omega\frac{d\beta}{d\omega}\frac{d^2\beta}{d\omega^2}\right] + \sin\beta\cdot\left[3\frac{d^2\beta}{d\omega^2} + \omega\frac{d^3\beta}{d\omega^3} - \omega\left(\frac{d\beta}{d\omega}\right)^3\right]\right\}\right|_{\omega_0}
\end{aligned}
$$

For small values of β (such as in the case of relatively weak angular dispersion from e.g. a prism setup), $(\sin\beta) \ll 1$ and $(\cos\beta) \approx 1$, therefore

$$
D_{2ang.} \approx \left.-\frac{x\omega_0}{c}\left(\frac{d\beta}{d\omega}\right)^2\right|_{\omega_0} \quad \text{and}
$$

$$
D_{3ang.} \approx \left.-\frac{3x}{c}\left[\left(\frac{d\beta}{d\omega}\right)^2 + \omega\frac{d\beta}{d\omega}\frac{d^2\beta}{d\omega^2}\right]\right|_{\omega_0}
$$

- In the above definition, $D_{2,ang}$ is always negative, irrespective of $(d\beta/d\omega)|_{\omega_0}$.

- The dispersion increases with the distance x from the dispersing element

- For gratings the above approximation is not adequate, since for broadband pulses in general β is not a small angle

These formulas just require to plug in the appropriate function for $\beta(\omega)$.

2.5 Prism compressor

- Optical arrangement:
  2 two identical prisms placed exactly antiparallel 17

- Function:
  Usually negative dispersion, because $D_{2,ang}$ is negative and "blue" passes less material than "red" (at least for $l \gg e_1, e_2$). If l is small, the geometrical path difference between blue and red in the 2nd prism might be small. Then the higher "blue" refractive index might lead to a longer optical path for blue. A prism compressor can provide both, either negative or positive dispersion.

- Calculation:
  Compute optical path through system, derive phase and D_m

$$
\varphi = \frac{2\pi}{\lambda}\cdot P_{opt}(\lambda) = \frac{\omega}{c}\cdot P_{opt}(\omega) \Rightarrow D_m = \frac{\partial^m \varphi(\omega)}{\partial \omega^m}
$$
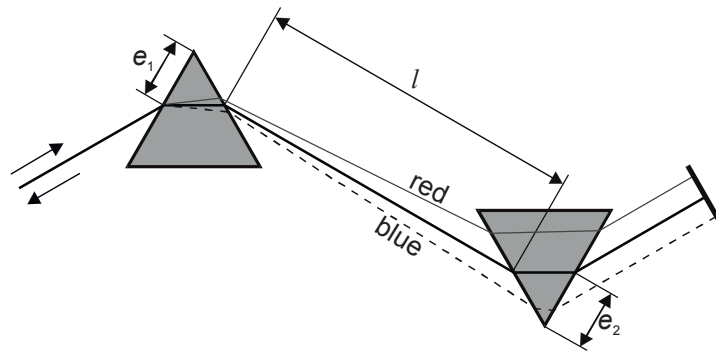
Figure 17: Prism compressor

Side consideration: Optical Prism

<u>Assume:</u>
prim with index of refraction $n(\lambda)$, apex angle α
incidence angle γ_1
incidence location e (dist. to apex)

- <u>angles $\delta_1, \delta_2, \gamma_2$</u>

- <u>distances f,g</u>

  express as functions of e, γ_1, α
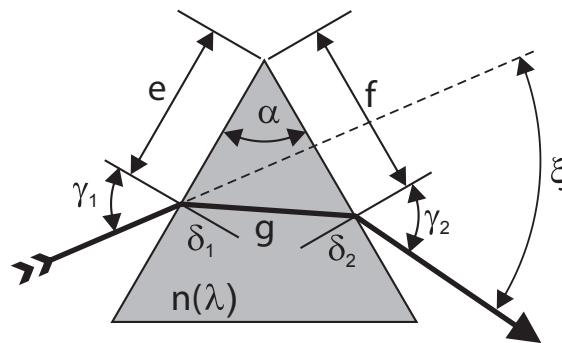
Figure 18: optical prism

<u>The following identities hold:</u>

1. $\frac{\sin \gamma_1}{\sin \delta_1} = n\left(\lambda\right) \Rightarrow \sin \gamma_1 = n\left(\lambda\right) \cdot \sin \delta_1$

$$\sin \gamma_2 = n\left(\lambda\right) \cdot \sin \delta_2 \qquad \text{(Snell's law)}$$

2. $\xi = (\gamma_1 - \delta_1) + (\gamma_2 - \delta_2) = (\gamma_1 + \gamma_2) - (\delta_1 + \delta_2)$

    (sum of deflections on 1st and 2nd surface)

3. $\alpha = \delta_1 + \delta_2$ (angle sum in triangle)

4. from 1: $\delta_1 = \arcsin\left(\frac{\sin\gamma_1}{n(\lambda)}\right)$

5. from 3: $\delta_2 = \alpha - \arcsin\left(\frac{\sin\gamma_1}{n(\lambda)}\right)$

6. from 5& 1: $\gamma_2 = \arcsin\left(n \cdot \sin\left(\alpha - \arcsin\left(\frac{\sin\gamma_1}{n(\lambda)}\right)\right)\right)$

7. from 2-6: $\xi = \gamma_1 + \arcsin\left(n \cdot sin\left(\alpha - \arcsin\left(\frac{\sin\gamma_1}{n(\lambda)}\right)\right)\right) - \alpha$

Since now all angles are known in terms of α, γ_1 and $n(\lambda)$, the distances f and g can be inferred using the law of sines:

$$\frac{a}{\sin(\alpha)} = \frac{b}{\sin(\beta)} = \frac{c}{\sin(\gamma)}$$

a,b,c are the three sides and a, b, g the three opposing angles, respectively. In our case, this yields:

$$\frac{g}{\sin\alpha} = \frac{e}{\sin(\pi/2 - \delta_2)} = \frac{e}{\cos\delta_2} \quad \Rightarrow g = \frac{\sin\alpha \cdot e}{\cos(\alpha - \arcsin(\sin\gamma_1/n(\lambda)))}$$

$$\frac{f}{\sin(\pi/2 - \delta_1)} = \frac{e}{\sin(\pi/2 - \delta_2)} = \frac{e}{\cos\delta_2} \quad \Rightarrow f = \frac{\cos(\arcsin(\sin\gamma_1/n(\lambda))) \cdot e}{\cos(\alpha - \arcsin(\sin\gamma_1/n(\lambda)))}$$

This fixes all unkonwn quantities in terms of e, α, γ_1 and $n(\lambda)$. In order to minimize the reflection losses of a prism dispersion setup, a is chosen such that if the incident rays hit the first surface at Brewster's angle, also the refracted ray (at central wavelength l_0) leaves the second surface at the same angle. Simplifications associated with this special case will be discussed below.

Firstly, the prism in such a configuration is used symmetrically (for λ_0), hence f = e:

$$\frac{f}{e} = \frac{\arcsin(\sin(\gamma_1/n(\lambda))}{\alpha - \arcsin(\sin\gamma_1/n(\lambda))} = 1 = \frac{\delta_1}{\alpha - \delta_1} \Rightarrow \alpha = 2\delta_1 = 2\delta_2$$

or

$$\sin\gamma_1 = n(\lambda)\sin(\alpha/2)$$

Brewster's angle is defined as $\tan\gamma_B = n(\lambda_0)$, hence

$$\sin\gamma_B = \tan\gamma_B \sin(\alpha/2) \text{ or } \sin(\alpha/2) = \cos(\gamma_B)$$

or finally:

$$\alpha = 2 \arcsin(\cos(\gamma_B))$$

This defines the apex angle for an isosceles Brewster prism (which can be inferred as a function of γ_B just as easily from geometrical considerations):

$$\alpha = \pi - 2\gamma_B = \pi - 2\arctan(n(\lambda))$$

As discussed in 2.2.3, angular dispersion results in wavelength dependent delay between different spectral components. Overall dispersion (GDD) is negative: sum of angular (negative) and material dispersion (positive in the visible and NIR range)

Features:

- identical prisms with antiparallel arrangement

- the first prism serves as the disperser while the second produces parallel rays

- higher throughput compared to the grating compressor (close to Brewster's angle.)

- fine tuning of the dispersion is possible due to the opposite sign of material dispersion

- *SPM in the last prism*

For the discussion of the prism compressor, we will separate the effects of the angular dispersion and material dispersion. In order to use the group dispersion formula for $D_{2,ang.}$ derived above, we assume that the apex of the second prism is located at B (see Fig.). x denotes the apex-apex distance.

For a symmetrical prism (angles γ of incident and refracted ray with first and second surface, respectively, are equal for the center frequency ω_0), β can be expressed using Snell's law:

$$\beta = \arcsin\left(n(\omega) \cdot \sin\left(\alpha - \arcsin\left(\frac{\sin\gamma}{n(\omega)}\right)\right)\right) - \alpha$$

In the case of a Brewster prism, α is given by

$$\alpha = \pi - 2\theta_b = \pi - 2\arctan(n(\omega))$$

Since now all optical paths are known from geometrical relations, we can give a closed expression for the 2nd and 3rd order dispersion coefficients of a prism compressor built from two isosceles Brewster prisms in symmetrical configuration. Let l_g be the total glass path and l the path of the central wavelength between the two prisms (see Fig. 17).

Then D_2 can be expressed as

$$D_2 = \frac{\lambda_0^3}{2\pi c^2} \left[l_g \frac{d^2 n}{d\lambda^2} - \left(4l + \frac{l_g}{n^3} \right) \left(\frac{dn}{d\lambda} \right)^2 \right] \Bigg|_{\lambda_0}$$

and D_3 is approximately (neglecting the angular dispersion in the glass):

$$D_3 = \frac{\lambda_0^4}{(2\pi c)^2 c} \left[12l \left(n'^2 \left[1 - \lambda_0 n'(n^{-3} - 2n) \right] + \lambda_0 n' n'' \right) - l_g (3n'' + \lambda_0 n''') \right] \Bigg|_{\lambda_0}$$

Taken from Diels...

In the above case of symmetrical beam path (minimum deviation) through the prism for the component ω_0 and with apex angle being chosen so that the Brewster condition is satisfied, it can be shown[2] that

$$\frac{d\beta}{dn} = -2, \text{ and } \frac{d^2\beta}{dn^2} = -4n + \frac{2}{n^3},$$

therefore

$$D_{2ang.} \approx -4 \frac{\lambda_0^3}{2\pi c^2} \left(\frac{dn}{d\lambda} \right)^2 \Bigg|_{\lambda_0} \cdot x$$

$$D_{3ang.} \approx \frac{12x\lambda_0^4}{(2\pi)^2 c^3} \left\{ \left(\frac{dn}{d\lambda} \right)^2 \left[1 - \lambda_0 \frac{dn}{d\lambda} \left(n^{-3} - 2n \right) \right] + \lambda_0 \left(\frac{dn}{d\lambda} \frac{d^2 n}{d\lambda^2} \right) \right\} \Bigg|_{\lambda_0}$$

Contribution of the material dispersion of the prism

Since the beam also passes through a certain amount of glass in each prism which contributes to the dispersion. So the contribution of material should also be considered. Let $x_m(\omega)$ be the total glass path for a ray with frequency ω, then the additional second and third order dispersion parameters are:

$$D_{2m} = \frac{\partial^2}{\partial\omega^2} \left(\frac{\omega}{c} n x_m \right) \Bigg|_{\omega_0} = \frac{1}{c} \left(2x_m \frac{\partial n}{\partial\omega} + 2n \frac{\partial x_m}{\partial\omega} + 2\omega \frac{\partial n}{\partial\omega} \frac{\partial x_m}{\partial\omega} + \omega x_m \frac{\partial^2 n}{\partial\omega^2} + \omega n \frac{\partial^2 x_m}{\partial\omega^2} \right) \Bigg|_{\omega_0}$$

$$D_{3m} = \frac{\partial^3}{\partial\omega^3} \left(\frac{\omega}{c} n x_m \right) \Bigg|_{\omega_0} =$$

$$= \frac{1}{c} \left(6 \frac{\partial x_m}{\partial\omega} \frac{\partial n}{\partial\omega} + 3n \frac{\partial^2 x_m}{\partial\omega^2} + 3x_m \frac{\partial^2 n}{\partial\omega^2} + 3\omega \frac{\partial^2 n}{\partial\omega^2} \frac{\partial x_m}{\partial\omega} + 3\omega \frac{\partial n}{\partial\omega} \frac{\partial x_m^2}{\partial\omega^2} + \omega x_m \frac{\partial^3 n}{\partial\omega^3} + \omega n \frac{\partial^3 x_m}{\partial\omega^3} \right) \Bigg|_{\omega_0}$$

$$= -\frac{\lambda_0^2}{(2\pi)^2 c^3} x_m \left[3\lambda^2 \frac{d^2 n}{d\lambda^2} + \lambda^3 \frac{d^3 n}{d\lambda^3} \right] \Bigg|_{\lambda_0}$$

---

[2]Fork et al., Opt. Lett. 9, 150 (1984)

nochmal pruefen

Therefore the total dispersion of the prism compressor for double pass configuration is given by

$$D_2 \approx 2\frac{\lambda_0^3}{2\pi c^2}\left(-4x\left(\left.\frac{dn}{d\lambda}\right|_{\lambda_0}\right)^2 + x_m\left.\frac{d^2n}{d\lambda^2}\right|_{\lambda_0} + x_m\left.\frac{2}{\lambda}\frac{dn}{d\lambda}\right|_{\lambda_0}\right)$$

$$D_3 \approx 2\frac{\lambda_0^2}{(2\pi)^2 c^3}\left\{12x\left[\left(\frac{dn}{d\lambda}\right)^2\left(1-\lambda\frac{dn}{d\lambda}\left(n^{-3}-2n\right)\right) + \lambda\left(\frac{dn}{d\lambda}\frac{d^2n}{d\lambda^2}\right)\right]\bigg|_{\lambda_0} - x_m\left(3\frac{d^2n}{d\lambda^2}+\lambda\frac{d^3n}{d\lambda^3}\right)\bigg|_{\lambda_0}\right\}$$

Advantages

- higher throughput compared to grating compressors

- fine tuning of the overall dispersion is possible due to the opposite sign of material dispersion

Disadvantage

- Self phase modulation (SPM) in the last prism, because the pulse is shortest in material just at the exit of the prism.

For prisms, the sign of 2nd and 3rd order dispersion is equal, just as in materials.

Alternative description: prism compressor, single pass:

Dispersion coefficients can be described as linear functions of l (prism inner distance, see Fig. 2.2) and $e = e_1 + e_2$ (sum of apex distances, i.e. propagation in material):

$$D_2 = A_2 \cdot l + B_2 \cdot e, \qquad\qquad D_3 = A_3 \cdot l + B_3 \cdot e$$

Linear coefficients A_i, B_i for a single pass:

$$A_2 = -4\omega \cdot (n')^2 \cdot \frac{1}{c}$$

$$B_2 = \frac{2}{\sqrt{1+n^2}} \cdot \left[2n' + \omega \cdot \left(n'' - \frac{(n')^2}{n^3}\right)\right] \cdot \frac{1}{c}$$

$$A_3 = 12n' \cdot \left[n' + \omega \cdot n'' + \omega \cdot (n')^2 \cdot n \cdot \left(2 - \frac{1}{n^4}\right)\right] \cdot \frac{1}{c}$$

$$B_3 = \frac{2}{\sqrt{1+n^2}} \cdot \left[3 \cdot \left(\frac{n''}{n} - \frac{(n')^2}{n^4}\right) + \omega\left(n''' - 3 \cdot \frac{n' \cdot n''}{n^3} + 3 \cdot (n^2 + 1) \cdot \left(\frac{n'}{n^2}\right)^3\right)\right] \cdot \frac{1}{c}$$

In practice: e not too small (otherwise spectral clipping at the apex)
$\Rightarrow 1cm \leq e \leq 5$ cm

Material	n	n' [fs]	n" [fs^2]	n"' [fs^3]	γ_{Br} [°]	A_2 [fs^2/cm]	B_2 [fs^2/cm]	A_3 [fs^3/cm]	B_3 [fs^3/cm]
Sapphire	1.760	0.0091	−3.33 E-4	0.00578	59.2	−26.00	572.2	−32.62	429.3
BK7	1.511	0.00674	−4.11 E-5	0.00413	67.0	−14.26	491.1	−18.68	354.2
Quartz	1.453	0.00587	−3.83 E-4	0.00398	69.1	−10.82	408.4	−12.15	324.0
SF14	1.743	0.01859	−6.92 E-3	0.00576	59.7	−108.54	1769.2	−279.39	836.1

Figure 19: Derivatives of refractive index with respect to frequency and linear coefficients A_i, B_i for the calculation of the dispersion coefficients ($D_i = A_i \cdot l + B_i \cdot e$) in a single-passed prism compressor (without end mirror), $\lambda_0 = 800$ nm:

2.6 Grating Compressor

Angular dispersion due to the diffraction from gratings results in wavelength-dependent delay between different spectral components.
"Red part" travels **longer** optical path
"Blue part" travels **shorter** optical path

Components:

- two identical diffraction gratings (transmission/reflection), *Exactly parallel including lines, near Littrow-angle of incidence for maximum efficiency.*

- end mirror (flat or roof mirror)

Features:

- larger dispersion compared to the bulk material, chirped/dispersive mirrors or prism compressor $\rightarrow$ compact

- exact compensation of higher order dispersion coefficients, excluding additional dispersion from the amplifier chain, with grating based stretcher and compressor using optical imaging technique.

- material dispersion of the amplifier chain can be compensated to at least 3rd order by the of angle of incidence and the grating separation in the stretcher or compressor

- however: 2nd and 3rd order dispersion are of opposite sign (exactly matched to grating stretcher, but not to bulk material), therefore a grating compressor cannot be used to compress pulses stretched in bulk material alone.

- *slight misalignment of gratings results in angular chirp and pulse front tilt*

- *higher losses compared to bulk-material and prism pairs*

- *self-phase modulation in case of transmission gratings*

- *limited acceptance of spectral bandwidth (Max. one octave)*

The grating equation for the first-order diffraction is given by:

$$\sin\gamma + \sin\beta = N \cdot \lambda$$

where

γ = angle of incidence

β = diffraction angle of wavelength λ

N= groove density (#/m) of the grating
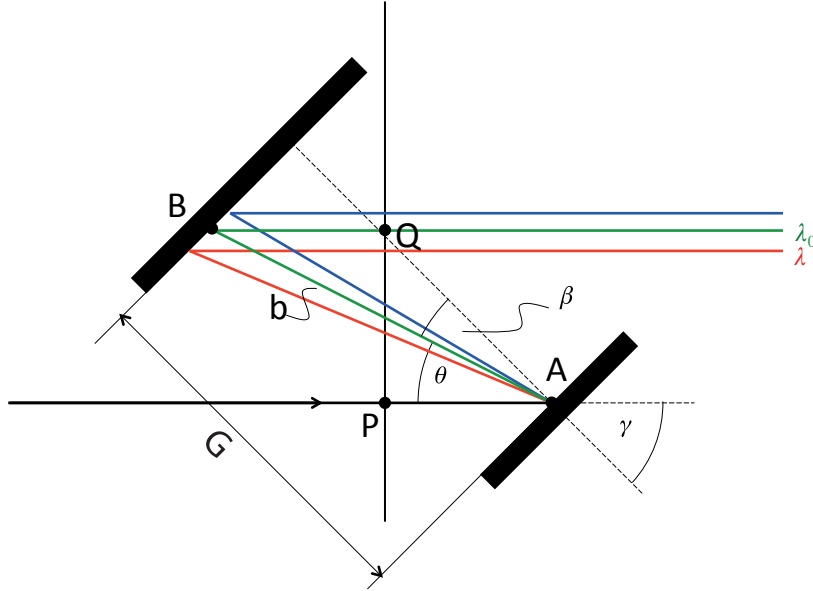
Figure 20: Dispersion via grating.

If G is the perpendicular distance between both gratings (see figure 20), for each color the slant distance $\overline{AB} := b$ is given by $b = \frac{G}{\cos\beta}$. Defining $\theta = \gamma - \beta$, the optical path of each ray along $\overline{PABQ}$ can be expressed as:

$$p = b \cdot (1 + \cos(\theta))$$

The spectral phase $\phi(\omega)$ between point **P** and **Q** is given by:

$$\phi(\omega) = \frac{\omega}{c} \cdot p + R(\omega),$$

Here $R(\omega)$ is a correction taking into account the 2π phase shift that accounts for the phase matching on the grating. For each grating line between the impact of the rays with λ and λ_0 on the second grating, 2π has to be added to the total phase. This can be done by adding to the geometrical phase $\frac{\omega}{c} \cdot p$ a term $R(\omega)$ equalling -2π times the number of lines between point B and the foot of the normal from A to the second grating:

$$R(\omega) = G \tan\beta \cdot \frac{2\pi}{d}$$

Here, $d = N^{-1}$ is the groove spacing in the same units as G.

In order to avoid spatial separation of the different frequencies after the second grating, commonly an end mirror (flat or rooftop) is placed after the second grating that back-reflects all rays for a second pass. This also has the advantage of doubling the dispersion of the setup.

In summary, we obtain for the phase after 4 reflections:

$$\varphi(\omega) = 2 \cdot \left(\frac{\omega}{c}p - \frac{2\pi G}{d}\tan\beta \right) = 2G \cdot \left(\frac{\omega}{c}\frac{1 + \cos\theta}{\cos\beta} - \frac{2\pi}{d}\tan\beta \right)$$

Hence, the phase and all dispersion coefficients scale linearly with G.

The group delay is the first derivative of $\varphi(\omega)$ with respect to ω,

$$GD = \frac{d\varphi(\omega)}{d\omega} = 2 \cdot \left(\frac{p}{c} + \frac{\omega}{c}\frac{dp}{d\omega} - \frac{2\pi G}{d}\frac{d\tan\beta}{d\omega} \right) = 2 \cdot \frac{p}{c}$$

since it can be shown that the 2nd and 3rd term are equal. This means that the groove correction, necessary for computing the phase, cancels out for all derivatives of the phase, and the group delay is indeed only given by the optical path difference of rays with different frequency divided by the speed of light.

Finding the dispersion coefficients to order n is best done numerically. In order to avoid artifacts from differentiating a piecewise linear dispersion curve as obtained by evaluating $GD(\omega)$ or discrete frequency values, it is advisable to perform a polynomial fit of $\varphi(\omega)$ of order n, and then differentiating that polynomial n times. Evaluating the nth derivative polynomial at ω_0 yields D_n.

Alternative description

Using simple geometrical relations, it can be shown that

$$b = a \cdot \sin\alpha \quad \text{and} \quad d = \frac{D_0}{\cos\beta} = D \cdot \frac{\cos\beta_0}{\cos\beta},$$

$$D = \quad \text{distance between gratings along } \lambda_0$$

$$R(\lambda) = \quad \text{phase jump between the intersection points of } \lambda \text{ and } \lambda_0 :$$

$$R(\lambda) = 2\pi \cdot a \cdot N$$

$$\Rightarrow \varphi(\lambda) = \frac{2\pi}{\lambda} \cdot (b + d) - 2\pi \cdot a \cdot N = \frac{2\pi}{\lambda} \cdot D \cdot \cos(\beta_0 - \beta(\lambda))$$

Or in terms of frequency:

$$\varphi(\omega) = \frac{\omega}{c} \cdot D \cdot \cos(\beta_0 - \beta(\omega))$$
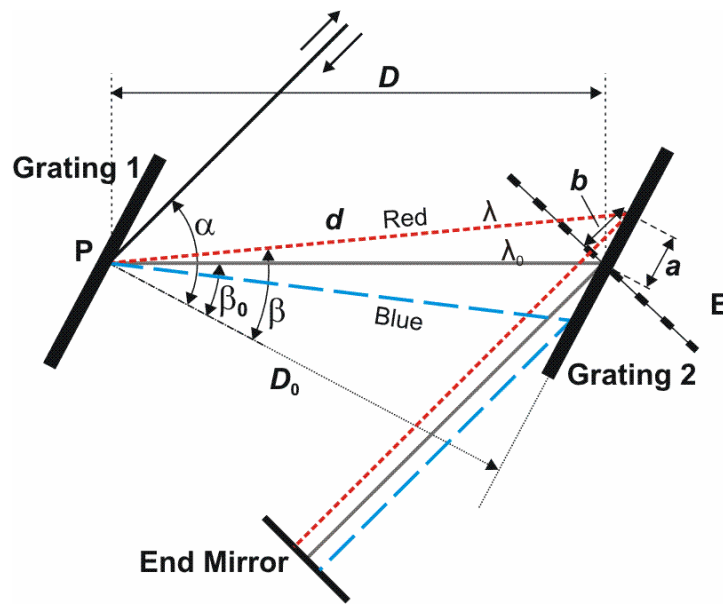
Figure 21: Grating compressor.
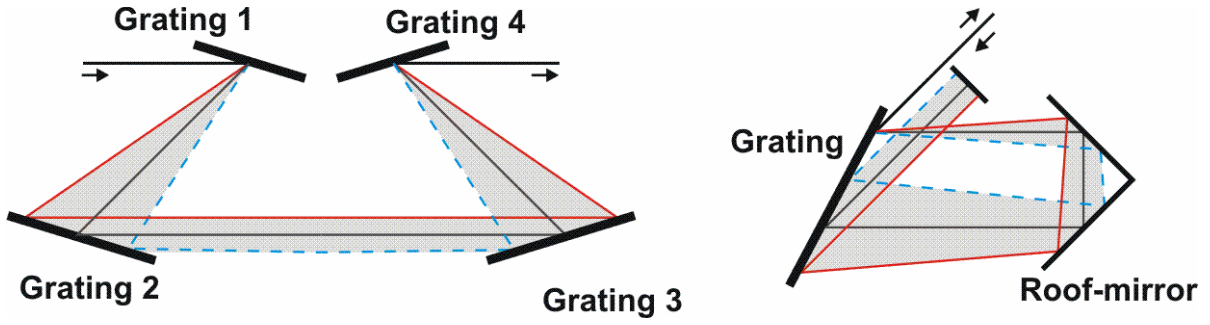
Figure 22: Types of grating compressor: Left 4-grating compressor, right 1-grating compressor

Dispersion Coefficients:

$$D_m = \left(\frac{\partial^m}{\partial \omega^m} \varphi(\omega) \right)_{\omega_0}$$

using $\quad \dfrac{d\beta(\omega)}{d\omega} = -\dfrac{2\pi \cdot c \cdot N}{\omega^2 \cdot \cos\beta}, \quad$ we have

$$D_1 = \quad 2 \cdot \frac{D}{c}$$

$$D_2 = -2 \cdot \frac{D}{c} \cdot \frac{\lambda}{2\pi \cdot c} \cdot \left(\frac{\lambda \cdot N}{\cos\beta_0} \right)^2$$

$$D_3 = -3 \cdot D_2 \cdot \frac{\lambda}{2\pi \cdot c} \cdot \left[1 + \frac{\lambda \cdot N \cdot \sin\beta_0}{cos^2\beta_0} \right]$$

$$D_4 = \quad 3 \cdot D_2 \cdot \left(\frac{\lambda}{2\pi \cdot c} \right)^2 \cdot \left[4 \cdot \left(1 + \frac{\lambda \cdot N \cdot \sin\beta_0}{cos^2\beta_0} \right)^2 + \left(\frac{\lambda \cdot N}{cos^2\beta_0} \right)^2 \right]$$
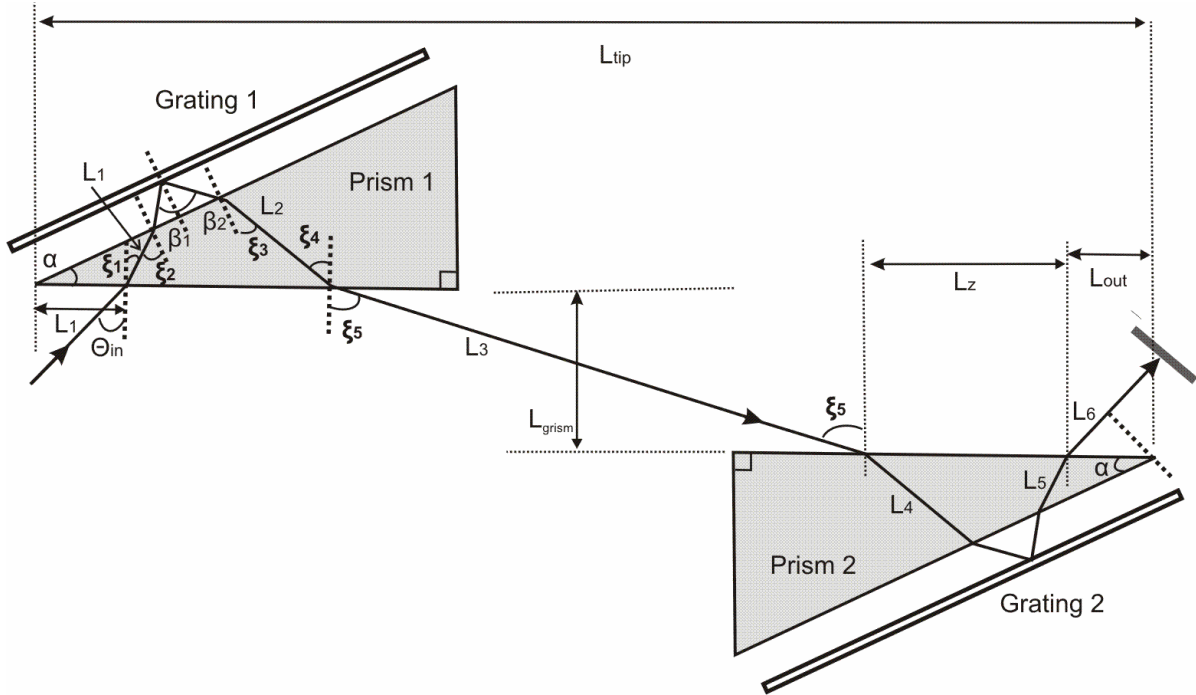
Figure 23: Grism compressor

2.7 Grism compressor

- combination of grating and prism

- more number of degrees of freedom for dispersion management, e.g., prism material, apex angle, angle of incidence, grooves density of grating

- GDD and TOD are of same sign → use bulk material as compressor (simple setup, high throughput)

- free from spherical aberrations

- limitation → uncompensated FOD

The ray path length in the grism stretcher is given by L1-L6 and are calculated by ray-tracing calculations assuming grating –prism separation ≈ 0

$$\varphi(\omega) = 2 \left[(L_3 + L_6) \frac{\omega}{c} + n(\omega) \cdot (L_1 + L_2 + L_4 + L_5) \frac{\omega}{c} + R(\omega) \right]$$

$R(\omega)$ = correction term due to the phase-shift stemming from different phase-matching along two points on the grating surface.

$$R(\omega) = -2\pi N L_\omega = -2\pi N \left[(L_2 + L_4) \sin \xi_3 + L_3 \sin (\xi_5 - \alpha) \right]$$

- N = groove density of the grating

- $L\omega$= distance between the normal on grating 2 (drawn from the point of incidence of the beam on grating 1) and the point of incidence of the wavelength-dependent beam on grating 2.

The coefficients of dispersion are then given by:

$$D_2 = \left.\frac{\partial^2 \phi(\omega)}{\partial \omega^2}\right|_{\omega_0} \quad \& \quad D_3 = \left.\frac{\partial^3 \phi(\omega)}{\partial \omega^3}\right|_{\omega_0}$$

Now using Snell's law and simple geometrical relations,

$$\xi_1 = \arcsin \frac{\sin \theta_{in}}{n}, \; \xi_2 = \xi_1 + \alpha$$

Using grating equation $\frac{m\lambda}{d} = \sin \beta_1 + \sin \beta_2$, where $d = \frac{1}{N} \& m = 1$ and applying Snell's law for angle β_1, we have $\xi_3 = \arcsin \left[\frac{\lambda N}{n} - \sin \xi_2 \right]$.

Similarly,
$\xi_4 = \xi_3 + \alpha$, and $\xi_5 = \arcsin (n \cdot \sin \xi_4)$

The distances L_1-L_6 can be calculated as follows

$$L_1 = L_{in} \frac{\sin \alpha}{\cos (\alpha + \xi_1)}, \quad L_2 = L_1 \frac{\cos \xi_1}{\cos \xi_4}, \quad L_3 = \frac{L_{grism}}{\cos \xi_5}, \quad L_4 = L_z \frac{\sin \alpha}{\cos \xi_4}$$

$$L_z = L_{tip} - L_1 \sin \xi_1 - L_2 \sin \xi_4 - L_3 \sin \xi_5 - L_{in}$$

$$L_5 = L_4 \frac{\cos \xi_4}{\cos \xi_1}, \quad L_{out} = L_5 \frac{\cos \xi_2}{\sin \alpha}, \quad L_6 = L_{out} \sin \theta_{in}$$

2.8 Grating Stretcher

- identical gratings with anti parallel arrangement

- identical angle of incidence both in the stretcher & compressor

- exact inverse-imaging using 1:1 telescope between the gratings

- offset of the gratings from the focal planes of the telescope determines the dispersion and hence required separation of grating compressor$\rightarrow$ distance of the virtual image of grating 2 from grating 1.

Features:

- Longer wavelengths travel shorter optical path, and the shorter wavelengths travel longer path.
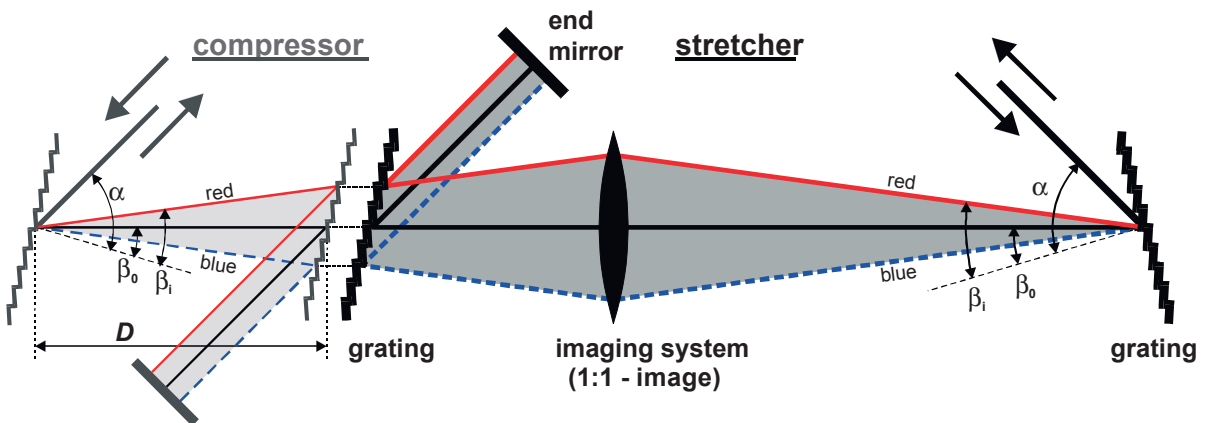
Figure 24: Grating stretcher-compressor system. Exact compensation of spectral phase

- Equal optical path length of all spectral components in stretcher + compressor → exact compensation of higher order dispersion. Material dispersion of laser chain is not compensated, but has to be minimized by deviating from exact stretcher-compressor match.

Different types of grating stretchers:

(a) Grating stretcher with Lens
Real: folded configuration ⇒ only one lens and one grating
⇒ Distance (Lens – folding mirror) = f

Equivalent to the absolute dispersion of grating-compressor with separation D if the distance grating – lens = f – D/2
Lens has to be achromatic!
Fine adjustment of TOD (D_3) by tuning angle and separation.

(b) Grating-stretcher with spherical mirror

Spherical mirror instead of lens
⇒ no additional pass through the material
Disadvantage: Spherical aberrations ⇒ small angles of incidence ⇒ large focal length mirrors and low-frequency grating for a given dispersion.

Alternative: parabolic mirror

(c) Öffner-stretcher

1:1- image with Öffner-telescope (low aberrations: near on-axis imaging) R_2 (convex mirror)= 2 x R_1 (concave mirror), concentric arrangement

Advantage: good correction of spherical abberations Disadvantage: large diameter mirror required (expensive!)

(d) Aberration-free stretcher

2 Gratings, 1 mirror: First grating in ROC of spherical mirror, 2nd grating at focus of mirror ($f=R/2$). Advantage: On-axis image for all colors Disadvantage: 2 Gratings have to be exactly aligned, 2nd Grating at focus only for central wavelength $\Rightarrow$ Spherochromatism!

Remedy: Choose input beam diameter small enough to keep Rayleigh length in focused beam longer than focus distance, choose input angle such that central wavelength is diffracted near grating normal.
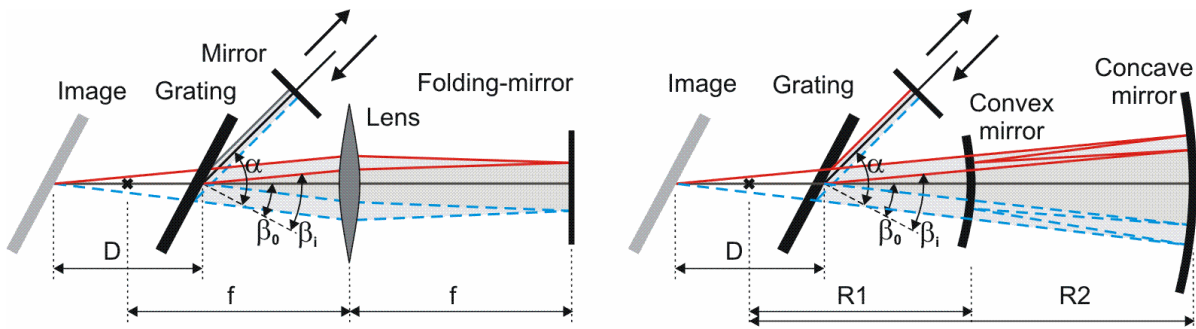
Figure 25: Examples of grating stretcher: (a) Lens stretcher (b) Öffner-stretcher.

Up to now, we represented the laser with a pencil beam, where sphärochromatism is not an issue. However, for extended beams we have to take into account the collimation of each color. In general, only 4-f telecopes provide proper collimation for all colors for a collimated input beam. Single lens/mirror designs (see Figs. 24, 26) frequently lead to different focus positions/divergences for different colors unless designed and installed properly. In general, the input waist has to be chosen such that the imaging element collimates all colors on the way to the second grating/end mirror. Of course the aberration-free design can be modified by using an Öffner telescope to produce and aberration-free Öffner stretcher that produces a collimated output beam for all colors provided the input is collimated.

2.9 Conclusions for system design

As discussed above for the example of a grating stretcher as the perfect conjugate of a grating compressor, for a matched stretcher/compressor pair (i.e. prism/prism,
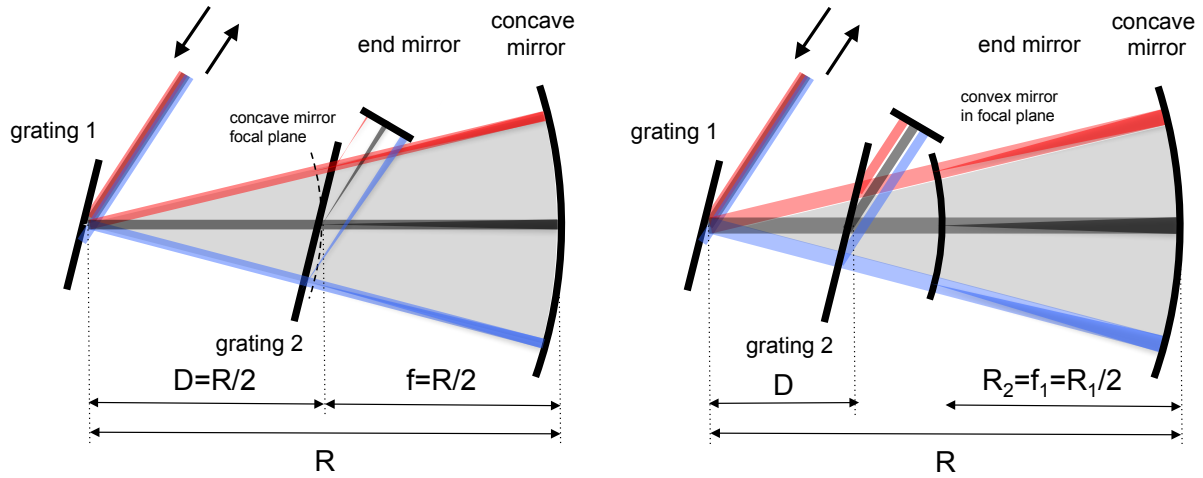
Figure 26: Aberration-free stretcher. Left: Single-mirror non-collimating design. For collimated input beams, the difference in focus distance is evident. In order to avoid spherochromatism, the input beam has to have a waist at the mirror's focal plane. Right: Oeffner design for collimated input beams. Note that the virtual grating separation equals the physical grating separation.
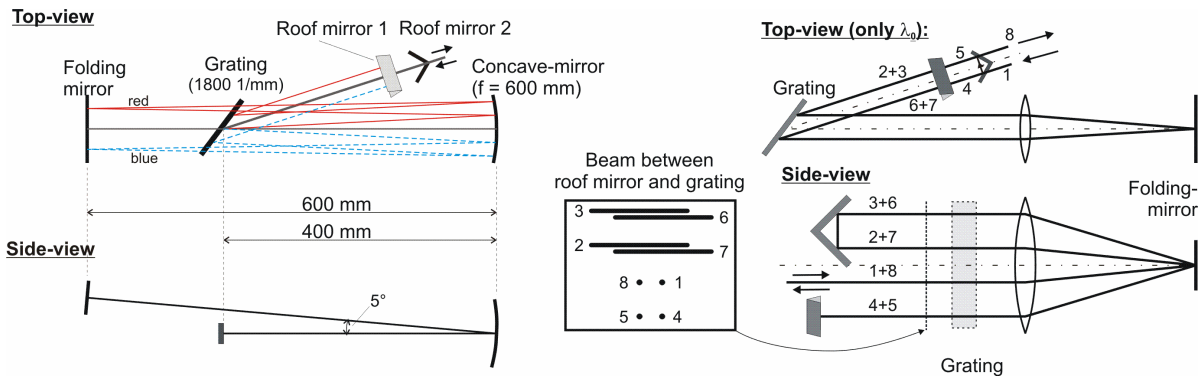
Figure 27: Single-grating stretcher with spherical mirror, real design; left: optical construction, Right: schematics of beam path.

grism/grism, grating/grating) the system dispersion can be made to vanish exactly. However, as soon as additional material in the system has to be accounted for, this is not possible anymore, since for any material there exists no perfect "conjugate material". This basic dilemma can be seen in the following table, where the signs of the 2nd to 4th order dispersion of materials and various compressor setups are listed. With the exception of a few materials with positive FOD, where a properly designed prism compressor might work up to forth order, all other compressors do not allow even to achieve the correct sign. Therefore, a broadband system design may involve any combination of stretchers and compressors of different type, sometimes even chirped mirrors

Order		Material	Prism	Grism	Grating
GDD		+	-	-	-
TOD		+	-	-/+	+
FOD		-(+)	-	-	-

Figure 28: Signs of dispersion components for material (as a stretcher) and prism/grism/grating based compressors.

designed to correct higher orders or even a programmable dispersive element (spatial light modulator (SLM) or acousto-optic programmable dispersive filter (AOPDF), i.e. DAZZLER).

2.10 Alignment of stretcher-compressor systems

The goal of stretcher-compressor systems is to achieve full recompression of the laser pulses after amplification, i.e. a spectral phase difference of zero across the whole amplified spectrum. For a system consisting of

> only stretcher and compressor:
>
> > $\Rightarrow$ this is theoretically feasible; depending only on the (stretcher)design and alignment
>
> additional dispersive material (i.e. laser components, air):
>
> > $\Rightarrow$ compensation of D_2 and D_3 is always possible by varying the incidence angle α and the grating separation D in the compressor.
> >
> > $\Rightarrow$ compensation of higher orders D_m: only via integrated design taking into account all system components.
> > (i.e. deviation from exact conjugate design of stretcher and compressor)

However, even in a perfectly designed system, adjustment errors can severely compromise the performance. A very common error and its implications will be discussed below:

Non-parallel compressor gratings (-prisms/-grisms): spatially varying pulse duration?

Extended beam (dimension x), varying grating separation $D = D(x)$:

$$D(x) = D(x_0) + \frac{(x - x_0) \cdot \varepsilon_x}{\cos \alpha \cdot \ \cos \beta_0}$$

> $\Rightarrow$ Even with perfect compensation of the chirp in the centre of the beam ($x = x_0$) off-axis ($x \neq x_0$) parts are not fully compressed
>
> $\Rightarrow$ spatially varying pulse duration
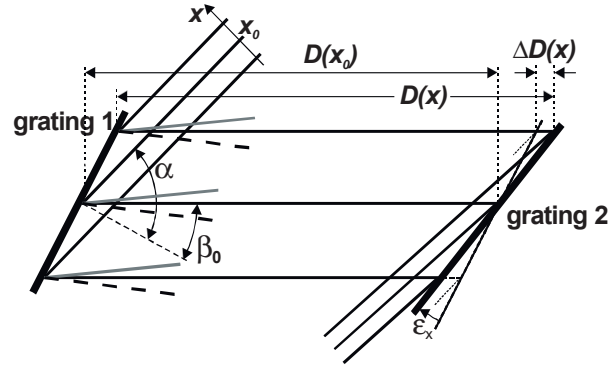
Figure 29: grating pair, non-parallel by angle ϵ_x
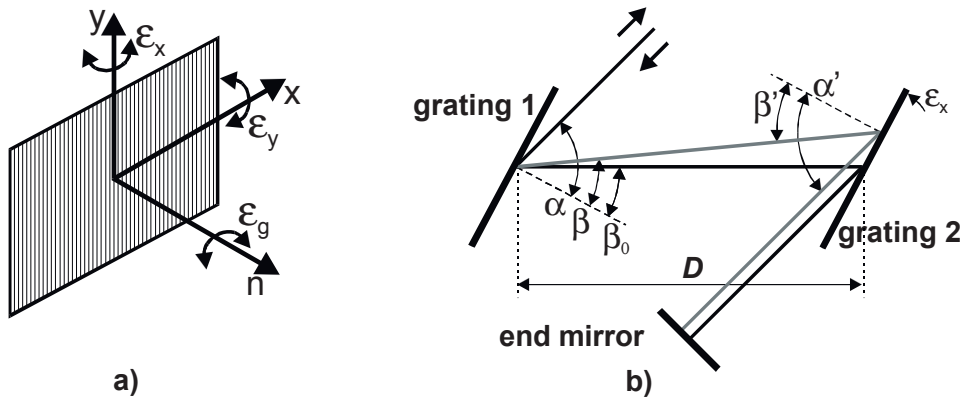
Figure 30: (a) definition of tilt axes of a reflection grating (b) angles in compressor with not fully parallel gratings

Assume tilt in drawing plane (by angle ϵ_x , see 30):

double reflected beam does not hit the end mirror parallel to the incident beam, but tilted by

$$\delta_x(\lambda) \; = \; (\alpha \; - \; \alpha') \; \approx \; \varepsilon_x \cdot \frac{\cos\beta(\lambda)}{\cos\alpha}$$

$\Rightarrow$ angular chirp (quantifies the different directions of the spectral components):

$$C_{a,x} \;\; = \;\; 2 \cdot \left|\frac{\mathrm{d}\delta_x}{\mathrm{d}\lambda}\right|_{\lambda=\lambda_0} \;\; = \;\; 2N \cdot \left|\varepsilon_x \; \cdot \frac{\tan\beta_0}{\cos\alpha}\right|_{\lambda=\lambda_0}$$

("2" accounts for double pass)

tilt by ϵ_y or ϵ_g around horizontal axes: vertical angular chirp

$$C_{a,y} = \left|\frac{d\,\delta_y}{d\,\lambda}\right|_{\lambda=\lambda_0} = 2N \cdot |\epsilon_y \cdot \tan\beta_0| \qquad \text{or:}$$
$$C_{a,y} = 2N \cdot |\epsilon_g|$$

Stretcher: errors in grating parallelism by alignment errors of imaging telescope:
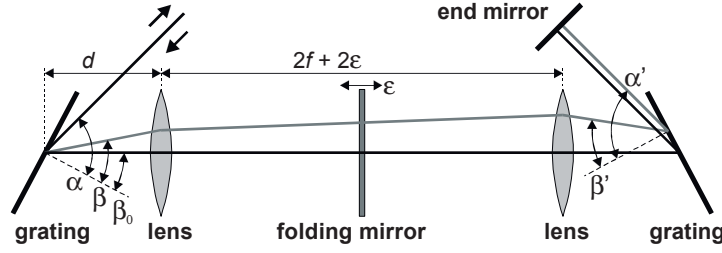
Figure 31: Angles in stretcher with misaligned folding mirror.

$$\beta' \;=\; \beta \;+\; 2\varepsilon \;\cdot\; \frac{f-d}{f^2} \;\cdot\; (\beta - \beta_0)$$

$$\delta_x(\lambda) \;=\; (\alpha - \alpha') \;\approx\; 4\varepsilon \;\cdot\; \frac{f-d}{f^2} \;\cdot\; (\beta - \beta_0) \;\cdot\; \frac{\cos\beta}{\cos\alpha}$$

$$\Rightarrow \text{angle chirp} \quad C_{a,x} \;=\; 2\cdot\left|\frac{\mathrm{d}\delta_x}{\mathrm{d}\lambda}\right|_{\lambda=\lambda_0} \;=\; 4N\cdot\left|\frac{f-d}{f^2} \;\cdot\; \frac{\varepsilon}{\cos\alpha}\right|$$

Effect of an angular chirp in the near field: **pulse front tilt**

Angular deviations $\delta(\lambda])$ of the spectral components lead to a transverse phase difference

$$\Delta\varphi(\lambda,x) \quad\approx\quad \frac{2\pi}{\lambda}\cdot\delta(\lambda)\cdot(x-x_0)$$

and to a transversally varying dispersion component D_1:

$$D_1(x) \;\;(= t_g(x)) \;=\; \left(\frac{\mathrm{d}\varphi(\omega,x)}{\mathrm{d}\omega}\right)_{\omega=\omega_0} \;=\; \frac{\lambda_0}{c}\cdot C_{a,x}\cdot(x_0-x)$$

i.e. the pulse envelope is tilted by α_t with respect to the phase fronts (which are always normal to the propagation direction):

$$\tan\alpha_t \;=\; \frac{t_g(x)\cdot c}{x-x_0} \qquad\Rightarrow\qquad |\alpha_t| \;\approx\; \lambda_0\cdot C_a$$

Alternative description:
If we define g as the frequency dependence of the x-component of the k-vector:

$$g = \frac{dk_x}{d\omega}, \tag{1}$$
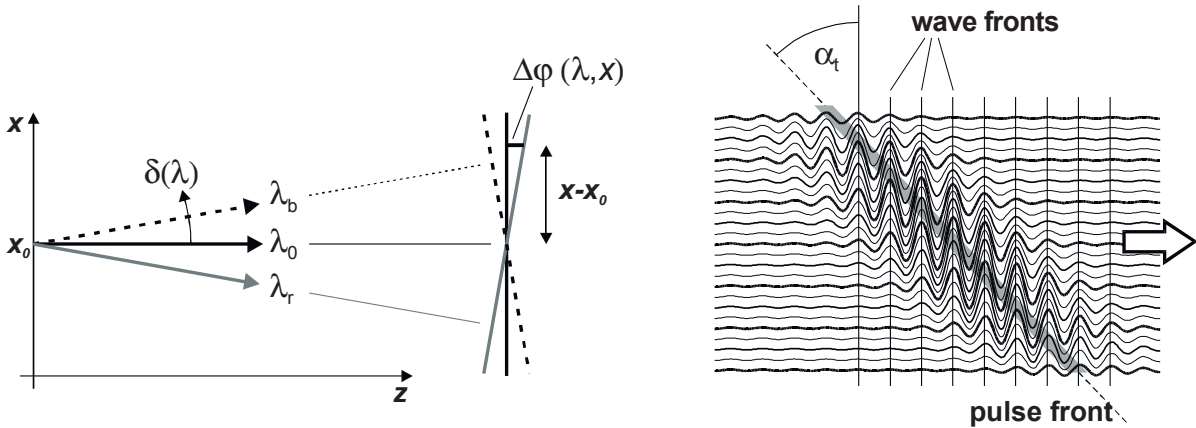
Figure 32: angular chirp: (a) spatially-varying spectral phase leads to (b) a tilt of the pulse front with angle α_t with respect to the wave fronts

then the electric field of the laser pulse is given by:

$$\hat{\tilde{E}}(k_x, \omega) = \qquad\qquad\qquad =\hat{\tilde{E}}_0(k_x + g(\omega - \omega_0), \omega)$$

$$\tilde{E}(x, \omega) = \mathcal{F}^{-1}\hat{\tilde{E}}(k_x, \omega)_{k_x \to x} \qquad =\tilde{E}_0(x, \omega)e^{ig(\omega - \omega_0)x}$$

$$E(x, t) = \mathcal{F}^{-1}\tilde{E}(x, \omega)_{\omega \to t} \qquad =E(x, t + gx)$$

This dual Fourier transform nicely illustrates how a frequency-dependent k-vector (=direction) turns into a tilted pulse front.

In the near-field this pulse front tilt has no easily discernible effects:

- Local pulse duration stays short

- Spatial beam profile stays unchanged in first approximation

- Wave fronts and propagation properties stay largely unchanged

In the far field (= focus), it leads to a strong reduction of focused intensity:

Assumptions:

- temporally/ spectrally gaussian pulse: $\xi_\lambda = \Delta\lambda/\sqrt{2 \cdot \ln 2}$

- spatially gaussian profile: $w_1 = d_{FWHM}/\sqrt{2 \cdot \ln 2}$

- angular chirp $C_{a,x}$ in x-dimension

Consequence:

in the focus every spectral component gets focussed to a spot of size

$$w_0 = \frac{\lambda \cdot f}{\pi \cdot w_1} \qquad \text{but every component is laterally offset by}$$

$$\Delta x = f \cdot \left(\frac{\mathrm{d}\delta_x}{\mathrm{d}\lambda} \cdot \Delta\lambda \right) = f \cdot C_{a,x} \cdot (\lambda - \lambda_0)$$
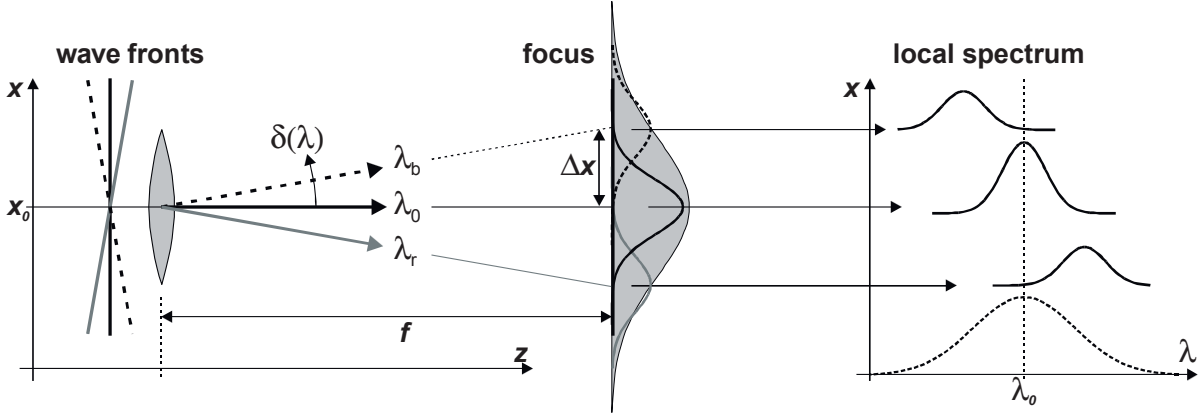
Figure 33: Effect of an angular chirp in the focus: (a) spectral components are focussed next to each other $\Rightarrow$ extension of focal spot area (b) at each point in focus the spectrum is narrower than the overall spectrum (dashed line) $\Rightarrow$ local lengthening of the pulse

(a) intensity distribution in focus:

$$I(x,\lambda) \propto \exp\left(-2 \cdot \left[\tfrac{\lambda-\lambda_0}{\xi_\lambda} \right]^2 \right) \cdot \exp\left(-2 \cdot \left[\tfrac{x - f \cdot C_{a,x} \cdot (\lambda-\lambda_0)}{w_0} \right]^2 \right)$$

$\Rightarrow$ in the center (x = 0) this leads to a spectral distribution

$$I(\lambda) \propto exp\left(-2 \cdot \left[\tfrac{\lambda-\lambda_0}{\xi_\lambda} \cdot \sqrt{1 - \left(\tfrac{C_{a,x} \cdot f \cdot \xi_\lambda}{w_0} \right)^2} \right]^2 \right)$$

$\Rightarrow$ under the assumption that the time-bandwidth-product $\Delta\tau \cdot \Delta\lambda$ is unchanged, this results in a pulse elongation in focus of

$$\xi \quad = \quad \frac{\Delta\tau}{\Delta\tau_0} \quad = \quad \sqrt{1 + \left(\tfrac{C_{a,x} \cdot f \cdot \xi_\lambda}{w_0} \right)^2} \quad = \quad \sqrt{1 + \left(C_{a,x} \cdot \tfrac{\pi}{2 \cdot \ln 2} \cdot \tfrac{\Delta\lambda}{\lambda_0} \cdot d_{FWHM} \right)^2}$$

(b) energy deposition at each point x:

$$E(x) \propto \int\limits_{-\infty}^{\infty} \exp\left(-2 \cdot \left(\left[\tfrac{\lambda-\lambda_0}{\xi_\lambda} \right]^2 + \left[\tfrac{x - C_{a,x} \cdot f \cdot (\lambda-\lambda_0)}{w_0} \right]^2 \right) \right) \mathrm{d}\,(\lambda - \lambda_0) = \exp\left(-2 \cdot \left[\tfrac{x}{w_0 \cdot \xi} \right]^2 \right)$$

$\Rightarrow$ Enlargement of focal area by a factor ξ.

In summary: An angular chirp C_a causes an intensity reduction in focus by a factor

$$I \quad = \quad \frac{I_0}{\xi^2}, \qquad \xi^2 = 1 + \left(\frac{C_a \cdot f \cdot \xi_\lambda}{w_0}\right)^2$$

3 Generation of ultrashort pulses

3.1 Optical resonator

(a) Longitudinal mode structure
Resonance condition:

$$\frac{2L}{\lambda} = \frac{2L \cdot \nu}{c} \overset{!}{=} n$$

$$\Rightarrow \Delta\lambda = \frac{\lambda^2}{2L}{}^a$$

$$\Rightarrow \Delta\nu = \frac{c}{2L} = \frac{1}{\tau_r}$$

$\tau_r \ldots$ round trip time

$\Delta\nu ..$ free spectral range

---

^{a}since $\Delta\lambda = \lambda/n$ and $\Delta\nu = \nu/n$
^{a}since $\Delta\lambda = \lambda/n$ and $\Delta\nu = \nu/n$
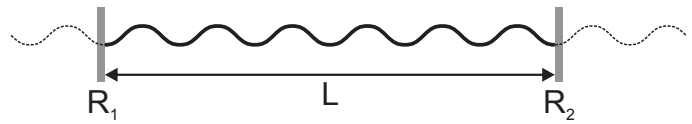
Figure 34: Fabry-Perot-resonator.

Mode width: $\delta\lambda = \dfrac{\Delta\lambda}{F}$

Finesse: $F \approx \dfrac{\pi \cdot \sqrt{r}}{1 - r}$

with $r = \sqrt{R_1 \cdot R_2}$
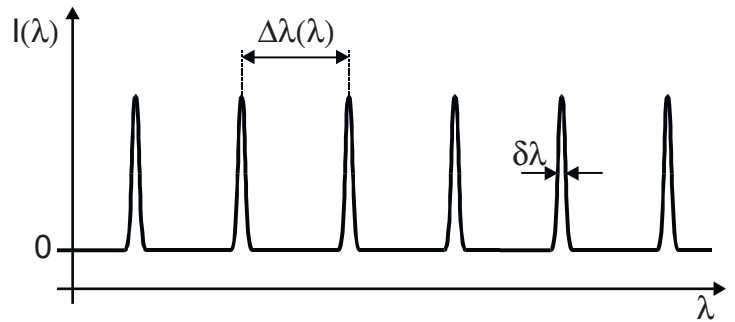
Figure 35: Longitudinal mode structure.

(b) Transverse mode structure
Beam propagation:

at cavity mirror 1: beam profile $I_0(r, \varphi)$
$\Downarrow$
1 round trip (change of beam profile by optical elements and diffraction)
$\Downarrow$
at cavity mirror 1: beam profile $I_1(r, \varphi)$

Resonance condition: $I_0(r, \Phi) = I_n(r, \Phi)$ ($n = 1, 2, \ldots$) can only be fulfilled for special profiles.

$\Rightarrow$ TEM-modes (**T**ransverse **E**lectro-**M**agnetic Modes)

51

Cylindrical coordinates:

$$I_{pl}(r, \Phi, x) = I_0 \cdot \rho^l \cdot (L_p^l(\rho) \cdot \cos(l\Phi))^2 \cdot e^{-\rho}$$

$$\text{with } \rho = 2 \cdot \left(\frac{r(x)}{w(x)} \right)^2$$

$L_p^l \ldots p^{th}$ order Laguerre-polynomial

$$\left(L_0^l = 1, L_1^0 = 1 - \rho, L_2^0 = 1 - 2\rho + \frac{\rho^2}{2} \right)$$

$p \ldots$ number of dark rings

$l \ldots$ number of symmetry axes

$l^* \ldots$ two l-modes (rotated by 90°)
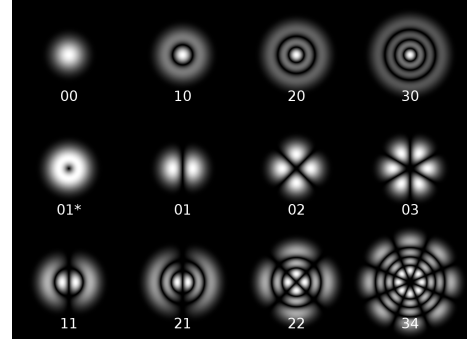
Figure 36: TEM_{pl} ("Laguerre-Gaussian") modes in cylindrical coordinates.

Cartesian coordinates:

$$I_{nm}(x, y, z) = I_0 \cdot \left[H_m \left(\frac{\sqrt{2}y}{w(x)} \right) \cdot e^{\left(\frac{y}{w(x)} \right)^2} \right]^2$$

$$\times \left[H_n \left(\frac{\sqrt{2}z}{w(x)} \right) \cdot e^{\left(\frac{z}{w(x)} \right)^2} \right]^2$$

$H_x(s) \ldots x^{th}$ order Hermite polynomial

$$\left(H_0(s) = 1, H_1(s) = 2s, H_2(s) = 4s^2 - 1 \right)$$
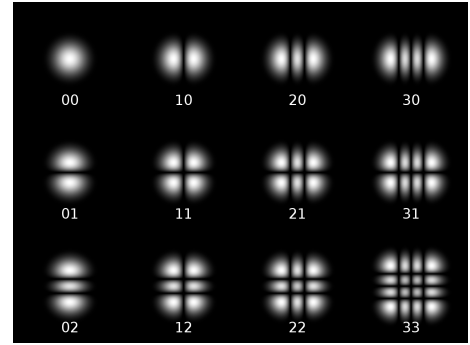
Figure 37: TEM_{nm} ("Hermite-Gaussian") modes in cartesian coordinates.

The actual beam profile is a linear combination of cylindrical or cartesian modes.

(c) Geometry of TEM_{00}-mode:

General description of resonator:

Two spherical cavity mirrors (focusing: $R > 0$, defocusing: $R < 0$)

 Beam radii:
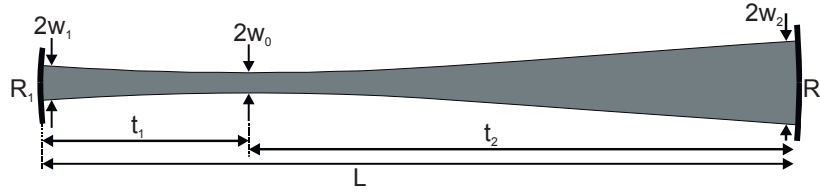
Figure 38: Beam path in resonator (TEM$_{00}$-mode).

$$w_1^4 = \left(\frac{\lambda R_1}{\pi}\right)^2 \cdot \frac{R_2 - L}{R_1 - L} \cdot \frac{L}{R_1 + R_2 - L}$$

$$w_2^4 = \left(\frac{\lambda R_2}{\pi}\right)^2 \cdot \frac{R_1 - L}{R_2 - L} \cdot \frac{L}{R_1 + R_2 - L}$$

$$w_0^4 = \left(\frac{\lambda}{\pi}\right)^2 \cdot \frac{L \cdot (R_1 - L)(R_2 - L)(R_1 + R_2 - L)}{(R_1 + R_2 - 2L)^2}$$

Position of waist:

$$t_1 = \frac{L \cdot (R_2 - L)}{R_1 + R_2 - 2L} \qquad t_2 = \frac{L \cdot (R_1 - L)}{R_1 + R_2 - 2L}$$

(d) Resonator stability: ("stable" means: TEM$_{00}$-mode can develop)
stability condition:

$$0 \leq \left(1 - \frac{L}{R_1}\right) \cdot \left(1 - \frac{L}{R_2}\right) \leq 1 \quad \text{with} \quad g_i = \left(1 - \frac{L}{R_i}\right)$$

$$0 \leq g_1 \cdot g_2 \leq 1$$

$R_i = L/2$	$g_i = -1.0$ (concentric)
$R_i = 2L/3$	$g_i = -0.5$
$R_i = L$	$g_i = 0.0$ (confocal)
$R_i = 2L$	$g_i = 0.5$
$R_i = \infty$	$g_i = 1.0$ (plane)
$R_i = -2L$	$g_i = 1.5$ (convex)
$R_i = -L$	$g_i = 2.0$
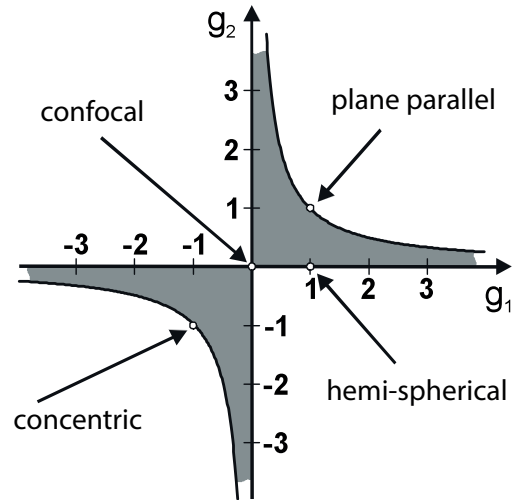
Figure 39: Stability range; gray area = stable

Example: resonator with two identical mirrors ($R_1 = R_2 = R$):

- stable for $0 < g^2 < 1 \Rightarrow |g| < 1 \Rightarrow L/2 < R < \infty$

- beam radius at the mirrors $(w_{1,2})^2 = \frac{\lambda R}{\pi} \cdot \sqrt{\frac{L}{2R-L}}$

- beam radius at waist position $(w_0)^2 = \frac{\lambda}{2\pi} \cdot \sqrt{L \cdot (2R - L)}$

3.2 The inverted medium

(a) basics

population:
N_i as absolute numbers or densities $[\mathrm{m}^{-3}]$
2-level-system:

$$E_2 - E_1 = h\nu_0$$

Boltzmann-distribution:

$$N_2 = N_1 \cdot \frac{g_2}{g_1} \cdot e^{-\frac{E_2 - E_1}{kT}}$$

g_i : degeneracy.
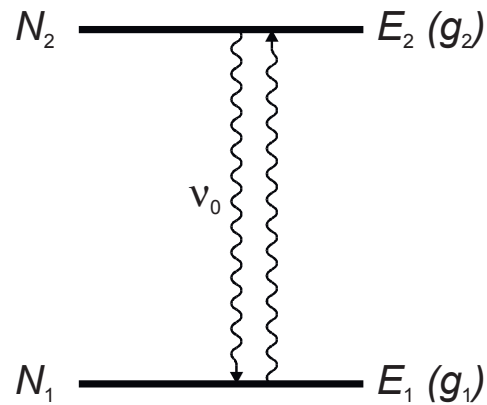
Figure 40: Two-level-system.

(b) Interaction of a radiation field with a two-level-system:
1. spontaneous processes:

spontaneous emission: $\left(\dfrac{\mathrm{d}N_2}{\mathrm{d}t}\right)_{se} = -A \cdot N_2$

radiationless: $\left(\dfrac{\mathrm{d}N_2}{\mathrm{d}t}\right)_{rl} = -\dfrac{N_2}{\tau_{rl}}$

total: $\left(\dfrac{\mathrm{d}N_2}{\mathrm{d}t}\right)_{sp} = -\dfrac{N_2}{\tau}$

$A[\mathrm{s}^{-1}]$ spontaneous emission rate
("Einstein A")

$\tau_r = 1/A$ radiative life time (depends only on the transition)

τ_{rl} radiationless life time (may depend on external conditions, i.e. collisions)

$\tau = 1/(\frac{1}{\tau_r} + \frac{1}{\tau_{rl}})$ spontaneous lifetime

2. Induced (stimulated) emission in external light field:

$$\left(\frac{dN_2}{dt}\right)_i = -W_{21} \cdot N_2 \quad W_{21}[\text{s}^{-1}] \text{ stimulated emission rate}$$

Alternative notations:

$$W_{21} = B_{21} \cdot \rho_{\nu_0} \qquad \begin{array}{ll} B_{21} & [\text{ m}^3/(\text{s}^2\text{J})] \\ \rho_{\nu_0} & [\text{J}/(\text{m}^3/(1/\text{s}))] \end{array} \qquad \begin{array}{r} \text{Einstein B-coefficient} \\ \text{spectral energy density} \end{array}$$

$$W_{21} = \sigma_{21} \cdot \Phi \qquad \begin{array}{ll} \sigma_{21} & [\text{m}^2] \\ \Phi = I/h\nu & [\text{photons}/(\text{m}^2\text{s})] \end{array} \qquad \begin{array}{r} \text{cross-section for induced emission} \\ \text{photon flux density} \end{array}$$

3. Absorption of light

$$\left(\frac{dN_1}{dt}\right)_a = -W_{12} \cdot N_1, \quad W_{12}[\text{s}^{-1}] \quad \text{absorption rate}$$

$$W_{12} = B_{12} \cdot \rho_{\nu_0} \quad \text{or}$$

$$W_{12} = \sigma_{12} \cdot \Phi$$

Dependence of stimulated and absorption quantitites:

$$g_2 \cdot \left\{ \begin{array}{c} W_{21} \\ \sigma_{21} \\ B_{21} \end{array} \right. = g_1 \cdot \left\{ \begin{array}{c} W_{12} \\ \sigma_{12} \\ B_{12} \end{array} \right.$$

example:

- weak light field (photon flux φ)
- interacts with 2-level-medium (populations N_1, N_2, thickness dx)
- neglect spontaneous processes and population changes:

$$d\varphi = \left(-\left(\frac{dN_2}{dt}\right)_i + \left(\frac{dN_1}{dt}\right)_a \right) dx = (W_{21} \cdot N_2 - W_{12} \cdot N_1) \, dx = \sigma_{21} \cdot \Phi \cdot \left(N_2 - \frac{g_2}{g_1} \cdot N_1 \right) dx$$

absorption ($d\varphi < 0$)   for $N_2 < \left(\dfrac{g_2}{g_1}\right) \cdot N_1$ (e.g. Boltzmann distribution)

amplification ($d\Phi > 0$)   for $N_2 > \left(\dfrac{g_2}{g_1}\right) \cdot N_1$

for lasing to occur: inversion

$$\Delta N = \left(N_2 - \frac{g_2}{g_1} N_1 \right) \stackrel{!}{>} 0$$

In a real 2-level system, the stimulated emission scales linearly with the population of the N_2-level, i.e. with the number of absorbed photons. Therefore the stimulated emission grows with the same rate as the absorption, and inversion cannot be reached.

(c) Idealised 3-level-system

Spontaneous life times:
Level 3: short-lived ($\tau \to 0$)
such that always $N_3 \approx 0$

Level 2: long-lived ($\tau \to \infty$)
lasing condition:

$$\Delta N = \left(N_2 - \frac{g_2}{g_1} N_1 \right) \overset{!}{>} 0$$

$\Rightarrow$ Assuming $g_1 = g_2$, more than half of all atoms have to be in N_2!
However: N_2 is not depopulated via induced emission by the pump.
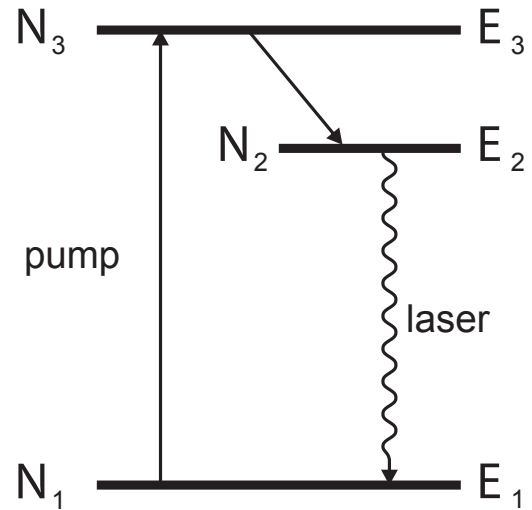
Figure 41: Three-level-system.

(d) The following 3-level system is impossible:

Level 2: short-lived ($\tau \to 0$)
such that always $N_2 \approx 0$
and inversion is achieved after pumping the system.

The pump that fills N_3 immediately depletes N_3, and nothing goes into N_2. Stimulated emission rate $\gg$ spontaneous decay rate! This therefore is a 2-level system!
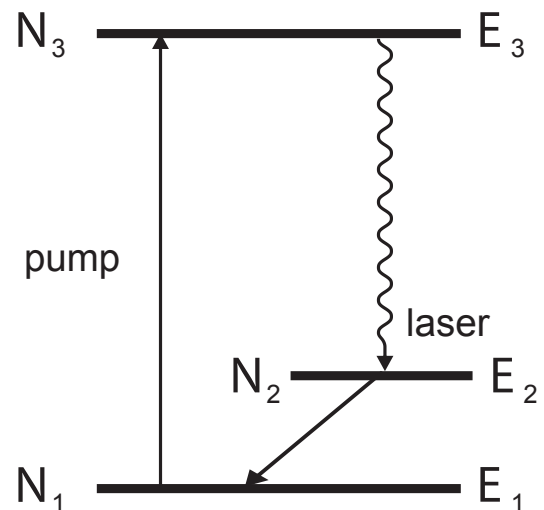
Figure 42: non-functional three-level-system.

(e) idealised 4-level-system
ground state: $N_0 = const$ $(N_0 \gg N_2)$

level 3: short-lived $\tau \to 0$ $(N_3 \approx 0)$
$\Rightarrow$ everything pumped into N_3 immediately
decays to N_2

level 1: short-lived $\tau \to 0$, $(N_1 \approx 0)$
$\Rightarrow$ everything decaying into N_1 (lower laser
level), immediately decays to N_0 (GS)

Lasing condition

$$\Delta N = (N_2 - \frac{g_3}{g_2} N_1) = N_2 > 0$$

$\Rightarrow$ inversion established as soon as medium
is pumped.
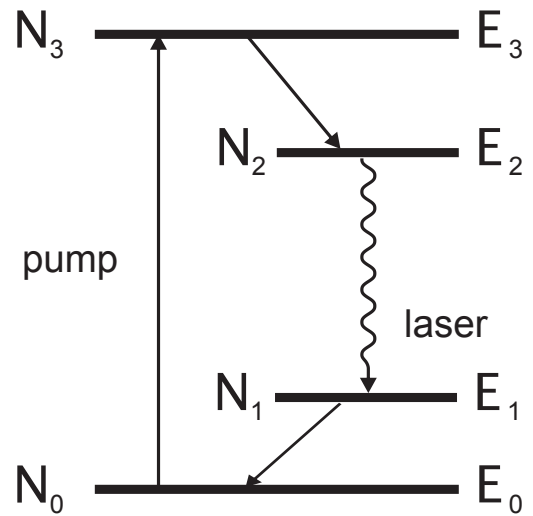
Figure 43: Four-level-system.

3.3 The Laser Resonator

(a) Rate equations:
Description of the temporal behaviour of the inverted medium using rate equations
for

- N_2 (spatial inversion density)
- Ψ (number of photons in resonator)
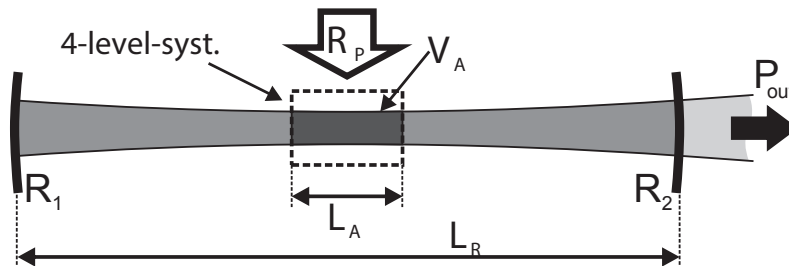
Figure 44: Scheme of laser resonator.

R_P pump rate per volume $[m^{-3}s^{-1}]$

$$\frac{dN_2}{dt} = R_P - K \cdot \Psi \cdot N_2 - \frac{N_2}{\tau}$$

$K = \frac{\sigma_{21} \cdot L_A \cdot c}{V_A \cdot L_R}$

$\tau_C = \frac{1}{\gamma} \cdot \frac{L_R}{c}$ mean cavity life time

$$\frac{d\Psi}{dt} = K \cdot V_A \cdot \Psi \cdot N_2 - \frac{\Psi}{\tau_C}$$

$\gamma = \gamma_i + \frac{\gamma_1 + \gamma_2}{2}$ loss rate per round trip
γ_i: medium; mirror 1&2: $\gamma_{1,2} \approx 1 - R$

(b) Start-up:

$$\Psi_0 \approx 1, \quad \frac{d\Psi}{dt} > 0 \quad \Rightarrow \quad K \cdot V_A \cdot N_2 > \frac{1}{\tau_C}$$

$$N_2 > \frac{\gamma}{\sigma L_A} = N_c \quad \text{critical inversion density}$$

$$\Rightarrow R_{P,c} = \frac{\gamma}{\sigma \cdot L_A \cdot \tau} = \frac{N_c}{\tau} \quad \text{critical pump power}$$

$R_{P,c}$ has to replenish the critical inversion density during τ !

(c) Stationary case:

$$R_p > R_{p,c} \quad \text{and} \quad \frac{d}{dt} = 0 \quad \Rightarrow N_2 = \frac{1}{K \cdot V_A \cdot \tau_C} = N_c$$

$$\Psi = V_A \cdot \tau_C \cdot \left(R_p - \frac{N_c}{\tau} \right) = A \cdot \frac{\gamma}{\sigma_{21}} \cdot \frac{\tau_C}{\tau} \cdot \left(\frac{R_p}{R_{p,c}} - 1 \right) \quad \text{A: beam area}$$

$$\Rightarrow P_{out} = \frac{\gamma_2}{2} \cdot \frac{c}{L_R} \cdot h\nu \cdot \Psi = \frac{\gamma_2}{2} \cdot I_S \cdot A \cdot \left(\frac{R_p}{R_{p,c}} - 1 \right) \quad \left(I_S = \frac{h\nu}{\sigma_{21} \cdot \tau} \text{ Saturation intensity} \right)$$

3.4 Generation of pulsed laser radiation

(a) pulsed pump (e.g. flashlamps):

$$\Delta\tau_{Laser} \approx \Delta\tau_{pump} \quad (\approx 10 - 100\mu s)$$

(b) Q-switch (modulation of cavity Q):

Phase 1: high resonator losses ("shutter closed"), pumped:

$$\frac{dN_2}{dt} = R_p - K \cdot \Psi \cdot N_2 - \frac{N_2}{\tau} \quad \text{with } \Psi = 0$$

$$\Rightarrow N_2(t) = N_\infty \cdot \left(1 - e^{-t/\tau} \right) \quad \text{with } N_\infty = R_p \cdot \tau = N_c \cdot \frac{R_p}{R_{p,c}}$$

<u>Phase 2:</u> low resonator losses ("shutter open"), neglect pump and spontaneous decay:

$$\left.\begin{array}{l} \frac{\mathrm{d}N_2}{\mathrm{d}t} = -K \cdot \Psi \cdot N_2 + \left(R_p - \frac{N_2}{\tau}\right) \\ \frac{\mathrm{d}\Psi}{\mathrm{d}t} = \left(K \cdot V_A \cdot N_2 - \frac{1}{\tau_C}\right) \cdot \Psi \end{array}\right\} \text{divide: } \frac{\mathrm{d}\Psi}{\mathrm{d}N_2} = -V_A \cdot \left(1 - \frac{N_c}{N_2}\right)$$

$$\Rightarrow \Psi = V_A \cdot \left[N_{2,\infty} - N_2 - N_c \cdot \ln\left(\frac{N_{2,\infty}}{N_2}\right)\right]$$

at maximum:

$$\frac{\mathrm{d}\Psi}{\mathrm{d}t} = 0 \quad \Rightarrow \quad N_2 = \frac{1}{K \cdot V_A \cdot \tau_C} = N_c \quad \Rightarrow \quad \text{no excess gain left!}$$

$$\Psi_{max} = V_A \cdot N_c \cdot \left[\frac{N_{2,\infty}}{N_c} - \ln\left(\frac{N_{2,\infty}}{N_c}\right) - 1\right]$$

Inversion accumulates during phase 1 (shutter closed and pump on), and stored energy is released after shutter is opened in phase 2. Typical time-scales are given by either the shutter opening time, or, for switching times faster than a resonator round trip, the round-trip time. For typical resonator lengths of the order of meters, the latter is in the ns-10ns regime. This dictates the shortest pulse duration achievable with external high-contrast switching of the resonator.

(c) Mode-locking
Shorter pulse durations can be achieved by exploiting the Fourier theorem: A short pulse can be thought of as a sum of cosine-functions with different frequencies and a fixed phase relation.
   Sum of many resonator modes:

$$E(t) = \sum_n E_{n,0} \cdot \sin(2\pi \cdot \nu_n t + \varphi_n)$$

Special case:

$$E_{n,0} = E_0, \ \varphi_n = 0$$

$$I(t) \propto I_0 \cdot \left[\frac{\sin(N \cdot \pi \cdot \Delta\nu \cdot \tau)}{\sin(\pi \cdot \Delta\nu \cdot \tau)}\right]^2 \quad \text{with } \Delta\nu = \frac{c}{2L}$$

In the context of a laser resonator this can be achieved by introducing a periodic loss modulation with the resonator eigenfrequency, which allows a single pulse to circulate in the resonator with relatively low losses. The faster the modulation rise/fall times around the pulse, the shorter the pulse can become. Fast modulations are best achieved in an instantaneous nonlinear process triggered by the pulse itself:
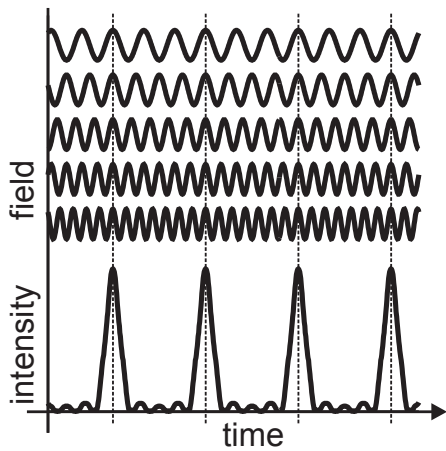
Figure 45: phase-locked superposition of 5 modes
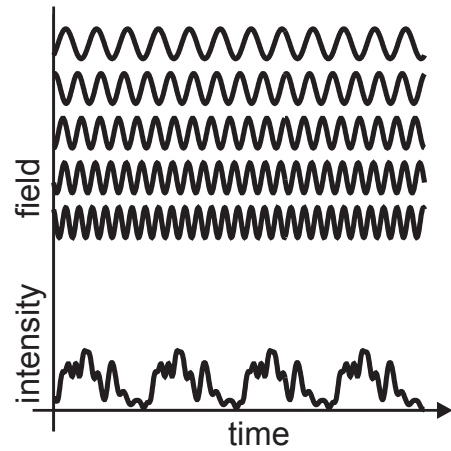
Figure 46: random superposition of 5 modes
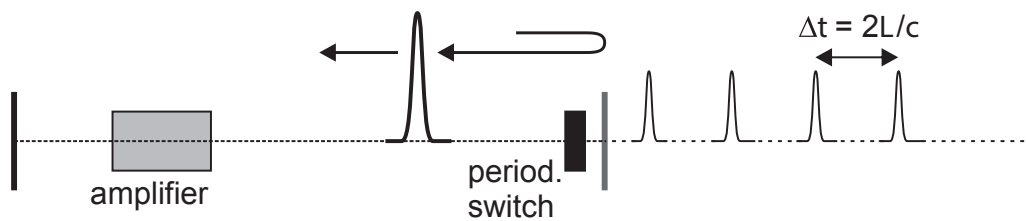
Figure 47: Schematic of mode-locked resonator.

3.5 The KLM-oscillator

(a) KLM (Kerr-lens-modelocking)

   loss modulation by self-focusing ("Kerr-lens") and iris

   $\Rightarrow$ intense light gets focused through the iris and experiences lower losses
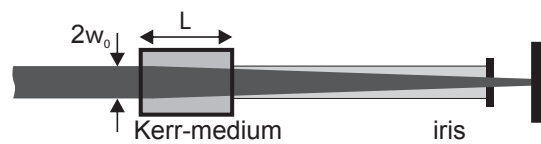
Figure 48: Kerr-lens modelocking: principle

(b) properties:

   • focal length of Kerr-lens:

$$f_{Kerr} \approx \frac{w_0^2}{4n_2 \cdot I_0 \cdot L}$$

- Kerr-lens sensitivity:

$$\delta = \frac{\frac{\mathrm{d}w}{w}}{\frac{\mathrm{d}P}{P_{cr}}} \overset{!}{<} -1 \quad \text{(at position of iris)}$$

- change in transmission:

$$\frac{\mathrm{d}T}{\mathrm{d}w} = -\frac{4R^2}{w^3} \cdot e^{-2\frac{R^2}{w^2}} \quad \text{gaussian beam through an iris with radius } R$$

$$\Rightarrow \text{ for } R \approx w: \quad \mathrm{d}T \approx -\frac{1}{2w} \cdot \mathrm{d}w$$

(c) Realization in an optical resonator:

The most common oscillator design for Kerr-lens mode locking is shown in Fig. 49 It comprises two flat and two spherical mirrors in a Z configuration. The lowest losses are achieved if the wavefront of the stationary mode is exactly flat at the position of the two flat end mirrors. In the absence of a laser medium, this is the case if S_1 and S_2 are close to confocal, and the beam has a waist exactly on l_1 and l_2. Of course, this is only possible of the astigmatism of the spherical mirrors can be compensated. As will be shown later, this is possible by cutting the laser crystal at Brewster's angle. With the crystal in place, everything said before holds true, except that the distance of the mirrors has to be adapted to accommodate for the additional optical path in the crystal in order to become confocal again. Such a resonator (confocal, Brewster-cut crystal to correct for the astigmatism of the off-axis focusing mirrors) exhibits the lowest losses for CW radiation, if the pump spot size matches the focus in the crystal. If the distance of the spherical mirrors is slightly increased to create a small separation δ between their foci in the crystal, the resonator is driven deeper into the stability region, albeit with larger losses. A Kerr lens, however, can bridge the gap between the two foci by keeping the beam small over a distance of δ, effectively restoring the "confocality". Hence, the cavity lengthened by δ has the lowest losses for pulsed radiation.

role of the inverted medium:

- generation of laser radiation

- Kerr lens: high nonlinear refractive index desired
  $\Rightarrow$ focus tightly into crystal

- iris: spatial amplification profile acts as soft aperture:
  $\Rightarrow$ match pump profile to mode profile with active Kerr-lens (and not to CW mode).
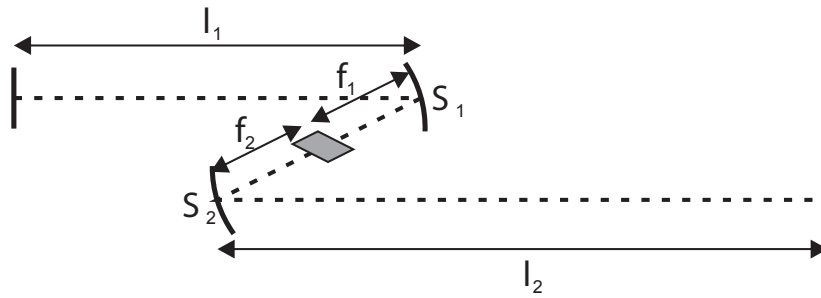
Figure 49: Setup for KLM.
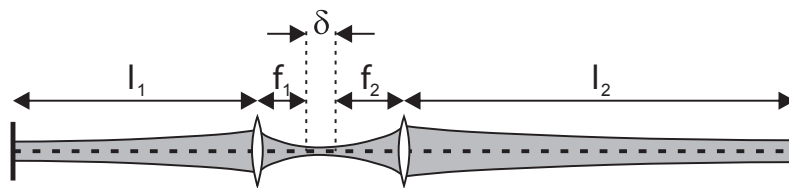
Figure 50: Schematic.

(d) Resonator stability: consider two identical focusing mirrors ($f_1 = f_2 = f$) equivalent two-mirror oscillator (cf. Fig. 50):

$$R_1 = \frac{f^2}{l_1} \quad R_2 = \frac{f^2}{l_2} \quad L = R_1 + R_2 - \delta$$

$$\Rightarrow g_1 = \left(1 - \frac{L}{R_1}\right) = \frac{l_1}{l_2} \cdot \left(\frac{l_2}{f^2} \cdot \delta - 1\right)$$

$$\Rightarrow \text{ stability for}$$

$$0 \le \left(1 - \delta \cdot \frac{l_2}{f^2}\right) \cdot \left(1 - \delta \cdot \frac{l_1}{f^2}\right) \le 1$$

$$\text{analyze } g_1' = \left(1 - \delta \cdot \frac{l_2}{f^2}\right)$$

for $l_1 \ne l_2$ two stability regions exist

(a) $0 \le \delta \le R_1$
(assumption: $l_1 > l_2$
Otherwise: swap indices)

(b) $R_2 \le \delta \le R_1 + R_2$
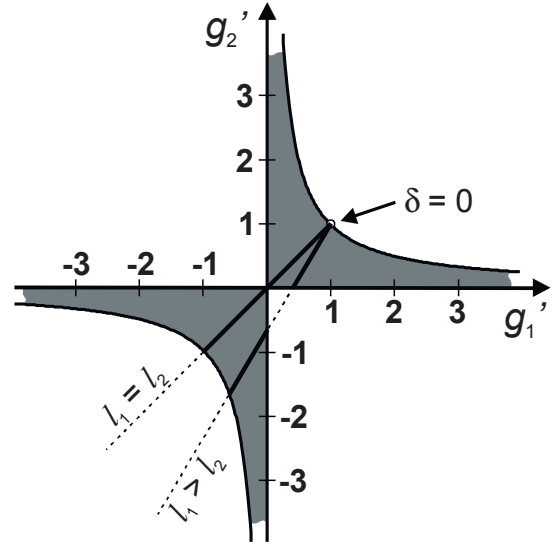
Figure 51: Stability diagram for a KLM-oscillator.

(e) compensation of astigmatism:

focusing with spherical mirror:
astigmatism (see Fig. 52(a)) :
2 focal lines instead of focal spot

Tangential plane:

$$f_T = \frac{R \cdot \cos(\theta)}{2} < \frac{R}{2}$$

Sagittal plane:

$$f_S = \frac{R}{2 \cdot \cos(\theta)} > \frac{R}{2}$$
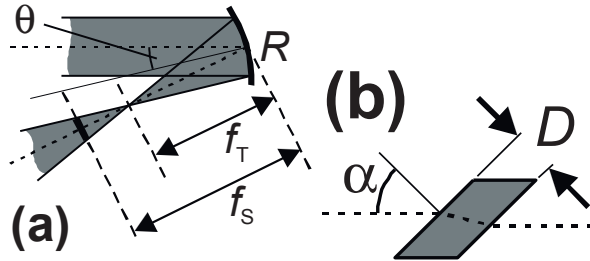
Figure 52: Astigmatism in a KLM-oscillator.

A pass through the crystal (thickness D, refractive index n) at Brewster's angle (Fig. 52 (b)):

$$\tan \alpha = n \quad \text{also leads to astigmatism.}$$

Compensation can be achieved for

$$\frac{(n^2 - 1) \cdot \sqrt{n^2 + 1}}{n^4} \cdot D = R \cdot \sin(\theta) \cdot \tan(\theta)$$

R :   Radius of curvature of both mirrors (assumed equal)

θ angle at both mirrors

D, n Crystal: thickness and refractive index

Substituting N

$$N = \frac{(n^2 - 1) \cdot \sqrt{n^2 + 1}}{n^4} \tag{2}$$

we get

$$\sin\theta \tan\theta = \frac{ND}{R} \tag{3}$$

which leads to a quadratic equation in $\cos\theta$:

$$\cos\theta^2 + \frac{ND}{R}\cos\theta - 1 = 0 \tag{4}$$

This has got the positive solution

$$\theta = \arccos\left[\sqrt{1 + \left(\frac{ND}{2R}\right)^2} - \frac{ND}{2R}\right] \tag{5}$$

(f) Dispersion control:

In order to maintain the phase relation for all modes constituting the pulse, the round-trip time has to be equal for all frequencies within a certain limit. This is given by maximum permissible deviation: $< \pi/2$ over resonator lifetime)

Oscillator material (crystal, air, mirrors) exhibits "positive dispersion" ($D_2 > 0$), typically $D_2 \approx 100 - 500\text{fs}^2$ per round trip.

Compensation by introducing an equal amount of negative dispersion

methods:

- Prism compressor: prism pair in front of one end mirror (see e.g. figure 53)

  Standard solution for pulses with $\Delta\tau \geq 20$ fs

Main problem: dispersion components D_2 and D_3 (almost always) cannot be compensated at the same time for $\lambda_0 = 800$nm (see table p.36). This fact limits the achievable pulse duration.

However: at one end mirror the pulse is spectrally dispersed. This allows to set the central wavelength, bandwidth and pulse duration

- chirped mirrors inside the resonator (e.g. figure 54)

For pulses down to $\Delta\tau \geq 5$fs

D_2 and D_3 can be compensated at the same time: ultra-short pulse durations. Fine-tuning with additional material in the resonator (e.g. two opposed wedges at Brewster's angle)

3.6 Oscillator concepts

Parameters:

- repetition rate: $10 - 120$MHz

- pulse duration: $5 - 150$fs

- pulse energy: $0.1 - 100$nJ

- pulse power: ≤ 1MW

- average power: $0.05 - 10$W

Oscilator configurations:
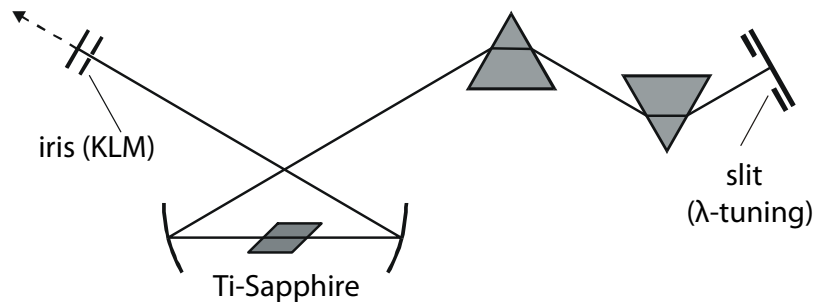
Figure 53: prism-compensated Fabry-Perot oscillator. Pulse duration: $20 - 150$fs, easy tuning of central wavelength
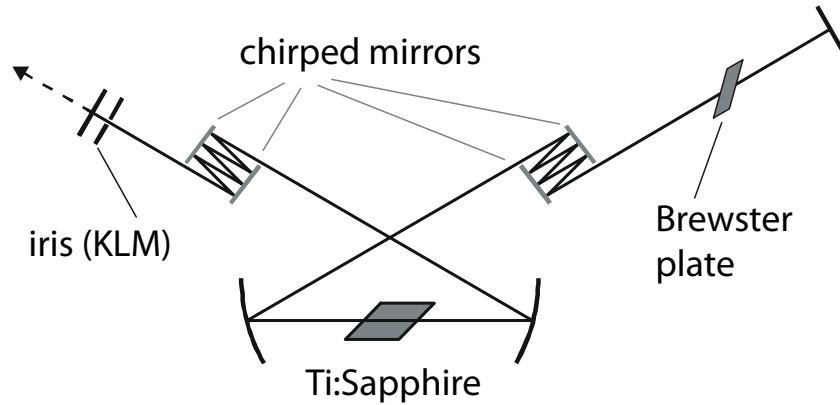
Figure 54: mirror-compensated Fabry-Perot oscillator. Pulse duration: $5 - 50$fs.
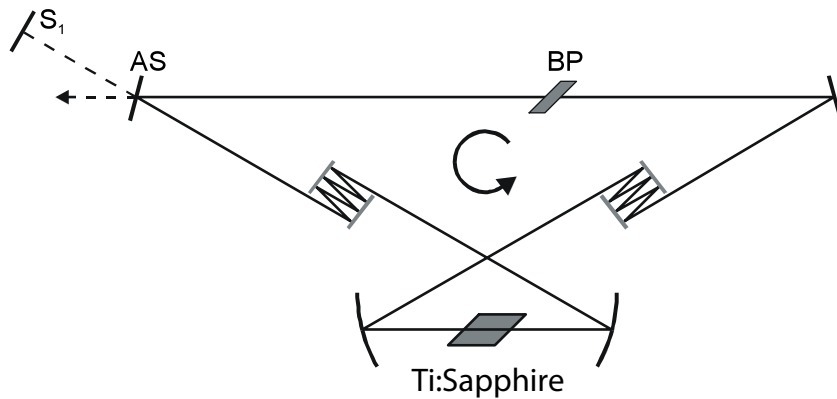
Figure 55: mirror-compensated ring-oscillator. pulse duration: $5 - 50$fs.
advantage: stable against back-reflections from outside the cavity
start-up/CW-operation: Condition: AS-S1-AS-Cr = AS-BP-Cr (back-reflected pulse reduces gain for "wrong" pulse).
ML-operation: mirror S_1 not needed.

4 Amplification of ultrashort pulses

Principle

Generation of an inversion in an active medium. Pass pulse once or more times through medium, until the stored energy is transferred to the pulse.

Comparison	Oscillator	Amplifier
Purpose:	Transfer of CW pump light into quasi-CW laser radiation. Low single pulse energy	Transfer of pump energy to one pulse. Extraction of a large part of the stored energy.
Principle:	equilibrium (gain compensates loss).	extreme nonequilibrium (gain $\gg$ losses).
Pulse forming:	necessary: spatial (mode structure) and spectro- temporal (KLM, dispersion control).	possible: spatial (influences final focusing), spectro-temporal (recompression).
Dispersion control:	with every round trip, always in equilibrium	once after the whole amplification

4.1 Monochromatic pulses

Physical description: semi-classical theory (Schrödinger- and Maxwell-Eqn. for matter and fields lead to Maxwell-Bloch equations. See e.g. Yariv: "Quantum Electronics")

Here: Description by rate equations (similar to oscillator):

(a) Assumption: inverted 4-level-system

Rate equations in lab frame $(\hat{x}, \hat{t})$ for

$\Delta N = N_2$ (inversion density: particles/m³)
Φ (photon density: photons/m³)

$$\frac{\partial \Delta N}{\partial \hat{t}} = R_p - \frac{\Delta N}{\tau} - \Delta N \cdot \Phi \cdot c \cdot \sigma$$

$$\frac{\partial \Phi}{\partial \hat{t}} = \underbrace{\Delta N \cdot \Phi \cdot c \cdot \sigma}_{\text{gain}} - \underbrace{c \cdot \frac{\partial \Phi}{\partial \hat{x}}}_{\text{long. pulse profile}}$$
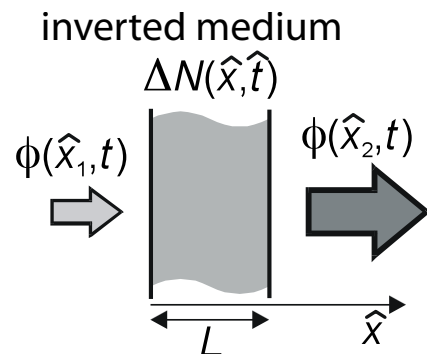
Figure 56: Amplification.

(b) Change to co-moving frame $(\hat{x}, \hat{t}) \rightarrow (x, t)$ with $t = \hat{t} - \hat{x} \cdot c$, $x = \hat{x}$

Intensity [energy/(area $\cdot$ time)] $I = \Phi \cdot h\nu \cdot c$

Neglect pump and spontaneous decay $R_p \approx 0$, $\Delta N / \tau \approx 0$

$$\Rightarrow \frac{\partial \Delta N(x, t)}{\partial t} = -\frac{\sigma}{h\nu} \cdot \Delta N(x, t) \cdot I(x, t) \tag{6}$$

$$\frac{\partial I(x, t)}{\partial x} = \sigma \cdot \Delta N(x, t) \cdot I(x, t) \tag{7}$$

(c) Integrate both equations over whole length L of the medium:
From equation 7

$$I_{out} = I_{in} \cdot G(t)$$
$$\text{with } G(t) = e^{\sigma \cdot n_{tot}(t)} \qquad \text{(amplification of pulse up to time } t\text{)}$$
$$n_{tot}(t) = \int_{x=0}^{x=L} \Delta N(x, t) \mathrm{d}x \qquad \text{(inversion areal density)}$$

Equation 7 into equation 6

$$\Rightarrow \frac{\mathrm{d}n_{tot}(t)}{\mathrm{d}t} = -\frac{I_{out}(t) - I_{in}(t)}{h\nu} \tag{8}$$

$$= -\frac{I_{in}(t)}{h\nu} \cdot \left(e^{\sigma \cdot n_{tot}(t)} - 1\right) = -\frac{I_{out}(t)}{h\nu} \cdot \left(e^{-\sigma \cdot n_{tot}(t)} - 1\right) \tag{9}$$

(d) Definition of integral energy density ("fluence"): (energy/area contained in the pulse before time t)

$$J_{in}(t) = \int_{t_0}^{t} I_{in}(t') \mathrm{d}t' \qquad \text{(at amp. input)}$$

$$J_{out}(t) = \int_{t_0}^{t} I_{out}(t') \mathrm{d}t' \qquad \text{(at amp. output)}$$
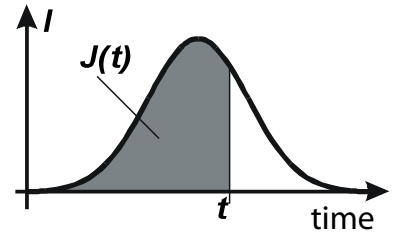
Figure 57: definition of energy density ("fluence") *J(t)*

(e) Definition of saturation fluence J_{sat} :

$$\frac{\partial \Delta N}{\partial t} = -\frac{\sigma}{h\nu} \cdot \Delta N(x,t) \cdot I(x,t) \quad \rightarrow \int_{t_0}^{t} ...\mathrm{d}t'$$

$$\Rightarrow \ln\left(\frac{\Delta N(x,t)}{\Delta N(x,t_0)}\right) = -\frac{J(x,t)}{J_{sat}}$$

$$J_{sat} = \frac{h\nu}{\sigma} \quad \text{saturation fluence}$$

$$J = J_{sat} \Rightarrow \Delta N = \frac{1}{e} \cdot \Delta N(t_0)$$

After the saturation fluence has been extracted, only $1/e$ of the original inversion is still present.

(f) Definition of initial values (at time t_0 before the pulse arrives):

$$n_0 = n_{tot}(t_0) = \int_{x=0}^{x=L} \Delta N(x,t_0)\mathrm{d}x \qquad\qquad \text{initial inversion areal density}$$

$$= \Delta N(t_0) \cdot L \qquad\qquad \text{if} \Delta N(t_0) \neq f(x) \text{ (homogeneous inversion)}$$

$$J_{st,0} = h\nu \cdot n_0 \qquad\qquad \text{max. stored energy density}$$

$$G_0 = G(t_0) = e^{\sigma \cdot n_0} = e^{\sigma \cdot \Delta N(t_0) \cdot L} \qquad\qquad \text{initial (small-signal) gain}$$

$$= e^{\frac{\sigma}{h\nu} \cdot h \cdot \nu \cdot n_0} = e^{\frac{J_{st,0}}{J_{sat}}}$$

(g) Gain of fluence in the pulse: $\left(\int_{t_0}^{t}(\text{eqn.9}) \, dt\right)$

$$\Rightarrow J_{in}(t) = J_{sat} \cdot \ln\left(\frac{1 - 1/G_0}{1 - 1/G(t)}\right) \qquad\qquad \Rightarrow G(t) = \frac{G_0}{G_0 - (G_0 - 1) \cdot e^{-(J_{in}(t)/J_{sat})}}$$

$$J_{out}(t) = J_{sat} \cdot \ln\left(\frac{G_0 - 1}{G(t) - 1}\right) \qquad\qquad \Rightarrow J_{out}(t) = J_{sat} \cdot \ln\left(1 + G_0 \cdot (e^{J_{in}(t)/J_{sat}} - 1)\right)$$

(h) Gain of the whole pulse:

$$G_p = \frac{J_{out}}{J_{in}} = \frac{J_{sat}}{J_{in}} \cdot \ln\left(1 + G_0 \cdot (e^{J_{in}/J_{sat}} - 1)\right)$$

(a) small signal gain ($J_{in} \ll J_{sat}$): $G_p \approx G_0 = e^{\Delta N(t_0) \cdot \sigma \cdot L}$

(b) saturated gain ($J_{in} \gg J_{sat}$): $G_p \approx 1 + \frac{J_{sat}}{J_{in}} \cdot \ln(G_0) = 1 + \frac{J_{sat}}{J_{in}} \cdot \Delta N(t_0) \cdot \sigma \cdot L$

(i) Extracted fluence:

$$J_{extr}(t) = J_{out}(t) - J_{in}(t) = J_{sat} \cdot \ln\left(\frac{G_0}{G(t)}\right)$$

Whole pulse: $\qquad\qquad\qquad\qquad\qquad\qquad\qquad\qquad J_{extr} = J_{sat} \cdot \ln\left(\frac{G_0}{G_f}\right)$

Final gain: $\qquad\qquad\qquad\qquad\qquad\qquad\qquad G_f = \dfrac{G_0}{G_0 - (G_0 - 1) \cdot e^{-(J_{in}/J_{sat})}}$

Amplifier efficiency: $\qquad\qquad\qquad\qquad \eta = \dfrac{J_{extr}}{J_{st,0}} = 1 - \dfrac{\ln G_f}{\ln G_0} \Rightarrow G_f = (G_0)^{1-\eta}$
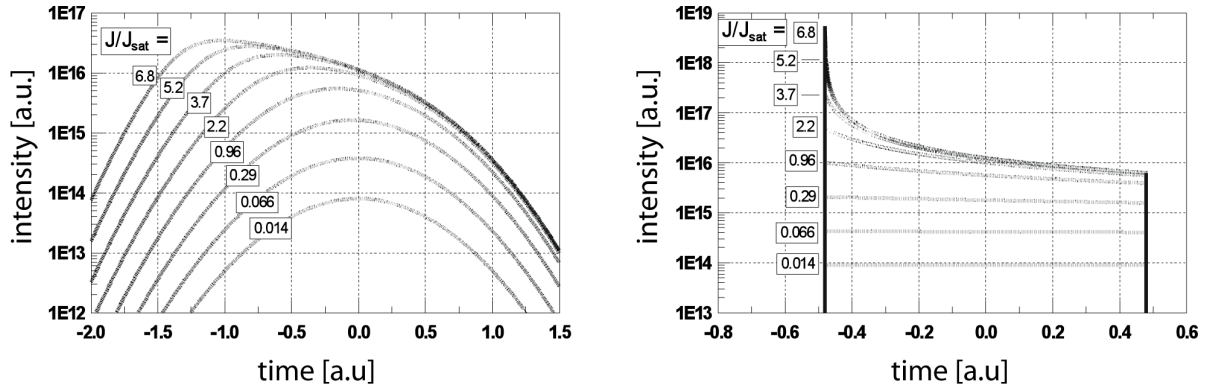
Figure 58: Example of gain-modified pulse shapes:
Gain medium: small signal gain $G_0 = 4.8$/cm, 7cm long.
Input pulse: fluence $J = 0.014 \cdot J_{sat}$. (a) gaussian, (b) rectangular temporal shape. Plots of pulse shape and instantaneous fluence J at input and after each cm of gain medium.

(j) Output pulse shape:

$$I_{out}(t) = I_{in}(t) \cdot G(t) = \frac{I_{in}(t) \cdot G_0}{G_0 - (G_0 - 1) \cdot e^{-(J_{in}(t)/J_{sat})}}$$

Saturation has a strong influence on the output pulse shape, if

- the stored energy is extracted efficiently ($\eta <\approx 1$):
  $\Rightarrow$ final gain $G_f \approx 1$ (i.e strong saturation)

- the initial gain is high ($G_0 \gg 1$):
  a large difference G_0–G_f has a big influence on the output shape

(k) Multi-pass configurations
In an inverted medium of length L, the low intensity of the pulses at the entrance leads to a low stimulated decay rate (see equation 6) and hence an incomplete extraction of energy at the entrance side in a single pass. This makes a long single pass amplifier inefficient if very large gain factors have to be reached. The obvious solution is to use the same gain medium a number of times by passing the laser beam through it in a repeated fashion. In such an arrangement, the whole inverted population can be used, even with very low input fluences.

N passes through the same inverted medium (standard configuration),
$G_{0,1}$ initial gain before the first pass (calculate from initial inversion density/pump rate),
$I_{in}(t)$, $J_{in,1}(t)$ initial energy and fluence profile of the pulse

- initial gain changes: $G_{0,n}$ for each pass n (for $n > 1$)

$$G_{0,n} = G_{f,n-1} = \frac{G_{0,n-1}}{G_{0,n-1} - (G_{0,n-1} - 1) \cdot e^{-(J_{in,n-1}/J_{sat})}}$$

- fluence gain per pass:

$$J_{out,n} = J_{in,n+1} = J_{in,n} + J_{sat} \cdot \left(\frac{G_{0,n}}{G_{f,n}} \right)$$

- Calculation of pulse shape: varying gain $G_n(t)$ during n^{th} pass:

$$G_n(t) = \frac{G_{0,n}}{G_{0,n} - (G_{0,n} - 1) \cdot e^{-(J_{in,n}(t)/J_{sat})}}$$

- fluence profile after n^{th} pass:

$$J_{out,n}(t) = J_{in,n+1}(t) = J_{in,n}(t) + J_{sat} \cdot \ln\left(\frac{G_{0,n}}{G_n(t)} \right)$$

- pulse shape (intensity profile) after N passes:

$$I_{out}(t) = I_{in}(t) \cdot (1 - \gamma)^N \cdot \prod_{n=1}^{N} G_n(t) \quad \gamma : \text{per-pass losses}$$

4.2 Chirped pulses

(a) spectral saturation:

    Depends on the type of broadening of the atomic transition.

    In the following, only homogeneously broadened transitions are discussed.
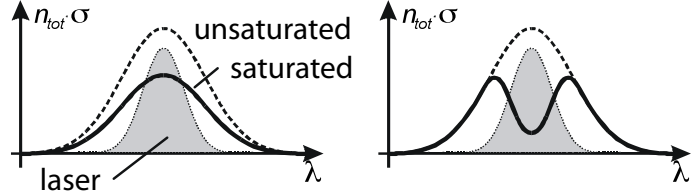
Figure 59: Saturation of the gain profile by a laser (grey) for a homogeneously (left) and inhomogeneously (right) broadened transition.

(b) Effect of saturation on chirped pulses:
In first approximation, in a chirped pulse the instantaneous frequency changes linear with t:

$$\omega(t) = \omega_0 + \frac{D_2}{\left(\Delta\tau_0/2 \cdot \sqrt{\ln 2}\right)^4 + D_2^2} \cdot t = \omega_0 + B \cdot t$$

$\Rightarrow$ Temporal saturation effects have an implication on the spectrum.
$\Rightarrow$ <u>Red-shift</u> (for positively chirped pulses) and gain-induced deformation.

(c) *Gain-narrowing*:
The gain coefficient is spectrally non-uniform (see fig. 59)
e.g. gaussian gain profile:

$$g(\omega) = n_0 \cdot \sigma(\omega) = g_0 \cdot e^{-\left(\frac{\omega-\omega_0}{\xi_g}\right)^2} \qquad \Delta\omega_g = \left(2 \cdot \sqrt{\ln 2}\right) \cdot \xi_g$$

Assume: input pulse gaussian as well:

$$I_{in}(\omega) = I_0 \cdot e^{-\left(\frac{\omega-\omega_0}{\xi_I}\right)^2} \qquad \Delta\tau_0 = \left(2 \cdot \sqrt{\ln 2}\right)/\xi_I$$

$\Rightarrow$ Non-uniform small signal gain:

$$I_{out}(\omega) = I_{in}(\omega) \cdot e^{g(\omega)} \approx I_0 \cdot e^{g_0} \cdot e^{-g_0 \cdot \left(\frac{\omega-\omega_0}{\xi}\right)^2}$$

$$\text{with} \quad \frac{1}{\xi^2} = \frac{1}{\xi_I^2} + g_0 \cdot \frac{1}{\xi_g^2} \qquad \text{(spectral narrowing)}$$

$$\Rightarrow \Delta\tau_1 = \sqrt{\Delta\tau_0^2 + \frac{\ln 2}{\pi^2} \cdot \frac{g_0}{\xi_g}} \qquad \text{(p ulse lengthening even for transform-limited pulses)}$$

(d) *Gain-shift:*

If amplification takes place outside the spectral gain maximum
$\Rightarrow$ spectrum $(\omega_0, \Delta\omega)$ gets shifted towards gain maximum:

$$G_0(\omega) = e^{n_0 \cdot \sigma(\omega)} \approx e^{n_0 \cdot \sigma(\omega_0)} \cdot e^{n_0 \frac{d\sigma}{d\omega}(\omega - \omega_0)}$$

$$\Rightarrow \omega_{max} = \omega_0 + 2 \cdot \ln 2 \cdot n_0 \cdot \frac{d\sigma}{d\omega} (\Delta\omega)^2$$
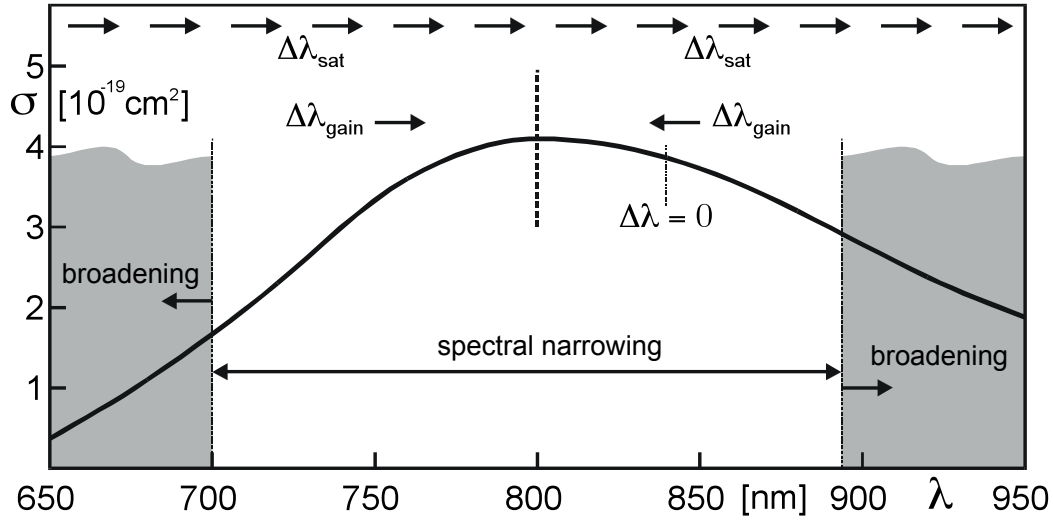
Figure 60: Gain band $\sigma(\lambda)$ of Ti:Sa and effects of spectral shifting/narrowing/broadening during amplification.

(e) Material properties for CPA amplification

Material	Ti:Sa	Nd:glass (silicate)	Nd:glass (phosphate)	Dye (Rh 6G)
λ_0[nm]	800	1062	1054	610
$\Delta\lambda_g$[nm]	220	27	21	50
τ_{sp}[μs]	3.2	340	310	0.003
σ_{ie}[cm^2]	$4.1 \cdot 10^{-19}$	$2.8 \cdot 10^{-20}$	$4.1 \cdot 10^{-20}$	$1.5 \cdot 10^{-16}$
J_{sat}[J/cm]	0.6	6.6	4.6	0.002
Pump	Nd:YAG (2ω), Ar+	Flashlamps, Diodes	Flashlamps,Diodes	Excimer-laser

4.3 Detrimental effects

Detrimental effects happen during amplification. They are caused by different effects which shall be presented in the following.

4.3.1 Spatial saturation

consider spatially homogeneous inverted medium:

during small signal gain:
spatial profile $J(y)$ is constant

after strong saturation $(J_{in} \gg J_{sat})$:

$$J_{out}(y) = J_{in}(y) + J_{sat} \cdot \ln G_0$$
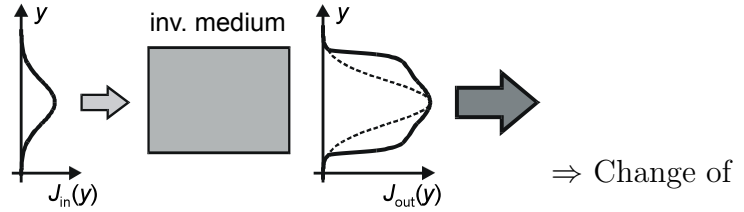
Figure 61: Change of spatial profile by saturation (dashed line: small signal gain).

$\Rightarrow$ Change of beam profile (here: approximation of square profile)

In general: profile of amplified pulses $\approx$ gain profile $\approx$ pump profile:

Shaping of pump is important!
Spatial saturation is not always detrimental. It helps with the transition from a Gaussian profile with good propagation characteristics in the preamplifiers to a top-hat profile with good energy extraction in the main amplifier. However, diffraction plays and important role during propagation of top-hat beams. Diffraction effects have to be taken into account and kept under control, e.g. by image-relaying the beam.

4.3.2 Thermal effects

Only a part $\eta = (h\nu_{Laser})/(h\nu_{pump}) = \lambda_{pump}/\lambda_{laser}$ of the absorbed pump radiation is used to create the inversion, the remainder is lost as heat in the amplifying medium.

Assumptions:

- heat deposition in the pumped volume is spatially homogeneous $\Rightarrow Q = P_H/V$ (power/vol.)

- cylindrical medium ("rod"), neglect axial heat flow

$$\Rightarrow \quad \text{1D-heat conduction:} \quad \frac{\mathrm{d}^2 T}{\mathrm{d}r^2} + \frac{1}{r} \cdot \frac{\mathrm{d}T}{\mathrm{d}r} + \frac{Q}{K} = 0 \quad (K: \text{heat conductivity})$$

$$\Rightarrow \quad \text{temperature profile:} \quad T(r) = T(R) + \frac{Q}{4K} \cdot \left(R^2 - r^2\right) \quad (R: \text{total radius of rod})$$

$$\text{with} \quad Q = \frac{P_H}{V} = \frac{P_H}{R^2 \cdot \pi \cdot L} \quad \Rightarrow \quad \Delta T = T(0) - T(R) = \frac{P_H}{4\pi \cdot K \cdot L}$$

Pulsed operation: the continuous heat load creates a parabolic temperature profile and a thermal lens. With a pulsed pump the last pump pulse (the one amplifying the actual

74

laser pulse) adds a temperature profile according to its energy deposition profile.

Effects of amplifier heating:

- Induced birefringence → generation of "wrong" polarization → high losses.

- Thermal change of refractive index (thermal lens):

$$\Delta n(T) = \frac{\mathrm{d}n}{\mathrm{d}T} \cdot \Delta T$$

$$\Rightarrow \quad n(r) = n_0 \cdot \left(1 - \frac{r^2}{B^2 \cdot R^2}\right) \qquad B^2 = \frac{2\pi \cdot L \cdot K}{P_H \cdot (\mathrm{d}n/\mathrm{d}T)}$$

$$\Rightarrow \quad \text{Gain medium becomes a lens with} \quad f \approx \frac{B^2 \cdot R^2}{2 \cdot n_0 \cdot L}$$

- Destruction by thermal shock

$$P_H \leq 8\pi \cdot S_{th} \cdot L \ (S_{th} \text{ thermal shock parameter})$$
$$S_{th} = 1/7.9/100 \text{ W/cm (glass / YAG / Ti:Sa)}$$

Cooling:

- Purpose:
  Reach a safe equilibrium
  At lower temperature, K increases for most laser materials $\Rightarrow \Delta T$ drops

- Method:
  Stream fluid with constant temperature T_F around the cylinder.
  In thermal equilibrium, P_H is extracted radially:

$$P_H = 2 \cdot L \cdot h \cdot (T(R) - T_F) \qquad h: \text{ heat transfer coefficient}$$

$$\Rightarrow T(r) = T_F + \frac{P_H}{2\pi \cdot L} \cdot \left(\frac{1}{R \cdot h} + \frac{1}{2K} \cdot \left(1 - \frac{r^2}{R^2}\right)\right)$$

4.3.3 Self-focussing

The intensity dependence of the refractive index (c.f. chapter 1.5.1) leads to a phase delay for high-intensity portions of the beam. Consequently, the beam is focused in these areas, which can even overcome diffraction, in a process called self-focusing. Since this may lead to optical damage, this effect is of particular concern in high-power laser amplifiers where the power can often exceed the critical power for self-focusing. Self-focusing takes place in two different regimes:

Small-scale self-focusing

Self-focusing (filamentation) at small local intensity spikes (e.g. diffration rings from dust on optical surfaces)
$\Rightarrow$ Beam break-up, local damage to the material.

Precautionary measure: typical size d_t of small structures in the beam must exceed

$$d_t > d_{cr} = \sqrt{\frac{2}{\pi}\frac{P_{cr}}{I}}$$

Reasons for generation and growth of spatial inhomogeneities:

- Inhomogeneity of the pump distribution

- Inhomogeneity of the laser materials

- Bad or dirty optical components

Countermeasure:

High spatial frequencies distribute intensity far outside the focal spot's radius, which relates to the beam diameter before the focusing optic. A spatial filter eliminates these frequencies, acting as a low-pass fourier filter.
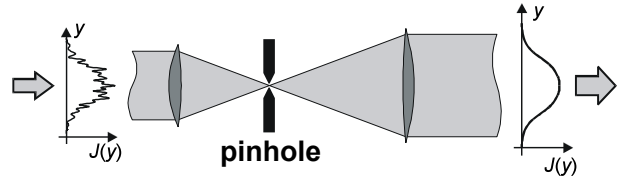
Figure 62: A spatial filter (pinhole around focal spot) generates a smooth spatial profile.

Whole-beam self-focusing

If the beam is sufficiently smooth and its power $P > P_{cr}$:
The whole beam collapses after a distance f_{SF} inside the medium into a single focal spot:

$$f_{SF} = \frac{b}{4 \cdot \sqrt{P/P_{cr} - 1}}$$

with $b = \dfrac{2\pi w_0^2}{\lambda}$ length of beam waist : "confocal parameter"

and w_0 Gaussian radius at the entrance to the medium

$\Rightarrow$ keep the accumulated optical path inside the medium $\ll f_{SF}$

Effects for chirped pulses:

Even though the SF may not be catastrophic, due to the non-uniform temporal intensity distribution the Kerr-lens varies significantly for different spectral components.

⇒ Beam divergence and focal position vary spectrally.

Rule of thumb: keep "B-integral" small:

$$B(\lambda_0) = \frac{2\pi}{\lambda_0} \cdot \int \frac{n_2 \cdot I(\lambda_0)}{n_0} \mathrm{d}l \leq 1$$

In that case all spectral components have the same (i.e. undistinguishable) beam geometry.

4.4 Loss mechanisms

4.4.1 Spontaneous decay

Takes place from the start of pumping until the end of the gain process and cannot be suppressed.

Rationale: Amplify quickly: amplification time $t_G \ll \tau$ (level decay time).

4.4.2 ASE (Amplified Spontaneous Emission)

Spontaneously emitted light bounces back and forth along the pass of the laser and depletes the inversion by getting amplified. Starts with the beginning of the pump and lasts until the inversion is depleted. Expecially problematic in amplifier chains.

⇒ Worst case scenario: ASE saturates, almost no inversion is left over for the pulse.

Countermeasures:

- temporal discrimination: optical switches

- spatial discrimination: spatial filtering between amplifiers

ASE may even lead to parasitic oscillations:

- In disk-shaped amplifier crystals, where high aspect ratio can cause high gain in the transverse dimension: total internal reflection traps light inside the crystal ⇒ strong lasing build-up.

  Countermeasures:
  - absorptive edge cladding (index-matched liquid), in order to suppress back-reflections from the crystal edges

- on-axis between optical components normal to it.

  Countermeasures:
    - Tilt all components away from the axis, Optically decouple them (optical switches, optical diodes).

4.4.3 Back-reflected laser light

Laser light gets back-reflected from optical components or the laser target and still sees gain in the amplifiers. Back-propagating through the chain, its beam size is reduced, while its energy increases. $\Rightarrow$ Worst case scenario: massive optical damage in parts with small beam size.

Causes:

- reflections off optical components or laser application

Countermeasures:

- optical switches (temporal discrimination), optical diodes (Faraday-rotators + polarizers).

4.4.4 Laser Induced Damage

Too high fluence on an optic will cause damage to the optic. For instance, small-scale self-focusing can cause catastrophic beam collapse over a sub-aperture of the beam and to ionization or generation of color centres in the bulk material. Likewise, a high average fluence in a material will cause heating due to residual absorption, and consequently to melting or cracking of the bulk. The severity of all these effects crucially depend on the material properties.

For most optical materials, bulk effects are insignificant in comparison to surface damage. On the surface the symmetry of the solid material is broken, leading to a high field enhancement and a dramaticaly lower laser induced damage threshold (LIDT). A huge number of different mechanisms cause surface damage, and may depend on pulse duration, pulse frequency, wavelength, surface roughness and/or contamination, environment (humidity) etc.

The following table gives a short overview of the most important damage causes with respect to pulse duration:

pulse duration	$t \leq 10^{-9}$ s	$10^{-9} \leq t \leq 10^{-7}$ s	$10^{-7} \leq t \leq 10^{-4}$ s	$t \geq 10^{-4}$ s
Damage mechanism	avalanche ionization	dielectric breakdown	dielectric breakdown / thermal	thermal
Typical values	0.1-1 J/cm^2	2-20 J/cm^2	100 J/cm^2	limited by cooling

Damage thresholds are specified according to ISO-21254-1:2011 standard, which defined test conditions. Most optics manufacturers specify the LIDT according to the above ISO norm with 10 ns, 1064 nm pulses, which is unusable for most ultrahigh-intensity applications. The following approximate scaling laws apply:

$$\text{adjusted LIDT} = \text{LIDT energy} \sqrt{\frac{\text{pulse duration}}{\text{LIDT pulse duration}}}$$

$$\text{adjusted LIDT} = \text{LIDT energy} \sqrt{\frac{\text{wavelength}}{\text{LIDT wavelength}}}$$

Note that below 10 ps, the LIDT energy scales much weaker with pulse duration:
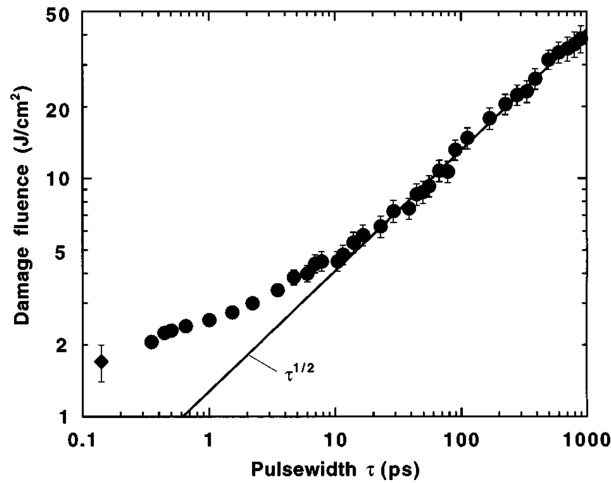
Figure 63: LIDT for different pulse lengths, from *B. C. Stuart et al., Optical ablation by high-power short-pulse lasers. J. Opt. Soc. Am.* ***B*** *13(2), p. 459-468 (1996)*

Finally, the beam radius has a strong influence on LIDT. For small beams (≈ 50 μm) the chance to illuminate a crack or imperfection on the surface drops dramatically, leading to a factor ≥ 10 higher LIDT. This illustrates the importance of an excellent surface polish.

4.4.5 Spatial inversion distribution

Longitudinal:
When the crystal is longitudinally pumped (absorption coefficient α):

⇒ Distribution of inversion density:

$$\Delta N(x) = \frac{\alpha \cdot J_{Pump,0}}{h\nu_{Pump}} \cdot e^{-\alpha \cdot x}$$

⇒ The strongest absorption, inversion, temperature etc. occurs at one end face. Countermeasure: pump from two sides.

Radial:

- Longitudinal pumping:
  Inversion density matches pump distribution, transverse shaping of the pump beam may be necessary.

- Radial pumping:
  Only careful design of pump source, reflector geometry and radial doping profile ensures an even illumination of the active material.

4.5 The regenerative amplifier

4.5.1 Basics

seeded, pulse-pumped laser resonator. The resonator's mode structure defines the spatial beam pattern, while the seed pulse determines the spectro-temporal characteristics of the output pulse. The seed pulse is switched in and out of the resonator after completing the desired number of round-trips. Since there is no Kerr-lens-ML, the compensation of dispersion is not necessary for achieving stable amplfication. However, the accumulated dispersion has to be taken into account in the overall dispersion management.
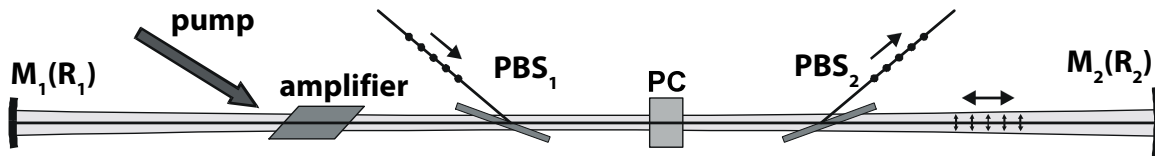
Figure 64: Regenerative amplifier: M_1, M_2 resonator mirrors (radii of curvature R_i), PC Pockels cell, PBS polarizing beam splitters.

4.5.2 Components

- mirrors:
  high-reflective, high LDT in a stable resonator configuration,

- gain medium:
  often used at Brewster's angle (no losses for p-polarized light),

- polarizing beam splitters (PBS): transmission for p-polarized light ($T_p \geq 95\%$), reflection for s-polarized light ($R_s \geq 80\%$) for the full bandwidth of the pulse ($\geq 4 \cdot \Delta\lambda$),

- Pockels cell (PC):
  off: no influence on polarization:
    - p-polarized light can circulate in the resonator,
      s-polarized light gets rejected by the polarizers;

  on: rotates the polarization of transmitted light by 90°:
    - p-polarized light gets s-polarized in the PC and is coupled out at the PBS's,
      p-polarized light gets s-polarized and transmitted by the PBS's.

4.5.3 Sequence of amplification

(1) PC off, pump on. (pump phase)
    $\Rightarrow$ Inversion and radiation build-up in the cavity.

(2) PC on, pump off. (incoupling)
    $\Rightarrow$ radiation from phase 1 gets switched out of the cavity (*cavity-dumping*), while a seed pulse gets switched in.

(3) PC off, before the seed pulse returns back to the PC from its first bounce off the end mirror. (amplification phase)
    $\Rightarrow$ the pulse stays in the cavity and is amplified, other seed pulses are blocked.

(4) PC on, when the gain is reaching saturation. (outcoupling)
    $\Rightarrow$ the amplified pulse is coupled out.

4.5.4 Role of resonator

- Only resonator modes are amplified efficiently.
  $\Rightarrow$ Amplified pulse has got "nice" spatial profile (TEM_{00}-mode: Gaussian beam).

- Mode-matched coupling of the seed pulse to the cavity!
  $\Rightarrow$ The waist of the seed beam and the fundamental mode of the resonator have to be of the same size and overlap spatially.
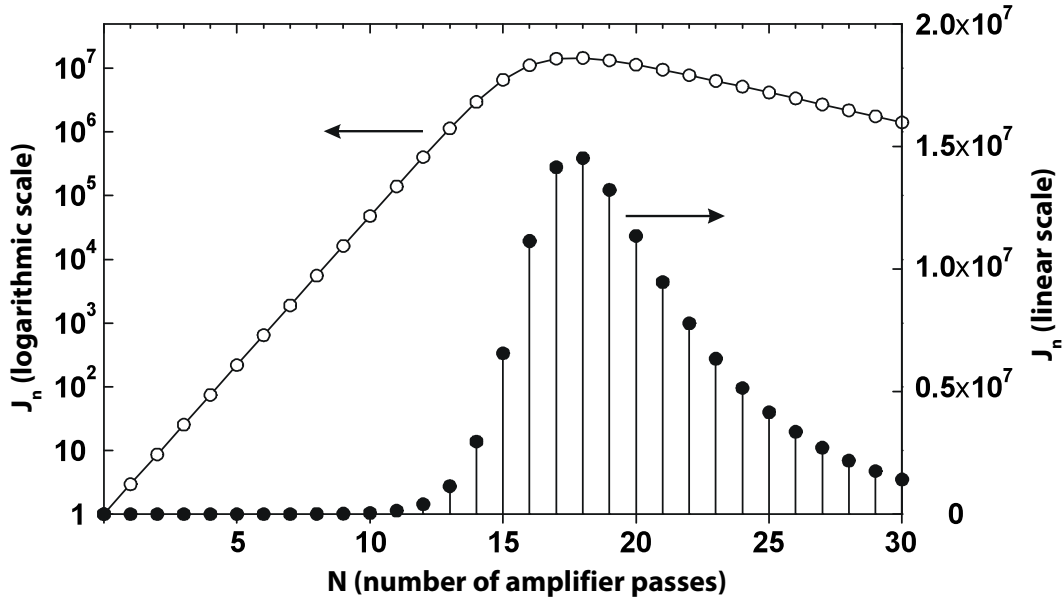
Figure 65: Amplification in a regenerative amplifier: fluence build-up and decay without an outcoupling switch ($G_0 = 2.94$, $J_0 = 4.6 \cdot 10^{-8} \cdot J_{sat}$, $\gamma = 0.2$). (plot of the same curve in linear and logarithmic scales).

4.5.5 Calculation of gain

Characteristics:

- losses: polarizers and pockels cells cause relatively high losses, additional losses via e.g. spectral filters ($\gamma = 10 - 30\%$ per single pass).

- gain per pass: relatively low, since many passes can take place. Good energy stability.

  - Small signal gain:

$$G_0 = e^{n_0 \cdot \sigma} = e^{\frac{J_{st,0}}{h\nu_{Laser}} \cdot \sigma} = e^{\frac{J_{st,0}}{J_{sat}}} \ (\text{typical } G_0 = 1.2 - 2.5, J_{st,0} = J_{stored})$$

  - Gain after n^{th} pass

$$G_n = \frac{G_{n-1}}{G_{n-1} + (1 - G_{n-1}) \cdot e^{-(J_{n-1}/J_{sat})}}$$

  - Fluence after n^{th} pass:

$$J_n = \left(J_{n-1} + J_{sat} \cdot \ln\left(\frac{G_{n-1}}{G_n}\right) \right) \cdot (1 - \gamma)$$

– Rough approximation: Number of passes N

$$N > \frac{J_{sat}}{J_{st,0}} \cdot \ln\left(\frac{J_{st,0}}{J_0}\right)$$

– Rough approximation: max fluence, at

$$e^{n_{tot}\cdot\sigma} \cdot (1 - \gamma) = 1$$

$$\Rightarrow E_{extr,max} \approx E_{st,0} \cdot \left(1 + \frac{\ln(1 - \gamma)}{\ln(G_0)}\right) \cdot (1 - \gamma)^k \quad k \approx 2, \text{ empirical, depends on } G_0, \gamma$$

4.5.6 Pre-pulses

- During the amplification all other oscillator pulses are passed on to the next amplifiers.
  ratio to desired pulse: $1/G_{ges}$, if the pulse train is not filtered by an additional PC.

- Attenuation ratio PC+PBS: $100 - 1000$. $\Rightarrow$ during each pass a part of the circulation pulse is coupled out. $\Rightarrow$ chain of prepulses.
  Remedy:
  Optical switch(es) after the regenerative amplifier.

- Oscillator pulses arriving early are also partially coupled in (bad attenuation ratio) and get amplified and coupled out.
  Remedy:
  Optical switch in front of amplifier.

- ASE (amplified spontaneous emission = incompressible background following the inversion level): at the time the seed pulse is coupled in, the ASE starts from zero, since in the switching process the previous ASE is cavity-dumped. Hence the ratio of seed pulse to spontaneous emission defines the ASE contrast level.

4.5.7 Spectral influence of a regenerative amplifer

Material dispersion: Many passes and long path in material (PC, crystal, PBS) cause high dispersion $\Rightarrow$ for ultrashort pulses ($\leq$ 25fs) a regenerative amplifier is difficult to compensate for.

Saturation effects: Low red shift, since low gain means the saturation is reached gradually in many steps, while the different spectral components of the pulse approximately see the same gain at each pass.

Gain-narrowing: strong, since the effective (= useable) gain is high and the losses γ necessitate an even higher total gain G_T:

$$G_T = G_{eff} \cdot (1 - \gamma)^{-N}$$

$$N \quad \text{number of passes}$$

$$G_{eff} = \frac{J_{extr}}{J_0} \quad \text{effective (net-)gain}$$

Compensation: Modulation of the spectral gain in order to selectively broaden, shift or shape the spectrum:

Method: reduce transmission in the center of the gain curve $\Rightarrow$ effective spectral broadening.

- place Fabry-Perot - interferometer with small finesse in the resonator

- use end mirrors with spectrally varying reflectivity

- place acousto-optic programmable spectral filter inside the resonator $\Rightarrow$ even more dispersion!

4.6 Multipass amplifier

4.6.1 Principle

Repeatedly send pulse through an inverted medium (i.e. in a folded path).
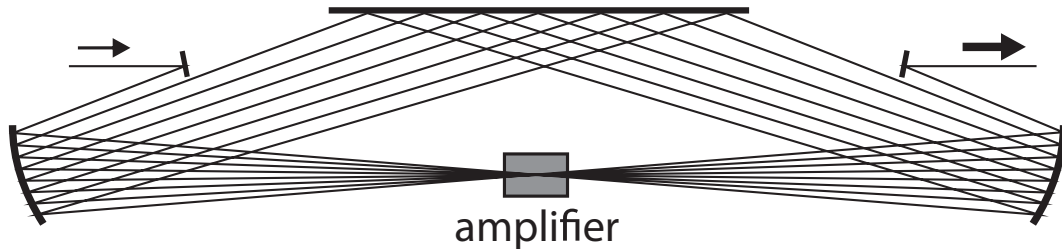
(a) High gain multipass as a low-loss, low-dispersion preamplifier
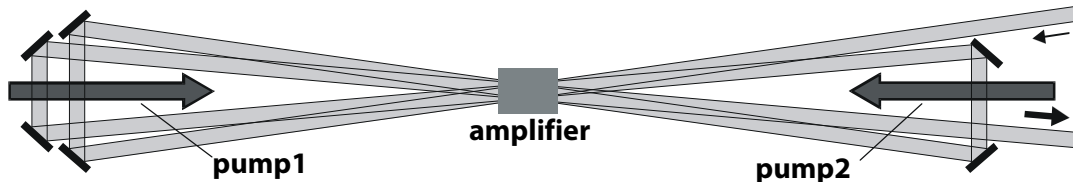
(b) Power amplifier for post-amplification of pulses with already high fluence

Figure 66: Two different multipass amplifiers.

4.6.2 Components

gain medium:
mostly normal incidence, AR-coated for pump and signal beams

Mirror array:
focusing or planar, depending of amplifier type.

Pump beams
two-sided pumping is advantageous due to a longitudinally more homogeneous pump distribution, transverse pump homogenization ensures transversally uniform gain.

4.6.3 Properties

- low losses ⇒ good efficiency

- rather few passes ⇒ high gain per pass ⇒ strong saturation effects.

- no smoothing of beam profile by a resonator mode
  $\Rightarrow$ Pump profile / inversion profile gets transferred onto the amplified beam

- no prepulses, but ASE (from the beginning of pumping until after the pulse)

4.6.4 Calculation of gain

Calculate pass after pass (as in regenerative amplifiers)
small signal gain:

$$G_0 = e^{n_0 \cdot \sigma} = e^{\frac{J_{st,0}}{h\nu_{Laser}} \cdot \sigma} = e^{\frac{J_{st,0}}{J_{sat}}} \quad \text{(typical: } G_0 = 3 - 10\text{)}.$$

Choice of N (number of passes) and d (pump size, gain): compromise between

- N large: complicated beam path, long path in material (dispersion, B-integral)

- N small: strong saturation and thermal effects

4.6.5 Types

- *high-gain-multipass-amplifier* (see figure 66(a)): (pre-)amplifier for up to 5mJ pulse energy.
  Pulse is focused into the crystal on each pass:
  May be set up with beam crossing point (= crystal position) and focal plane separated, allowing larger mode size in the crystal.
  Low losses and dispersion, efficient conversion of pump energy, smaller gain-narrowing.

- *power-amplifier*: Post-amplifier for pulses with $E > 1$mJ.
  Collimated beam travels through the crystal many times $\Rightarrow$ effects of thermal lens are multiplied

  Compensation of thermal lens:
    - Precompensation: use divergent input beam,

    - Compensation at origin: negative lenses between passes,

    - Include "thermal eigenmodes" into design: calculate stable mode in equivalent resonator (crystal = therm. lens $\leftrightarrow$ resonator mirrors) and couple input beam to that mode: $\Rightarrow$ beam keeps its shape in each pass.

4.7 Ultra-high-power lasers

This chapter presents some of the concepts for ultra-high-power lasers.

(a) Ultra-short-pulse-laser: $\Delta\tau \leq 10\mathrm{fs}$, $E_P \leq 1\mathrm{mJ}$, $P \leq 0.1\mathrm{TW}$, $\nu_{rep} = 1\mathrm{kHz}$, $I_{foc} \leq 2 \cdot 10^{17}\mathrm{W/cm2}$

- sub -10-fs - oscillator + glass block stretcher (to $\Delta \approx$ few ps)
- High-gain-multipass-amplifier (Ti:sapphire)
- Compressor: prisms + chirped mirrors for fine compensation of D_3 (1mJ, $\geq$ 20fs)
- Gas filled capillary (spectral broadening)
- Recompression to $\Delta\tau \approx 5\mathrm{fs}$ using dispersive mirrors.
- Post amplification in OPCPA stages possible up to J- (PW)level

(b) TW-PW Ti:Sa laser: $\Delta\tau \approx 20 - 100\mathrm{fs}$, $E_P = 1 - 100\mathrm{J}$, $P = 10 - 1000\mathrm{TW}$, $\nu_{rep} = 0.1 - 10\mathrm{Hz}$, $I_{foc} \approx 10^{19} - 10^{22}$ $\mathrm{W/cm}^2$

- 20fs - oscillator + grating stretcher (to $\Delta\tau \approx$ several 100ps); high-gain multipass & pulse cleaning as contrast booster
- Regenerative amplifier (Ti:sapphire) to multi-mJ
- One or more power-amplifiers (Ti:sapphire), to $1 - 100\mathrm{J}$
- grating compressor

(c) PW glass laser: $\Delta\tau \approx 150 - 1000\mathrm{fs}$, $E_P \leq 1\mathrm{kJ}$, $P \leq 2\mathrm{PW}$, $\nu_{rep} = 1/\mathrm{h}$, $I_{foc} \approx 1 \cdot 10^{21}\mathrm{W/cm}^2$

- 100fs - oscillator (Ti:sapphire at 1060nm) + grating stretcher (to $\Delta\tau > 1\mathrm{ns}$)
- OPCPA frontend to $> 10\mathrm{mJ}$
- 2–5 power-amplifier (Nd:glass), up to 1kJ
- Grating compressor (up to 1m beam size)

5 Pulse diagnostics

5.1 Quantities

wanted: complete description of electric field:

---
in frequency space
---

amplitude $\qquad\qquad\qquad\qquad\qquad \tilde{E}(\omega) = E_A(\omega) \cdot e^{i\varphi(\omega)}$

ampl. not observable $\Rightarrow$ intensity $\quad I(\omega) = |\tilde{E}(\omega)|^2 = (E_A(\omega))^2$

spectral phase $\varphi(\omega)$ $\qquad\qquad\qquad D_K = \left.\frac{\partial^k}{\partial\omega^k}\varphi(\omega)\right|_{\omega=\omega_0}$

---
in time
---

amplitude $\qquad\qquad\qquad\qquad\qquad \tilde{E}(t) = E_A(t) \cdot e^{i\varphi(t)} \quad (E(t) = \tilde{E}(t) \cdot e^{i\omega t})$

ampl. not observable $\Rightarrow$ intensity $\quad I(t) = |\tilde{E}(t)|^2 = (E_A(t))^2$

temporal phase $\varphi(t)$ contains
information on pulse chirp:

bandwidth limited pulse (no chirp): $\quad \varphi(t) = \varphi_0 + A \cdot t$
linear chirp (e.g. after stretcher): $\qquad \varphi(t) = \varphi_0 + A \cdot t + (B/2) \cdot t^2$

Context: complete description in either temporal or frequency space is sufficient:

$$\tilde{E}(t) = \mathrm{FT}\left(\tilde{E}(\omega)\right), \quad \tilde{E}(\omega) = \mathrm{IFT}\left(\tilde{E}(t)\right)$$

E.g. Gaussian pulses with dispersion component D_2 in frequency space:

$$\Rightarrow \text{ temporal space: intensity: } \quad \Delta\tau(D_2) = \Delta\tau_0 \cdot \sqrt{1 + \left(4 \cdot \ln 2 \cdot \frac{D_2}{\Delta\tau_0^2}\right)^2}$$

$$\text{lin. } chirp: \quad B(D_2) = -\frac{D_2}{\left((\Delta\tau_0^2/(4 \cdot \ln 2))^2 + D_2^2\right)}$$

Measurement of temporal phenomena:

In general: sampling of signal to be measured $M(t)$ with a shorter probe signal $A(t)$ (seconds on a clock, sampling interval of oscilloscope ...)

$$\Rightarrow \text{ cross-correlation } \quad S(\tau) = \int_{-\infty}^{\infty} M(t) \cdot A(t - \tau) \mathrm{d}t$$

Temporal resolution: duration of probe signal (sampling rate etc.)

In case no shorter probe signal is available: probe $M(t)$ with itself (either directly or by a modified version)

$$\Rightarrow \text{ auto-correlation } \quad S(\tau) = \int_{-\infty}^{\infty} M(t) \cdot M(t - \tau) \mathrm{d}t$$

But: loss of information, since often $M(t)$ cannot be retrieved unambiguously.

5.2 1st order auto-correlation

5.2.1 Field auto-correlation

Setup:

Two-beam interferometer, e.g.
Michelson-interferometer, see Fig.

Measured quantity:

Interference fringes change with a change
in position of the delay mirror

Principle:

"Interference only occurs to the degree
of temporal overlap"
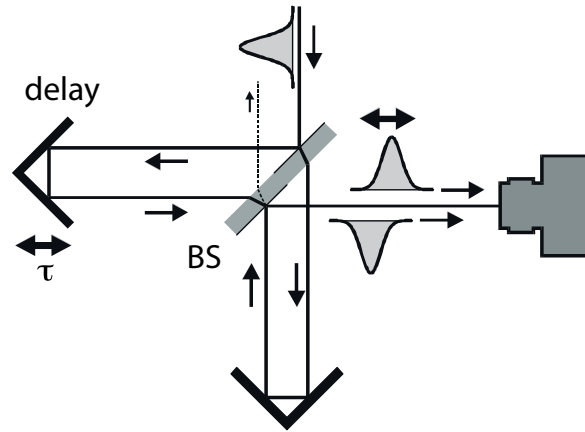
Signal:

$$S(\tau) = \int_{-\infty}^{\infty} I_{ges} \mathrm{d}t = \frac{\epsilon_0 c}{2} \cdot \int_{-\infty}^{\infty} |E_1(t) + E_2(t - \tau)|^2 \, \mathrm{d}t =$$

$$= \int_{-\infty}^{\infty} I \mathrm{d}t + \frac{\epsilon_0 c}{2} \cdot \left(e^{-i\omega_0 \tau} \int_{-\infty}^{\infty} \left(\tilde{E}_1(t) \cdot \tilde{E}_2^*(t - \tau) \right) \mathrm{d}t + e^{i\omega_0 \tau} \cdot \int_{-\infty}^{\infty} \left(\tilde{E}_1^*(t) \cdot \tilde{E}_2(t - \tau) \right) \mathrm{d}t \right)$$

$$= S_0 \cdot [1 + \cos(\omega_0 \tau) \cdot K \cdot \text{FT} (I(\omega))]$$

K normalizing constant (normalizes FT$(I(\omega))$ to 1)

$\Rightarrow$ $S(\tau)$ only depends on spectral amplitude, not spectral phase:
chirp has no effect on measured signal.

$\Rightarrow$ Field auto-correlation does not determine pulse duration, but coherence length. It thus only yields information on the intensity spectrum and the shortest possible (but not the actual!) pulse duration.

Gaussian pulses with spectral FWHM $\Delta\lambda$:

$$\text{Intensity FWHM}(w/o\ chirp): \quad \Delta\tau_I = \frac{2 \cdot \ln 2}{\pi} \cdot \frac{\lambda^2}{\Delta\lambda \cdot c}$$

$$\text{Electric field FWHM }(w/o\ chirp): \quad \Delta\tau_E = \sqrt{2} \cdot \frac{2 \cdot \ln 2}{\pi} \cdot \frac{\lambda^2}{\Delta\lambda \cdot c}$$

$$\text{Field auto correlation FWHM (arbitrary }chirp): \quad \Delta\tau_I = 2 \cdot \frac{2 \cdot \ln 2}{\pi} \cdot \frac{\lambda^2}{\Delta\lambda \cdot c}$$

For transform-limited Gaussian pulses, the intensity duration is exactly half the field AC duration!

Measurement with field AC (simulation):
laser pulse with:
$\lambda = 800$ nm, $\Delta\lambda = 90$ nm
result:
coherence length = shortest possible pulse duration
No information on actual pulse duration!
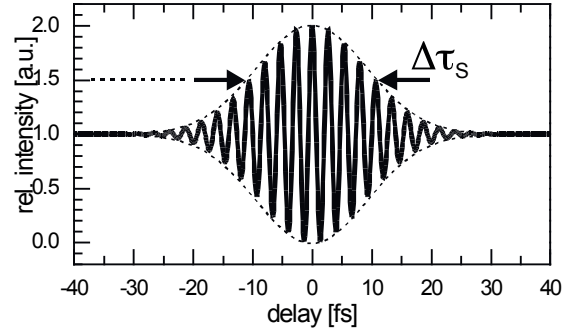
5.2.2 IFAC - inverted field auto-correlator[3]

- Purpose:
  Detection of pulse front tilt angle $\alpha_t = \lambda_0 \cdot C_a$ of short laser pulses in presence of angular chirp C_a.

- Method:
  Measure the relative delay between maximum 1st-order AC across the near field
  $\Rightarrow$ Field AC with spatial inversion of one of the two beams in the interferometer
  $\rightarrow$ IFAC

- Realization:
  Only inversion in one spatial dimension (see Fig. 67 right). This permits the introduction of a tilt in the other spatial dimension $\rightarrow$ horizontal interference fringes.

---

[3](G. Pretzler et al., Appl. Phys. B 70, 1 (2000))

If the input beam exhibits a pulse front tilt, these horizontal fringes move across the image horizontally with a change in delay τ. Quantitative determination of the angular chirp through analysis of the contrast function. Angular chirp in other spatial dimension can be determined by rotation of the input beam or by rotation of the field AC set-up.
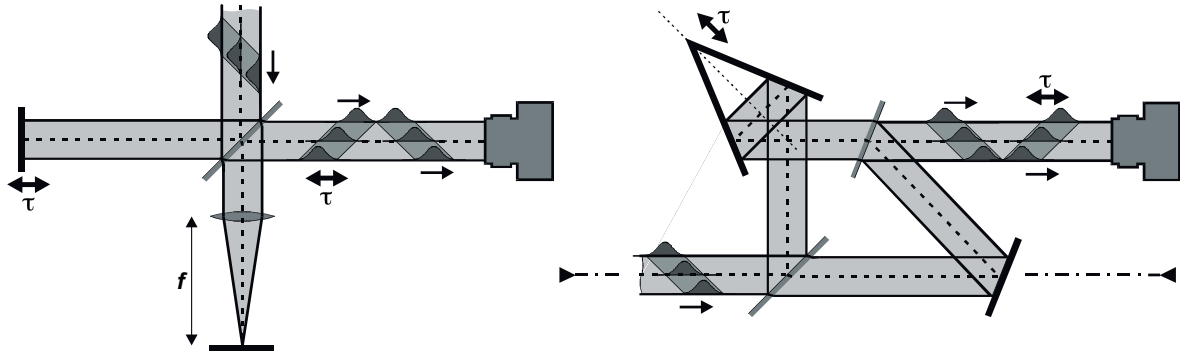
Figure 67: Inverted field AC for measuring the pulse front tilt:
left: Michelson-interferometer with 2D inversion (180°) by a lens.
right: Mach-Zehnder-Interferometer with 1-D inversion
(60° roof mirror in one arm). Setup can be rotated around the input axis for detecting pulse front tilt in any plane.
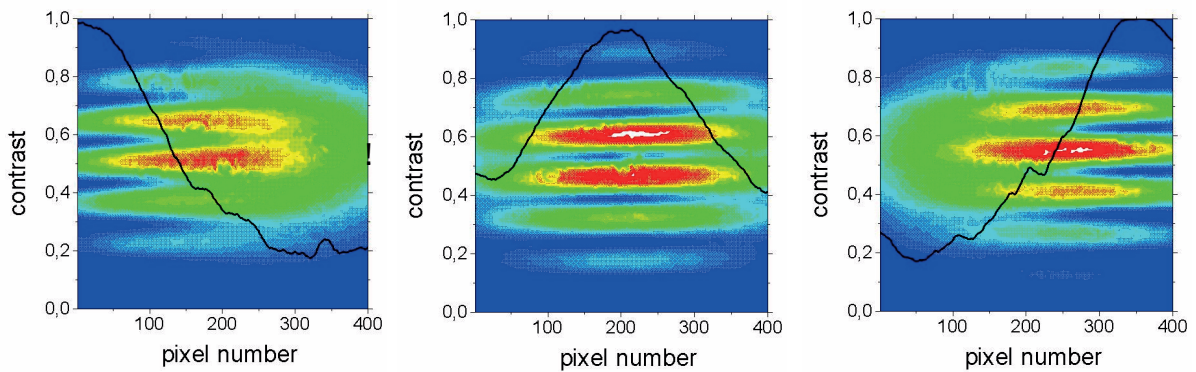
Figure 68: Result of an IFAC-measurement: between two images the delay is changed by 30μm. The contrast curves (black) indicate a pulse front tilt of 125 fs over the beam diameter.

5.3 2nd order auto-correlation

Idea: Introduction of a nonlinear effect in order to detect an intensity dependent correlation.

usually: second harmonic generation (SHG) in a nonlinear crystal (KDP, BBO) Efficiency: $\leq 50\%$ (depending on intensity and crystal thickness). Time-bandwidth product and spectral phase are conserved. Non-linearity:

$$E_{A,2\omega}(t) \propto (E_{A,\omega}(t))^2$$

5.3.1 Interferometric auto-correlation (IAC)

Principle:
Both beams are focused collinearly into the crystal, only the generated 2ω-radiation is detected:

$$S(\tau) = \int I_{2\omega}(t,\tau)\mathrm{d}t \propto \int (E_{2\omega}(t,\tau))^2 \, \mathrm{d}t \propto \int (E_\omega(t) + E_\omega(t-\tau))^4 \, \mathrm{d}t$$

Signal w/o overlap $(\tau \gg \tau_p)$:

$$S_0 = 2 \cdot \int (E_\omega(t))^4 \mathrm{d}t$$

Signal shape: $(S(\tau=0)/S_0) = 8$, complete fringe modulation only in the center. Symmetric to $\tau = 0$. If not: different dispersion of the beams in AC.
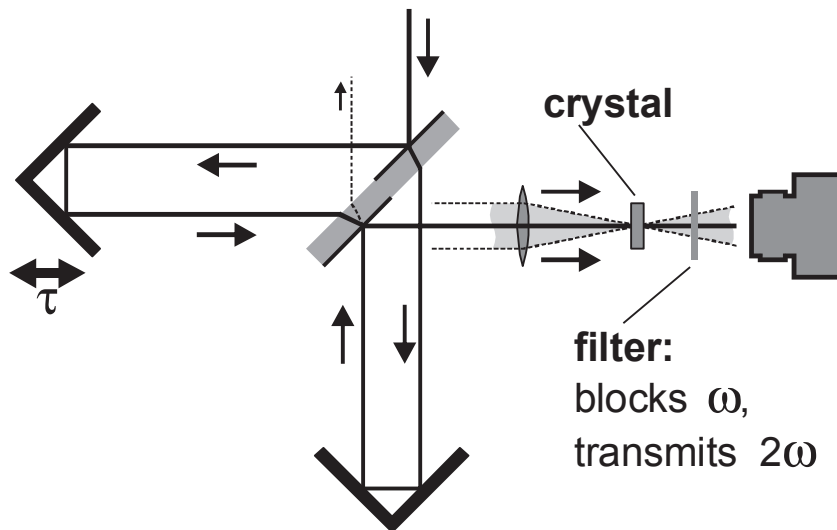
Figure 69: Interferometric auto-correlator

Analysis: Good estimate of pulse quality, duration of chirped pulses is hard to determine.
  Pulses with *little chirp*: estimate of duration and *chirp* by analysing the wings.
  Pulses with *large chirp*: analyse upper and lower envelope of interference pattern.
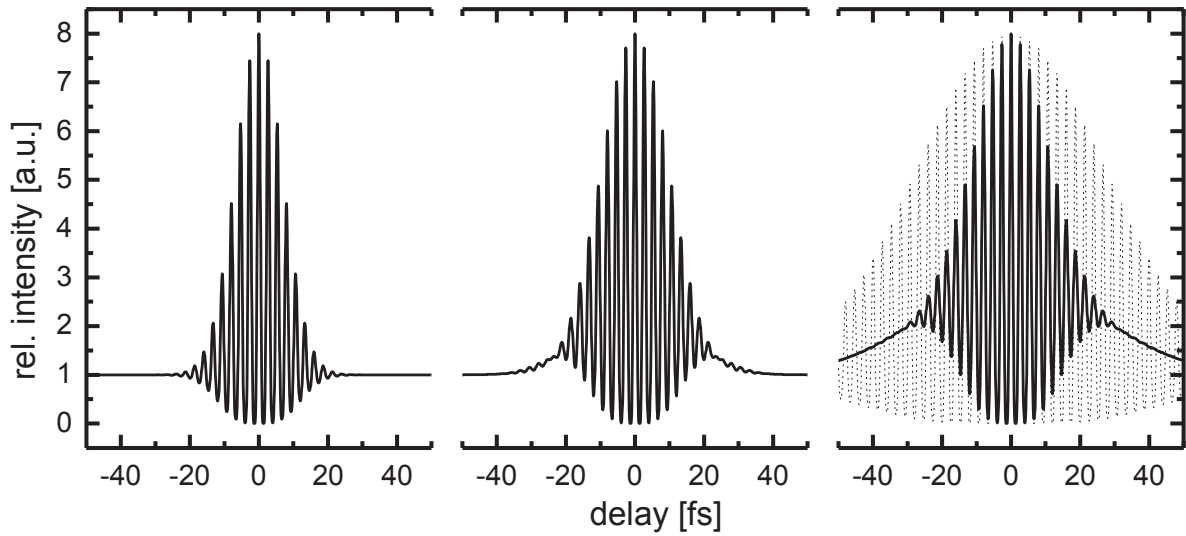
Figure 70: Signals in an interferometric AC (simulation):
left: bandwidth-limited gaussian pulse, $\Delta\lambda = 90$ nm, $\Delta\tau = 10.4$ fs,
middle: pulse with same spectrum, but $D_2 = 70\text{fs}^2 \to \Delta\tau = 21$ fs,
right: pulse with same spectrum, but $D_2 = 155\text{fs}^2 \Delta\tau = 42$ fs.
For comparison (dotted line): pulse with $\Delta\lambda = 22.5$ nm, $D_2 = 0, \Delta\tau = 42$ fs.

5.3.2 Background-free auto-correlation (BFAC)

Principle: Only measure the sum signal of both beams. The beams are focused under
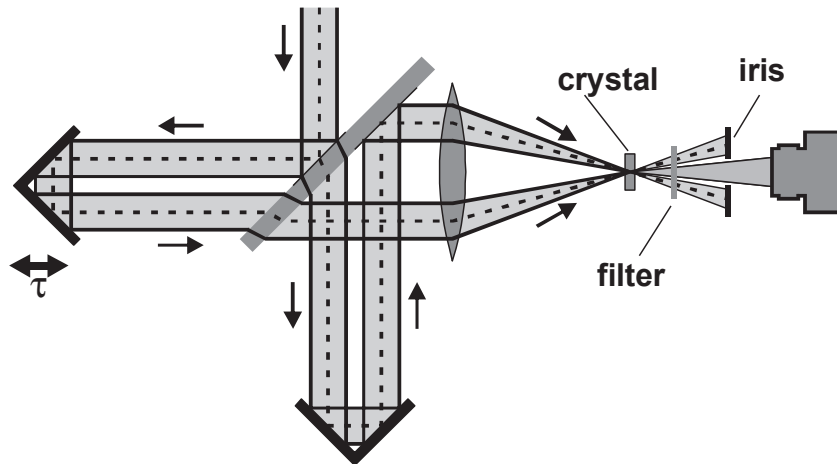
Figure 71: Background-free AC

an angle into the crystal.
signal: only photons emitted along the half-angle by sum frequency generation are de-

tected.

$$E_{2\omega,s}(t,\tau) \propto E_\omega(t) \cdot E_\omega(t-\tau)$$

$$S(\tau) = \int I_{2\omega}(t,\tau)\mathrm{d}t \propto \int (E_\omega(t) \cdot E\omega(t-\tau))^2 \mathrm{d}t = \int I_\omega(t) \cdot I_\omega(t-\tau)\mathrm{d}t$$

Signal shape: $S(\tau)$ is symmetric to $\tau = 0$. If not: measurement error/different dispersion. Pulse can be characterized far into the temporal wings, since no background is present.

For gaussian $I(t)$: $\Delta\tau_S = \sqrt{2}\Delta\tau_I$, for a sech$(t)$ shape: $\Delta\tau_S = 1.543 \cdot \Delta\tau_I$

Analysis: Good (but by no means exact) estimate for the pulse duration, since pulse shape is still unknown.

(common method: measure τ_S, assume pulse shape (gaussian), "calculate" τ_I.)

Deviations from "nice" pulse shape (pre-pulses, uncompensated dispersion) can be observed over many orders of magnitude in intensity.

Problem: since signal is symmetric, pre- or after-pulses are undistinguishable.

If spectrum is known $\rightarrow$ uncompensated dispersion components can be estimated
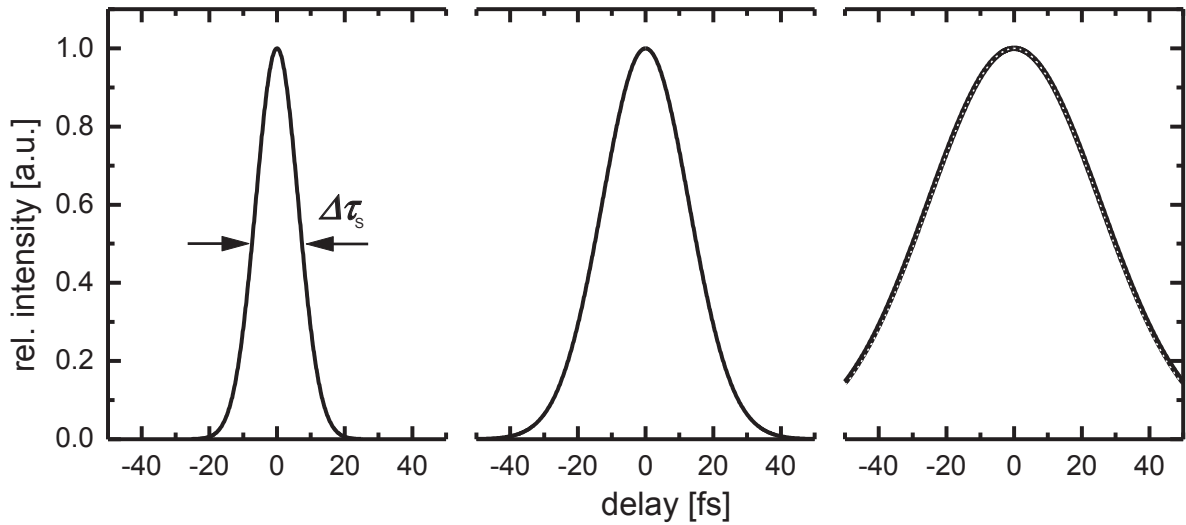
Figure 72: Signals in an BG-free AC (simulation):
left: bandwidth-limited gaussian pulse, $\Delta\lambda = 90$ nm, $\Delta\tau = 10.4$ fs,
middle: pulse with same spectrum, but $D_2 = 70\mathrm{fs}^2 \rightarrow \Delta\tau = 21$ fs,
right: pulse with same spectrum, but $D_2 = 155\mathrm{fs}^2 \Delta\tau = 42\mathrm{fs}$.
For comparison (dotted line): pulse with $\Delta\lambda = 22.5$nm, $D_2 = 0, \Delta\tau = 42\mathrm{fs}$.

5.3.3 2nd order single-shot auto-correlator

Principle: BFAC in the near field (unfocussed beams in a large doubling crystal). Every position y across the beam is correlated to a different delay in the crystal τ. Signal corresponds to the BFAC, but can be produced by a single pulse. Applications:
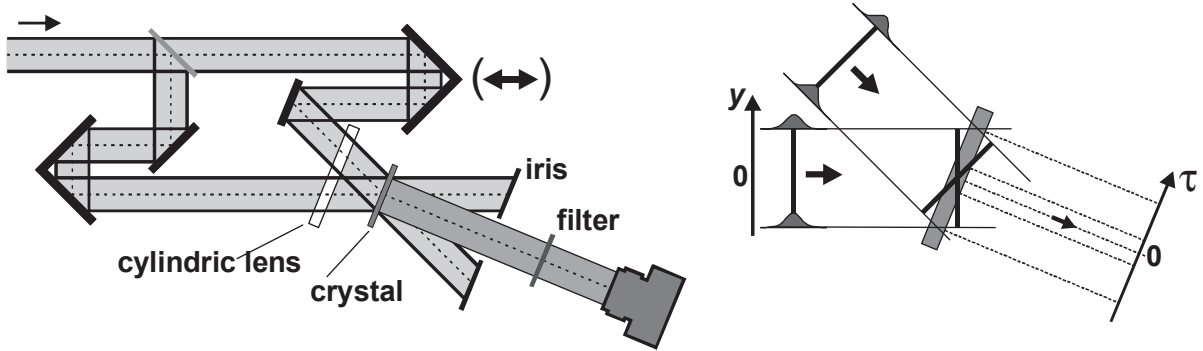
Figure 73: 2nd order single-shot AC. left: Set-up, right: Principle

- Lasers with low repetition rate (single shot, 10Hz).

- High pulse energy is needed for SFG in the near field.

- Smooth spatial profile needed.

Realization:

- 1D-detector needed (CCD-strip)

- Detector either close to the crystal or the crystal is imaged onto the detector.

- Delay change is used to calibrate the time axis.

5.3.4 3rd order auto-correlation

Purpose: breaking the symmetry in order to distinguish pre- from after-pulses. Signal:

$$S(\tau) = \int I_{3\omega}(t,\tau)\mathrm{d}t \propto \int I_{2\omega}(t) \cdot I_\omega(t-\tau)\,\mathrm{d}t \propto \int (I_\omega(t))^2 \cdot I_\omega(t-\tau)\mathrm{d}t$$

Use:

- Single-shot AC (see Fig. 74) with high-power lasers

- *Scanning autocorrelator* (analogous figure 74) with lasers of high repetition rate.

- 2 nonlinear processes: demanding on pulse profile and stability
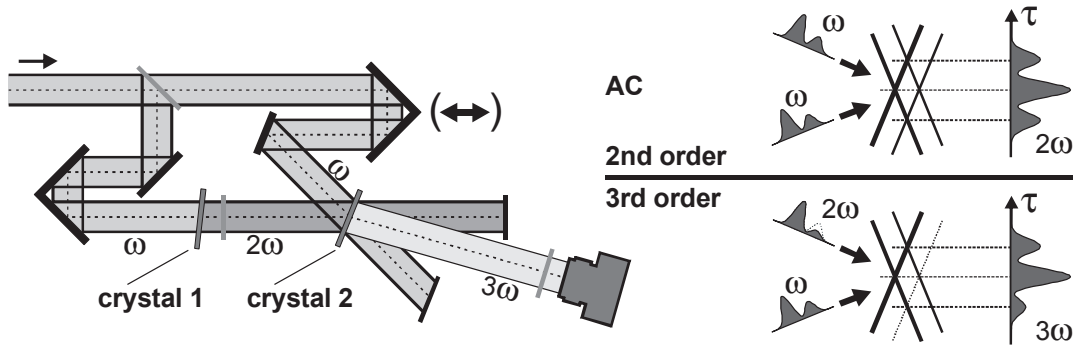
Figure 74: 3rd order single-shot AC. left: set-up, right: Comparison between signals from a 2nd and 3rd order AC with a strong prepulse.

5.4 FROG

5.4.1 Optical Gating: auto-correlation using a fast optical gate

Principle:

An optical gate for the tested pulse is opened by another pulse. Transmission is proportional to the instantaneous power in the gate pulse.
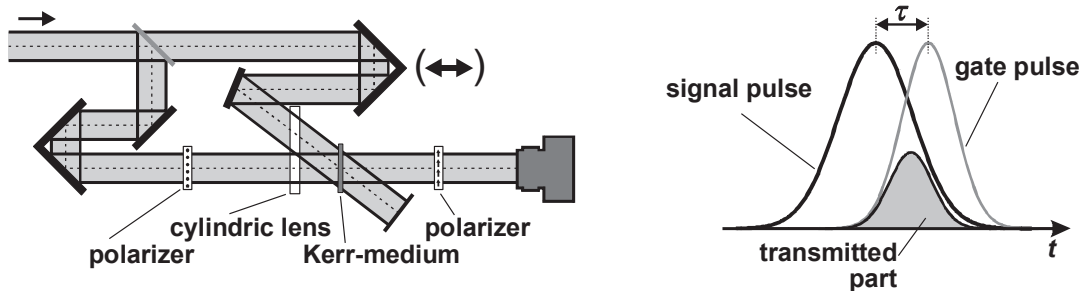
Figure 75: Single shot AC with optical polarization gate. Left: set-up, right: signal generation

Setup: Two crossed polarizers do not permit the main pulse to enter the detector. The switching pulse uses the Kerr medium in order to instantaneously generate birefringence.

$\Rightarrow$ Index difference $\Delta n(t) = (n_e - n_0)(t) \propto E_s^2(t)$ proportional to pulse envelope

$\Rightarrow$ $E_{tr} = E_T \cdot \sin\left((2\pi/\lambda) \cdot l \cdot (n_e - n_0)\right)$ enters detector

$\Rightarrow$ Signal: $S(\tau) = \int I_{tr}(t,\tau)\mathrm{d}t \propto \int (E(t) \cdot I(t-\tau))^2 \mathrm{d}t$

96

Properties:

- Signal is asymmetric to ($\tau = 0$), analogous AK 3rd order.

- Set-up is not background-free (extinction ratio $< 10^{-3}$).

- Tune I_S , to allow only a small fraction of E_{tr}/E_T to enter the detector: ($sin(\alpha) \approx \alpha$), where α is the polarization rotation.

- Single shot (figure 75) with spatially resolved detector or *scanning autocorrelator* (set-up see figure 5.7).

5.4.2 FROG: (Frequency Resolved Optical Gating) [4]

Principle: Signal of an optical gating auto-correlator will be spectrally analyzed. Different delays correspond to different positions in the laser pulse.

Analysis:

- Integration over spectral range yields AC-function.

- Integration over time yields frequency spectrum

- A best match of amplitude and phase to the measured data can be achieved with iterative methods.
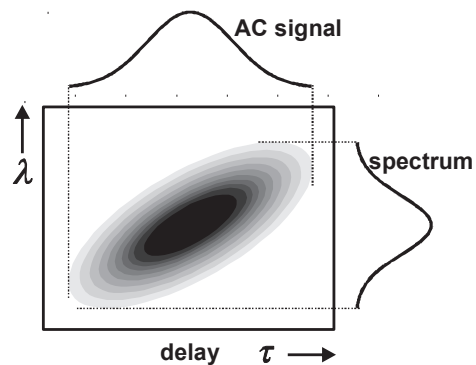
Figure 76: Single shot frog signal with linear Chirp.

Good reconstruction only by good beam smoothness (*single shot*)/ excellent pulse-to-pulse stability (*scanning*-methods).

5.4.3 Related time-frequency space methods[5]

All other AC signals can be frequency resolved to yield 2D-signals like in figure 76. All these variants are called FROG.

For all higher-order nonlinear techniques, it is possible to reconstruct the phase and amplitude of the pulse by employing iterative fitting routines. SHG-Frog (2nd order nonlinearity) yields symmetric signals in time, and therefore is ambiguous with respect to time.

---

[4]R. Trebino & D. Kane, JOSA A 10, 1101 (1993)
[5]K.W. DeLong et al., JOSA B 11, 1595 (1994)

$$E_{tr}(t,\tau) = E(t) \cdot |E(t-\tau)|^2 \qquad E_{tr}(t,\tau) = E^2(t) \cdot E^*(t-\tau) \qquad E_{tr}(t,\tau) = E(t) \cdot E(t-\tau) \qquad E_{tr}(t,\tau) = E^2(t) \cdot E(t-\tau)$$
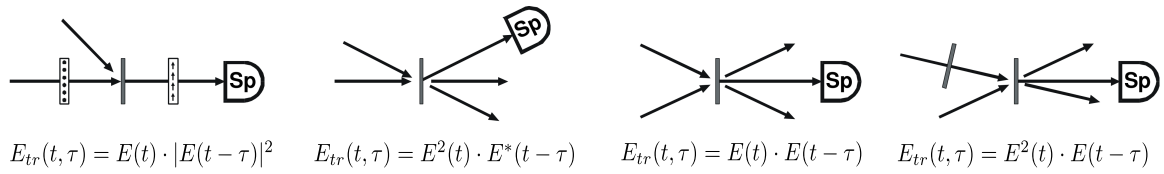
Figure 77: Schemes for some alternative FROG-Set-ups (Sp: spectrometer). From left: polarisation-gating(PG-FROG), three wave mixing (*self diffraction*, SD-FROG), 2nd order AC (SHG-FROG), 3rd order AC (THG-FROG).
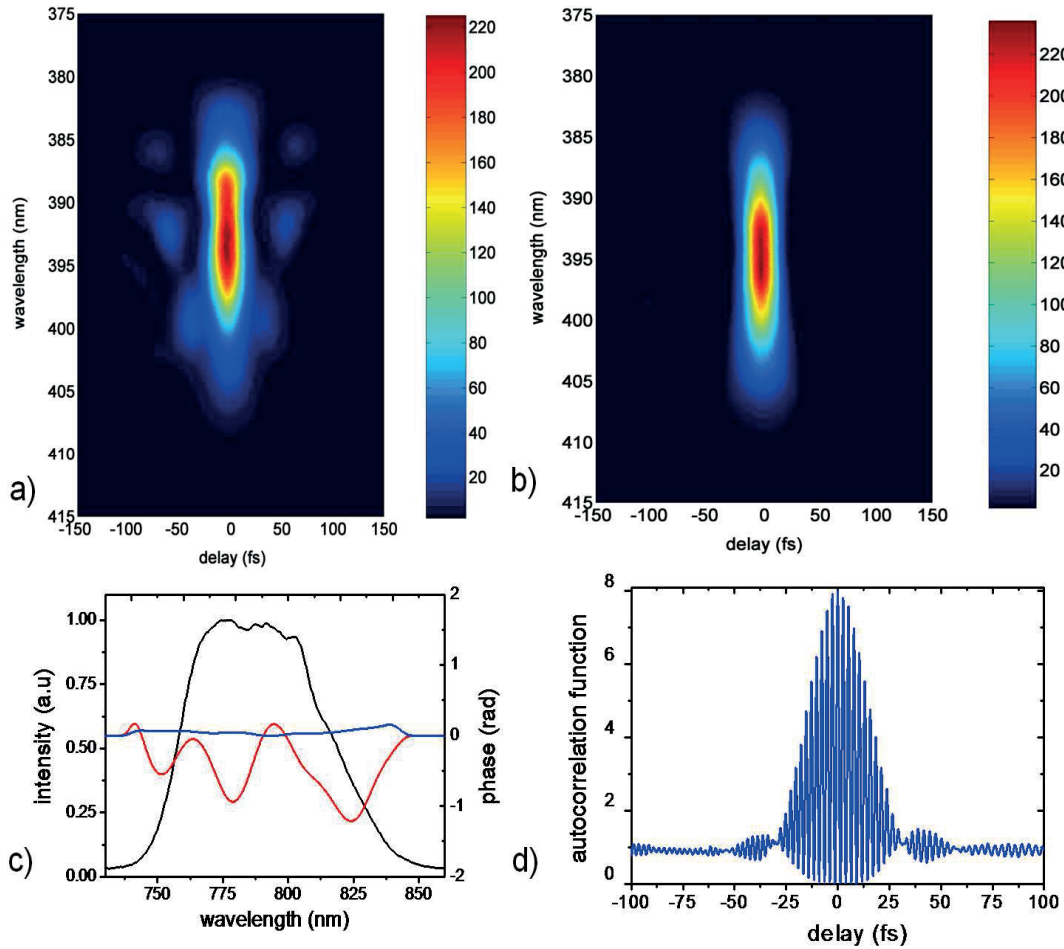
Figure 78: top row: Frog measurement of two laser pulses. Left: 21-fs Pulse with residual high-order phase. Right: 19 fs-pulse with high-order phase removed. Bottom row: Left: Spectrum and phase of both pulses. Right: Interferometric autocorrelation trace of 19-fs pulse

5.5 Frequency domain techniques

In the following chapter the techniques of measurement in frequency space are presented.

5.5.1 FDPM (frequency domain phase measurement)[6]

Principle:
By cutting out a narrowband part of the tested pulse, a second, long pulse is generated. The relative delay of the long pulse against the original pulse is measured and yields the dispersion component D_1, i.e. the derivative of the spectral phase.

$$t_g(\omega) = D_1(\omega) = \frac{\mathrm{d}\varphi(\omega)}{\mathrm{d}\omega}$$

From this, the higher order phase components and together with the intensity spectrum the pulse itself can be derived.
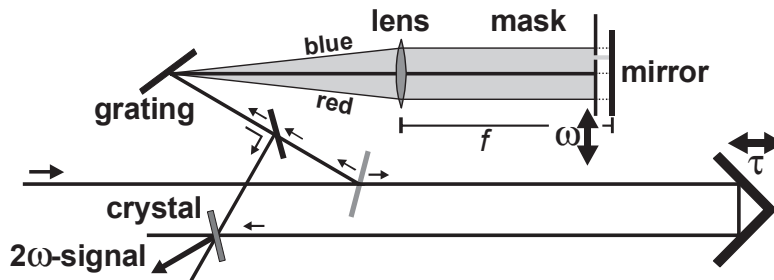
Figure 79: Setup for frequency domain phase measurement.

In practice:

- a scanning measurement (at low pulse energies) is complex, since for each setting of the wavelength mask a full scanning AC has to be measured.

- Relatively poor temporal accuracy leads to overall bad accuracy, especially for long pulses.

- Can be modified to single-shot setup for high pulse energies.

---

[6]J. Chilla & O. Martinez, IEEE J.Qu.El. 27, 1228 (1991)

5.5.2 SPIDER (spectral phase interferometry for direct electric-field reconstruction)[7]

Principle: Two slightly frequency shifted pulses are interfered in a spectrometer (spectral differential interferometry). This allows the deduction of the spectral phase.

1st step: if two mutually delayed pulses are spectrally analyzed, interference fringes occur in the spectrum (maxima for $\Delta L = n \cdot \lambda$), i.e. the frequency spacing is $\Delta \omega = 2\pi c / \Delta L$, <u>independent of the local frequency</u>. If the pulse in one arm of the interferometer is altered this can be detected in the signal (frequency domain-interferometry).
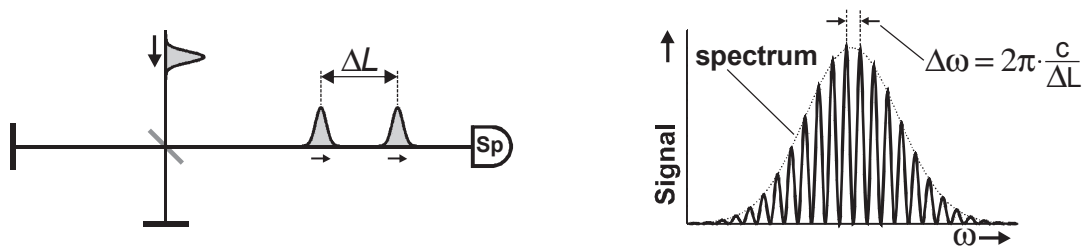
Figure 80: Frequency domain-interferometry. Left: set up (Sp: spectrometer), right: signal.

SPIDER-Setup: A double pulse interacts with a stretched pulse in a nonlinear crystal. Sum frequency generation (SFG) generates two pulses at approx. 2ω, which are sightly shifted in frequency.
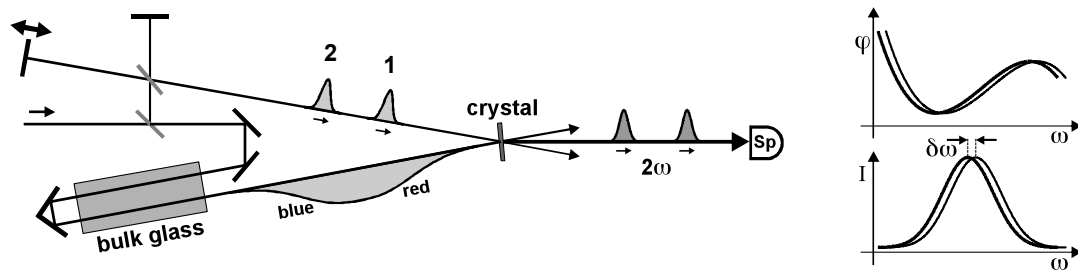
Figure 81: SPIDER. left: schematical set up, right: phase and spectrum of the two spectrally interfering pulses.

SPIDER signal (interferogram):

$$S(\omega) = |E(\omega)|^2 + |E(\omega + \delta\omega)|^2 + 2 \cdot |E(\omega) \cdot E(\omega + \delta\omega)| \cdot \left(\omega \cdot \frac{\Delta L}{c} + \varphi(\omega + \delta\omega) - \varphi(\omega) \right)$$

---

[7]C. Iaconis & I. Walmsley, IEEE J.Qu.El. 35, 501 (1999)

Knowing the spectra $I(\omega)$ and $I(\omega+\delta\omega)$ of the two pulses, and hence $E(\omega)$ and $E(\omega+\delta\omega)$, both the pulse delay ΔL and the phase difference $\varphi(\omega+\delta\omega)-\varphi(\omega)$ can be deduced. (by analyzing the frequency-dependent deviation from an otherwise constant fringe density).

In practice:

- pulse delay defines fringe density

- stretching factor (relative to pulse delay) defines resolution $\delta\omega$.

- Phase is measured at 2ω. For a full reconstruction of the E-field the spectrum at ω needs to be measured as well.

- Absolute (efficiency) calibration only necessary for ω-detector, but not for 2ω (a change in efficiency has little effect on phase measurement)

Figure 82: NA